HIGHWAY RESEARCH RECORD

Number 313

Bituminous Materials, Mixes, and Compaction

7 Reports

Subject Areas

25 Pavement Design
31 Bituminous Materials and Mixes
33 Construction

HIGHWAY RESEARCH BOARD
DIVISION OF ENGINEERING NATIONAL RESEARCH COUNCIL
NATIONAL ACADEMY OF SCIENCES—NATIONAL ACADEMY OF ENGINEERING
WASHINGTON, D.C. 1970

Standard Book Number 309-01812-9

Price: $3.00

Available from

Highway Research Board
National Academy of Sciences
2101 Constitution Avenue
Washington, D.C. 20418

Department of Materials and Construction

R. L. Peyton, Chairman
State Highway Commission of Kansas, Topeka

R. E. Bollen and W. G. Gunderman
Highway Research Board Staff

BITUMINOUS DIVISION

Jack H. Dillard, Chairman
Virginia Department of Highways, Charlottesville

COMMITTEE ON MECHANICAL PROPERTIES OF BITUMINOUS PAVING MIXTURES

(As of December 31, 1969)

Rudolf A. Jimenez, Chairman
The University of Arizona, Tucson

Grant J. Allen
Philip J. Arena, Jr.
Herbert W. Busching
A. B. Cornthwaite
A. W. Eatman
Jon A. Epps
William J. Harper
Yang Hsien Huang
Donald I. Inghram
I. V. Kalcheff
Bernard F. Kallas
J. Hode Keyser
Ralph W. Kiefer
Donald R. Lamb
W. H. Larson
Dah-yinn Lee
Kamran Majidzadeh
C. T. Metcalf
Fred Moavenzadeh
Carl L. Monismith
Charles A. Pagen
Charles F. Potts
C. K. Preus
Donald H. Remick
James H. Schaub
Jack E. Stephens
William T. Sterling
Ronald L. Terrel
B. A. Vallerga
L. E. Wood
George H. Zuehlke

CONSTRUCTION DIVISION

H. W. Humphres, Chairman
Washington Department of Highways, Olympia

COMMITTEE ON CONSTRUCTION PRACTICES—FLEXIBLE PAVEMENT

(As of December 31, 1969)

F. M. Drake, Chairman
The Asphalt Institute, Kansas City, Missouri

Verdi Adam
Charles W. Beagle
R. W. Beaty
Paul E. Blouin
Leo C. Brooks
B. W. Butt
James M. Desmond
W. L. Echstenkamper
Oren S. Fletcher
Charles R. Foster
William Gartner, Jr.
Willis B. Gibboney
Hans I. Hansen
J. F. Jorgensen
John J. Lyons
E. C. Meredith
Carl E. Minor
Charles F. Parker
Edward T. Perry
John T. Reinhard
James M. Rice
Orrin Riley
Roy M. Rucker
E. F. Sandlin
R. R. Stander
J. F. Tribble
David G. Tunnicliff
Lansing Tuttle

Foreword

The investigations appearing in this RECORD are of interest to the practicing pavement design engineer and also to the researcher of bituminous materials. The reports are concerned with (a) experimental test sections of rubberized asphaltic concrete and (b) laboratory studies related to shrinkage cracking, fatigue, and viscoelastic characteristics of asphaltic paving materials.

Darter et al. discuss the initial findings from an experiment designed to determine the effects of 5 factors on pavement performance. Those factors are variability in thickness of surface and base, variability in asphalt content and viscosity, and amount of rubber content. Preliminary evaluations showed that rubber content had an influence on mixture properties, pavement density, and extracted asphalt properties.

Professors Lai and Fitzgerald present results obtained from laboratory evaluations of rubber-asphalt mixtures used in the Darter investigation. Various types of creep and relaxation tests were performed to determine the effects of rubber on the thermorheological and viscoelastic properties of asphaltic concrete. The results indicated that mixtures with the higher viscosity asphalt had lower strength at 20 F, but at low (-20 F) temperature the effect was reversed. Also, high asphalt content with rubber yielded the higher strengths, especially at the low temperature. Viscoelastic analysis of the data indicated that the theory of linearity was approximately true.

The report by Haas and Phang is related to low temperature shrinkage cracking of pavements. Laboratory measurements showed that "high cracking frequencies were associated with stiff bituminous surfaces at low temperatures". It is reported that a mixture's tendency toward fracture could be predicted and that this tendency was associated with asphalt source more so than with the "hardness" of the asphalt.

Majidzadeh, Chan, and Ramsamooj use principles from fracture mechanics to predict the fatigue life of a sand-asphalt mixture. Fatigue life is expressed as a function of K_C, a critical stress intensity; a factor (set) giving the rate of crack growth; and C_O, the "initial flaw size." Determination of these factors is discussed, and a comparison between experimental and predicted fatigue life is presented.

The effect of particle shape on the fatigue life of asphaltic concrete is presented by Maupin. In the study, 3 aggregate shapes of "flat and slabby," rounded, and an intermediate form were used in asphaltic concrete beams tested under repeated constant center deflection. The data indicated a significantly shorter fatigue life for the mixture containing the slabby particles than for the gravel mixture. A log-log plot of rupture modulus versus fatigue cycles showed a linear and parallel relationship for all mixtures.

The paper entitled "Time and Load Independent Properties of Bituminous Mixtures" presents a unique analysis toward characterizing "the time dependent behavior of asphaltic concrete" under sinusoidal loading. The authors,

Swami, Goetz, and Harr, state that the characterization is represented by a transfer function that can be obtained from laboratory measurements. The form of the function is presented and broken into components that are believed to be better indicators of material performance than others, such as Young's modulus and Poisson's ratio that are affected by rate of loading. Experimental verification involved testing specimens under alternating axial forces of tension and compression and also static compressive forces. The results showed "excellent agreement between the calculated and measured values of displacement."

Epps, Gallaway, and Scott in their paper "Long Term Compaction of Asphalt Concrete Pavements" describe tests on 15 sites in Texas where field compaction was compared to laboratory compaction. Their study showed that, although 85 percent of the samples showed less than 95 percent initial compaction, after 2 years of traffic all but 2 sites exceeded 95 percent relative compaction. Only 20 percent of the sites reached 100 percent relative compaction.

Contents

Design, Construction, and Initial Evaluation of Experimental Test Sections of Asphalt Containing Synthetic Rubber

MICHAEL I. DARTER, DALE E. PETERSON, and GEORGE M. JONES,
Utah State Department of Highways, and
ROLAND VOKAC, Institute of Synthetic Rubber Producers, Inc.

The 16 test sections of asphalt containing rubber were constructed as part of a primary highway project in southeastern Utah. The experiment consists of 5 factors at 2 levels, each incorporated in a one-half replicate of a 2^5 fractional factorial experiment. The design provides the basis for determining the effect of each of 5 factors and each of 10 two-way interactions on pavement construction, performance, and design. The effect of each variable was determined for the construction process, and an initial evaluation was made. A description of the construction process, including the rubberizing process, is given. Evaluation is continuing through many observations and physical tests on the pavements and paving materials. Failure rate of pavements will be accelerated by the reduction of half the design thickness. The design provides a sound method of analysis and offers a definite basis to determine which factors and interactions are significantly affecting pavement performance and design.

•THIS PAPER DESCRIBES the experimental design, construction, and initial evaluation of test sections of asphalt containing rubber constructed as part of a federal-aid primary highway project. This experiment will provide data to evaluate all of the main effects of 5 factors involved and the first order interactions among them. The laboratory and field tests of the field experimental test sections will be relied on to determine the following:

1. The significant relationships among the performances under actual traffic of regularly designed and constructed specification asphalt pavement when the paving mixture is varied by asphalt content, viscosity, and addition of synthetic rubber;
2. The effect that varying the thickness of surface and base course to half the full design thickness has on the material properties, asphalt content, viscosity, and rubber additive, and also on pavement performance;
3. Whether any interaction of the 5 factors with each other is related to aspects of pavement performance and design;
4. The value of physical tests, such as the dynaflect deflections and asphalt properties, on the performance of the pavements and the significant correlations, if any, among these many tests;
5. Estimates of statistical parameters for the various tests and material properties;
6. The significant trends and results that will be helpful in future highway design and pavement evaluations;
7. The relation of the thermorheological properties of the pavement at various time periods to pavement performance and design; and
8. The significant relationships among the number of equivalent 18-kip axle loads, which were calculated from regular traffic loadings, and the main factors and interactions involved in the experiment.

Paper sponsored by Committee on Mechanical Properties of Bituminous Paving Mixtures.

TABLE 1

FACTORS AFFECTING PAVEMENT PERFORMANCE

Factor	Symbol	Level	Value
Synthetic rubber solids in rubber-asphalt compound	+S	High	3 percent by weight of asphalt
	-S	Low	0 percent
Kinematic viscosity of asphalt	+V	High	85 to 100 penetration grade, 292 centistokes at 275 F, 1,326 stokes at 140 F
	-V	Low	85 to 100 penetration grade, 199 centistokes at 275 F, 719 stokes at 140 F
Rubber-asphalt compound in paving mixture	+C	Rich	1.1 × design percentage or 6.48 percent
	-C	Lean	0.9 × design percentage or 5.24 percent
Thickness of asphaltic surface course	+T	High	1.0 × design or 6 in.
	-T	Low	0.5 × design or 3 in.
Thickness of untreated granular base course	+B	High	1.0 × design or 4 in.
	-B	Low	0.5 × design or 2 in.

EXPERIMENTAL DESIGN

Design

Based on findings of the first phase of a rubber-in-asphalt program of study, 5 factors were selected as representing the minimum number that significantly affect the strength, quality, and performance capability of an asphalt pavement. These are given in Table 1. A designed experiment (3), described as half replicate of a 2^5 factorial, was set up and required only 16 treatments or test sections. The chief advantages of a factorial experiment are that (a) the main effects of each factor may be determined from the response data measured in each test, and (b) the interactions of each factor with another will be disclosed in the analysis of such data. The latter is usually not possible in the traditional way of testing. The experiment of 5 factors in 16 treatment combinations makes it possible to measure all the main effects and the 10 interaction effects of the 5 factors. The 2 levels of each factor are indicated by minus and plus signs for low level and high level respectively. Table 2 gives the levels of the 5 factors present in each of the 16 test sections, the main effects, and the interactions.

The effect of the factor is the change in response produced by a change in the level of a factor; i.e., the effect is the difference between the average response of all tests carried out at the first level of the factor (-) and that of all tests at the second level (+). If the effect of one factor depends on the level of another factor, the two are said to interact. A set of levels of all factors employed in a given test section is a treatment; for example, section 1 comprises a given treatment.

TABLE 2

SUMMARY OF FACTORS AND THEIR LEVELS, EFFECTS, AND INTERACTIONS

Test Section	Treatment	Levels					Main Effects and Interactions
		T	B	S	V	C	
12	1	-	-	-	-	-	I
11	(C)T	+	-	-	-	+	T
10	(C)B	-	+	-	-	+	B
9	TB	+	+	-	-	-	TB
13	(C)S	-	-	+	-	+	S
14	TS	+	-	+	-	-	TS
15	BS	-	+	+	-	-	BS
16	(C)TBS	+	+	+	-	+	-CV
4	(C)V	-	-	-	+	+	V
3	TV	+	-	-	+	-	TV
2	BV	-	+	-	+	-	BV
1	(C)TBV	+	+	-	+	+	-CS
5	SV	-	-	+	+	-	SV
6	(C)TSV	+	-	+	+	+	-CB
7	(C)BSV	-	+	+	+	+	-CT
8	TBSV	+	+	+	+	-	-C

Project Layout

A typical cross section of the roadway is shown in Figure 1. The test sections are 150 ft in length with transitions between groups of four. This was for the convenience of construction only. The center 100 ft of each test section was used as the official section to avoid any end effects. From the data given in Table 2, the components of all 16 test sections can be determined.

The full and experimental pavement design was as follows:

Item	Full (in.)	Experimental (in.)
Bituminous surface (T)	6	3
Untreated base (B)	4	2
Total	10	5

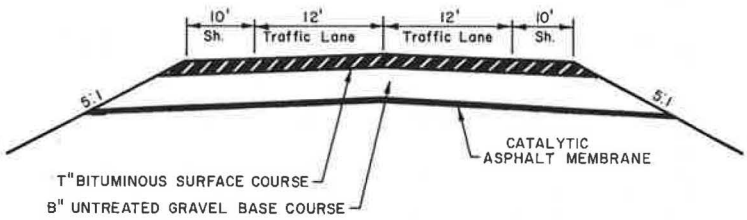

Figure 1. Typical cross section of roadway.

CONSTRUCTION AND MATERIALS

The test sections were constructed on a 7-mile project of which the test sections comprised about 4,000 ft. Construction was started in March 1968 and completed in August 1968. The test sections were constructed in phase with the rest of the project.

The sequence of construction was as follows: The natural ground was cleared and compacted. The subgrade was placed and compacted in layers. A summary of the physical characteristics of the subgrade are given in Table 3. An MC-70 prime coat was sprayed on the subgrade after final compaction in preparation for the catalytically blown asphalt membrane (penetration 50 to 60) that was then sprayed on the subgrade. The base gravel course was then placed to required thickness, compacted, and sprayed with MC-70 prime coat. A summary of the physical characteristics of the base gravel is given in Table 4.

Construction of the asphaltic concrete surface demanded a great deal of planning and careful procedures. Construction involved 8 different mixture combinations in 2 thicknesses for 16 different roadway sections each 150 ft long.

Asphalt Properties

During construction of each test section the asphalt in the storage tank was

TABLE 3

PHYSICAL CHARACTERISTICS OF SUBGRADE MATERIAL

Characteristic	Amount by AASHO Soil Classification	
	A-6	A-4
Plasticity index	13	5
Liquid limit	32	21
Percentage passing No. 200 sieve	59	62
Dry density (AASHO T-99D), lb/cu ft	112.2	121.6
Optimum moisture (AASHO T-99D), percent	16.0	11.5
R-value at 300 psi exudation pressure, psi	—	22.0

TABLE 4

PHYSICAL CHARACTERISTICS OF BASE GRAVEL MATERIAL

Characteristic	Amount
Absorption (AASHO T-84 and T-85), percent	1.7
Abrasion L. A. machine (AASHO T-96), percent	27.1
Fractured face count (USDH 8-929)[a], percent	62.0
Soundness (AASHO T-104), percent	
-4 material	5.47
+4 material	11.78
Specific gravity (AASHO T-84 and T-85)	
-4 material	2.43
+4 material	2.63
Liquid limit (AASHO T-89)	10
Plasticity index (AASHO T-90)	N. P.
Laboratory (AASHO T-180-61)	
moisture, percent	6.8
density, lb/cu ft	134.7

[a]Utah State Department of Highways standard test.

TABLE 5

PROPERTIES OF ORIGINAL ASPHALT TAKEN FROM STORAGE TANK AND ASPHALT RECOVERED FROM PAVEMENT MIXTURES

Mixture	Kinematic Viscosity at 140 F (stokes)	Kinematic Viscosity at 275 F (stokes)	Cannon-Cone Viscosity at 77 F (kilopoises)	Penetration at 77 F	Specific Gravity at 77 F
+V					
Original	1,326	2.92	619	103	1.031
Recovered	1,611	2.98	562	84	1.030
+V+S					
Original	2,422	12.94	348	92	1.020
Recovered	5,799	9.80	829	64	1.032
-V					
Original	691	1.99	735	95	1.013
Recovered	1,039	2.63	571	103	1.014
-V+S					
Original	1,615	7.19	497	82	1.009
Recovered	3,876	7.28	1,025	74	1.015

sampled. Samples of uncompacted mix were also taken from behind the paver during laydown. These samples were compacted and tested in the laboratory for rice density, stability, flow, density, voids, and the like. The properties of the asphalt cements used are given in Table 5.

Mix Design

The best combination of asphalt and aggregates was determined by the Marshall method, which is used for all mix designs in Utah. A complete mix design was made

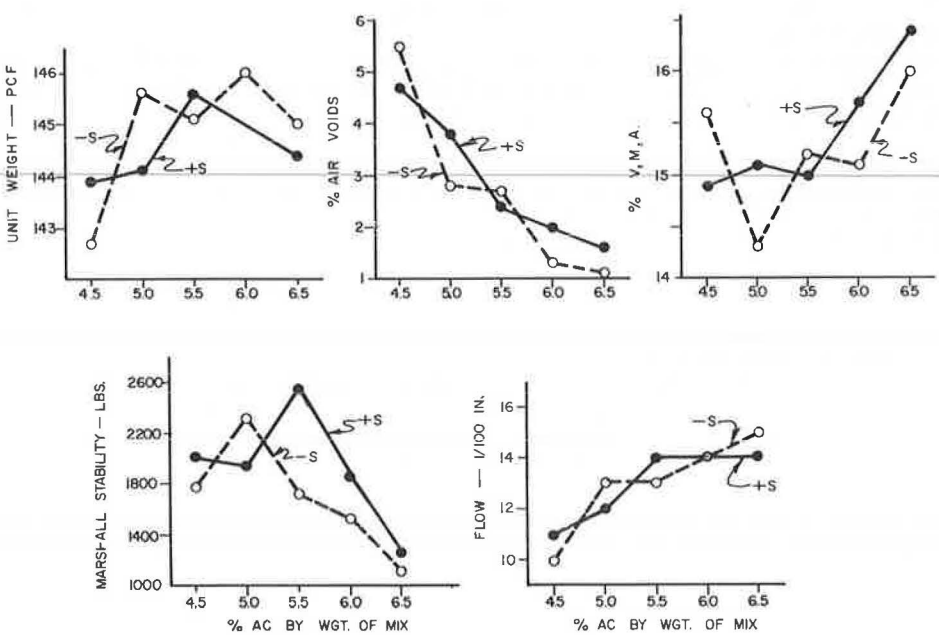

Figure 2. Marshall design for low-viscosity asphalt with and without rubber solids.

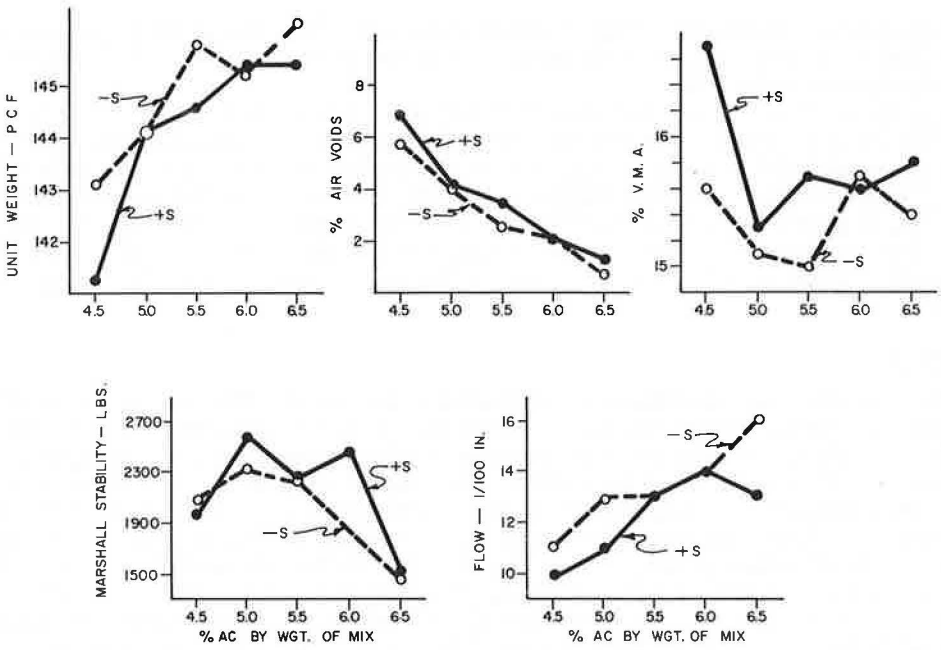

Figure 3. Marshall design for high-viscosity asphalt with and without rubber solids.

for each of the 4 combinations of rubber and asphalt. The resulting graphs are shown in Figures 2 and 3. The optimum asphalt contents are as follows:

Mixture	Percent Asphalt
-V-S	5.3
-V+S	5.5
+V-S	5.7
+V+S	6.0
Avg.	5.6

The average of these 4 values, 5.6 percent, was then multiplied by 1.1 and 0.9 to give the high and low levels of asphalt content.

Rich mixtures = 6.2 percent, actual obtained = 6.48 percent
Lean mixtures = 5.0 percent, actual obtained = 5.24 percent

The mix design involves a factorial design with 5 levels of asphalt content (C), 2 levels of viscosity (V), and 2 levels of rubber solids (S). The factors that significantly affected the mix design are as follows:

Stability—Rubber solids, viscosity, and asphalt content all had significant (0.1 percent level) effects on the resulting stability. High-viscosity mixtures showed increased stability (295 lb) over low-viscosity mixtures. The average effect of rubber solids was to increase stability 171 lb and to increase the maximum optimum asphalt content of the mix about 0.5 percent greater than the content of the -S mixtures with about the same stability.

Flow—Rubber solids and asphalt content had a significant (0.1 percent level) effect on the flow. The flow of the +S mixture shows a marked leveling off at 5.5 percent

asphalt content and greater. The -S mixes show increased flow in the usual manner. The effect of S was to decrease the mean flow of the mixture of 3 in. x 10^{-2} less than that of mixtures without S.

Density—Asphalt content (0.1 percent level) and rubber solids (5 percent level) were the main factors significantly affecting the bulk density of the Marshall specimens. The +S mixtures showed an average density of 0.3 lb/cu ft less than that of the -S mixtures.

Air Voids—Asphalt content (0.1 percent level), rubber solids (1.0 percent level), and viscosity (5 percent level) all significantly affected the air voids content. The +S mixes showed an average void content of 0.6 percent greater than that of the -S mixes. The +V mixes showed an average void content of 0.5 percent greater than that of the -V mixes.

Hot Plant

The hot plant was a continuous-flow Barber Green plant. The rate of aggregates, asphalt, and rubber solids was calibrated so that proper combinations of mixtures would be obtained. A procedure for addition of rubber latex to the mix was suggested by Goodyear Tire and Rubber Company and is shown in Figure 4. The rubber latex flow was controlled by a calibrated slot weir. This procedure required an extra man to operate. Rubber was added to the pugmill directly behind the asphalt spray bar as shown. The procedure produced good dispersion of rubber throughout the mix. The rubber latex was placed in a 500-gal tank. The tank was pressurized to force the latex to the top of the pugmill. The synthetic rubber, obtained from Goodyear, is called Pliopave Latex, type L 170, and containes 70 percent solids and 30 percent water.

Field Construction

The surface course was compacted with a 9-ton, steel-wheel roller. Compaction was monitored with a Seaman nuclear density gage. Density growth curves were obtained for each of the 8 basic combinations of asphalt and rubber materials. Typical curves are shown in Figures 5 and 6 for the low-viscosity asphalt with and without rubber solids and for successive roller passes. The corresponding viscosity of the asphalt is shown below the density growth curve. The viscosity was determined at 140 and 275 F for samples of asphalt recovered from uncompacted mixes that were taken from the roadway just after the paver-pass for each test section. The viscosity at 140 and 275 F were then plotted on standard ASTM temperature-viscosity paper. The viscosity at the temperature of each roller pass was determined and plotted on the graphs in Figures 5 and 6.

The +S mixtures were laid at a much higher temperature than the -S mixtures (47 F higher). The roller was able to roll the pavement at this hotter temperature with no "pick up." Viscosities of the 4 different mixture combinations were averaged and are given in Table 6. There appears to be no significant difference in viscosity among the mixtures at initial laying and up to 30 min after the paver-pass.

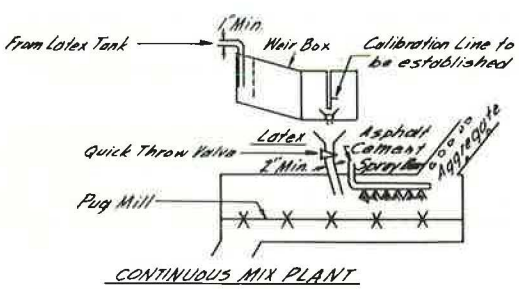

Figure 4. Rubberizing process for the continuous mix plant.

Utah highway department specifications for this project state that required density should be obtained before the viscosity reaches 5,000 centistokes (cs) as determined from the viscosity tests on the original asphalt. Figures 5 and 6 show that very little additional compaction is obtained 30 min after laydown. The corresponding minimum temperature at the 5,000-cs limit is given in the last row in Table 6. This temperature was determined from tests on the original asphalt. The 5,000-cs limiting viscosity appears to be a reasonable limit because little additional density is obtained after this limit is reached.

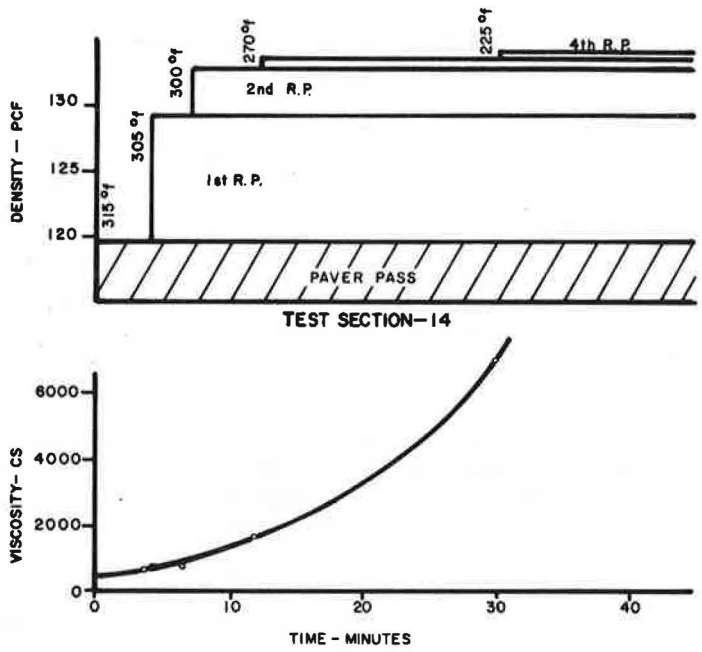

Figure 5. Density growth-viscosity for low-viscosity asphalt with rubber solids.

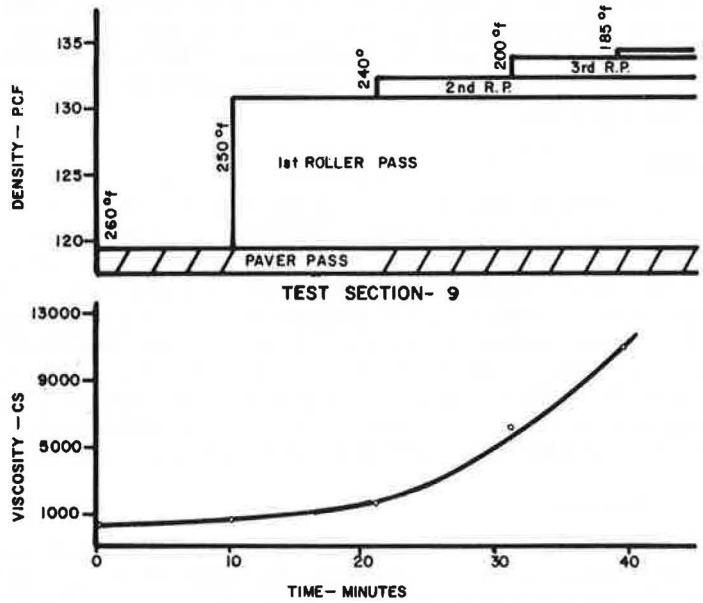

Figure 6. Density growth-viscosity for low-viscosity asphalt without rubber solids.

TABLE 6

AVERAGE VISCOSITIES OF RUBBER-ASPHALT COMPOUND MIXTURES DURING COMPACTION ON TEST SECTIONS 5, 6, 7, AND 8

Item	Mixture			
	+V+S	+V-S	-V+S	-V-S
Paver-pass	900 at 302	1,050 at 257	850 at 295	950 at 250
Time since paver-pass				
10 min	1,450 at 283	1,550 at 246	1,900 at 264	1,200 at 242
20 min	3,750 at 250	2,900 at 231	4,100 at 240	3,250 at 212
30 min	7,000 at 231	7,500 at 210	8,000 at 220	7,000 at 195
Minimum viscosity	5,000 at 230	5,000 at 193	5,000 at 212	5,000 at 183

Note: All amounts in centistokes at deg F.

The asphalt cement was held at a constant temperature, and the temperature of the aggregate was changed when rubber was added to the mixture. To rubberize an entire project would require the temperatures of both asphalt and aggregate be increased to levels required to obtain proper compaction viscosities.

INITIAL EVALUATION

An initial evaluation of several important items relating to the subgrade, base gravel course, and asphaltic concrete surface was made.

Subgrade

An analysis of the final dry densities obtained by the depth probe was made. The densities were highly variable ranging from 80 to 140 lb/cu ft. The results show that (a) the average subgrade densities are significantly different for the different test sections, and (b) there is no significant difference among densities at 1, 2, and 3 ft below the surface. Further analysis showed that certain test sections to be overlaid with certain combinations of T, B, S, V, and C have different densities. The most significant differences were between the sections to be overlaid with +S and -S mixes. Subgrade density for the +S sections was 122 lb/cu ft and for the -S test sections, 107 lb/cu ft. The BV and TC interactions also showed significance. This nonuniformity in subgrade density will undoubtedly have a considerable effect on future performance and must be considered in future analysis.

Base Gravel Course

An analysis of the resulting densities was made. Thickness level of the base course was somewhat significant (5 percent level) in affecting the density. The thickness of the +B sections had an average density of 3.7 lb/cu ft greater than that of the -B sections. V also showed some significance (5 percent level), indicating about a 3.0-lb/cu ft difference in base course density of those sections to be overlaid with high- and low-viscosity asphalt. The thickness of the base course was measured at random places in each section. B is the only factor that showed any significance. The average thickness is +B = 4.05 in. and -B = 2.22 in. Samples from both lanes show no significant difference in thickness, and the ends and centers of the sections are equally representative of thickness. Average gradations, given in Table 7, are within the specification limits.

Asphaltic Concrete Surface

Density—The final compaction of the test sections was determined from cores cut out of the pavement 2 weeks after construction. The analysis of variance is given in Table 8. The results show S and C are highly significant (at the 0.1 percent level) in affecting the final density of the pavements. The mean effect, which is the average difference of density among the different levels of the factors, of S and C along with the

TABLE 7

AVERAGE GRADATION OF BASE GRAVEL COURSE AND ASPHALTIC CONCRETE SURFACE

Sieve	Base Gravel Course		Asphaltic Concrete Surface		
	Specification	Percent Passing (n = 4)	Specification	Mix Design	Percent Passing (n = 24)
3/4 in.	100	100.0	100	100	100.0
3/8 in.	69 to 100	83.0	71 to 100	82	82.6
No. 4	46 to 75	63.8	51 to 76	60	64.4
No. 8			37 to 57	50	49.9
No. 16	22 to 49	39.8	26 to 42	41	39.1
No. 50	10 to 28	23.3	13 to 24	23	22.1
No. 200	4 to 13	9.8	6 to 13	10	7.7

average of the experiment can be used to obtain the average density at each level of S and C.

$$+C = 138.2 + (4.7/2) = 140.6 \text{ lb/cu ft}$$
$$-C = 138.2 - (4.7/2) = 135.8 \text{ lb/cu ft}$$
$$+S = 138.2 + (-1.8/2) = 137.3 \text{ lb/cu ft}$$
$$-S = 138.2 - (-1.8/2) = 139.1 \text{ lb/cu ft}$$

The other variance tables can be interpreted in the same way. The +C pavements are on the average 4.7 lb/cu ft denser than the -C pavements. This result is to be expected within limits. The reason that the +S mixtures are less dense than the -S is not so apparent because the viscosities at time of compaction are the same for the +S and -S mixtures. The +S mixtures perhaps are stiffer because of the strands of rubber present. The Marshall briquettes also showed this result. The resulting average pavement density is 96 percent of the average laboratory briquette density.

Asphalt Content—Asphalt content was determined by vacuum extraction of the uncompacted mixture and on core samples taken after compaction. Results of percentage of

TABLE 8

DENSITY OF INITIAL PAVEMENT CORES

Source of Variation	Degrees of Freedom	Mean Effect x 10^{-3} (lb/cu ft)	Mean Square x 10^{-5}	Comments
Main effects				
T	1	-0.1	0.0	
B	1	0.3	0.5	
S	1	-1.8	12.4	Significant at 0.1 percent level
V	1	0.3	0.4	
C	1	4.7	89.8	Significant at 0.1 percent level
Interactions				
TB	1	-0.3	0.4	
TS	1	-0.2	0.1	
BS	1	0.2	0.2	
CV	1	-0.1	0.0	
TV	1	-0.1	0.0	= 2.1, error = 0.2, df = 10
BV	1	-0.2	0.1	
CS	1	-0.1	0.0	
SV	1	-0.3	0.3	
BC	1	-0.4	0.5	
TC	1	-0.3	0.3	
Treatments	(15)		1,570.0	Significant at 0.1 percent level
Replications	2		22.0	Significant at 0.1 percent level
Lifts	1		0.0	
Lanes	1		6.0	
Error	124		1.5	
Total	143			

Additional factors: n = 144, $\bar{X}$ = 138.3 lb/cu ft.

asphalt extracted from several replicate samples from each section show the level of C is highly significant (0.1 percent level) in affecting the content in the pavements. This is the expected result with the mean effect being +1.24 percent. The +C = 6.48 percent and -C = 5.24 percent.

Gradation—The gradations of all uncompacted and core samples were determined. The averages, given in Table 7, are within specification limits.

Thickness—The thickness of each core cut from the pavement was determined. The mean effect of T was +2.7 in. The +T pavements averaged 5.7 in. and the -T pavements averaged 3.0 in. The results also show that there is no significant difference in thickness of surface due to the lanes samples, the replications within lanes, or any other factor in the 16 sections except T.

Air Voids—Air voids were determined for cores cut from the pavements. An analysis of variance was made on the resulting air voids and is given in Table 9. The results show that the level of C highly affects air voids. The mean effect is -5.4 percent. Average voids are +C = 4.4 percent and -C = 9.8 percent. The level of S significantly affected the air voids, the mean effect being 1.2 percent. This agrees directly with the resulting densities of the +S and -S sections; the +S show less density than the -S pavements.

Stability—Stability of the Marshall briquettes, which were compacted out of uncompacted mixture, was determined, and the results of the analysis are given in Table 10. Rubber solids and asphalt content were both highly significant in affecting stability. The rubberized mixture had a stability 385 lb greater than that of the nonrubberized mixture. The mixture containing high-asphalt content had a stability 486 lb less than that of the low-asphalt content mixture. The stability of cores cut from the pavements was determined, and the results are given in Table 11 and summarized as follows:

1. The effect of asphalt content is highly significant. The cores have open cut surfaces on the sides allowing considerable water to penetrate. +C specimens had a stability 238 lb greater than that of -C specimens because of the absorption of water into the core specimens. When the pavements are soaked this same phenomenon may take place.
2. V also shows some significance. The +V mixtures indicate an average stability 95 lb greater than that of the -V mixtures.

TABLE 9

AIR VOIDS IN INITIAL PAVEMENT CORES

Source of Variation	Degrees of Freedom	Mean Effect (percent)	Mean Square	Comments
Main effects				
T	1	0.33	0.42	
B	1	0.13	0.06	
S	1	1.15	5.29	Significant at 1 percent level
V	1	-0.20	0.16	
C	1	-5.38	115.56	Significant at 0.1 percent level
Interactions				
TB	1	-0.08	0.02	= 3.03, error = 0.303, df = 10
TS	1	0.25	0.25	
BS	1	-0.35	0.49	
CV	1	-0.10	0.04	
TV	1	0.50	0.01	
BV	1	-0.35	0.49	
CS	1	-0.15	0.09	
SV	1	0.43	0.72	
BC	1	0.48	0.90	
TC	1	0.08	0.02	
Treatments	(15)		74.25	Significant at 0.1 percent level
Replications	2		6.95	Significant at 0.1 percent level
Lifts	1		0.95	
Lanes	1		1.82	
Error	124		0.59	
Total	143			

Additional factors: n = 144, $\bar{X}$ = 7.1 percent.

TABLE 10

STABILITY OF UNCOMPACTED MIXTURE COMPACTED IN THE FIELD LABORATORY

Source of Variation	Degrees of Freedom	Mean Effect (lb)	Mean Square	Comments
Main effects				
T	1	40	6,320	
B	1	-10	400	
S	1	385	592,130	Significant at 0.1 percent level
V	1	100	39,601	
C	1	-486	946,729	Significant at 0.1 percent level
Interactions				
TB	1	113	51,302	
TS	1	-32	4,096	
BS	1	-42	7,140	
CV	1	116	53,361	
TV	1	53	11,130	
BV	1	8	289	= 132,668, error = 13,267, df = 10
CS	1	35	4,830	
SV	1	-9	306	
BC	1	-1	4	
TC	1	-7	210	
Treatments	(15)		514,798	Significant at 0.1 percent level
Replications	2		1,648	
Lifts, top and bottom			21,559	
Error	53		22,206	
Total	71			

Additional factors: n = 72, $\bar{X}$ = 1,707 lb.

3. S did not significantly influence the stability of the cores as it did the Marshall briquettes.

Asphalt Properties—Kinematic viscosity measurements were made on the original storage-tank asphalt. The samples representing the test sections containing rubber were rubberized in the laboratory. Viscosity of asphalt and rubber solids both highly affect the resulting viscosity of the original asphalt. Viscosity tests were also performed on the recovered asphalt from the uncompacted mixture samples, and Table 12

TABLE 11

STABILITY OF INITIAL PAVEMENT CORES

Source of Variation	Degrees of Freedom	Mean Effect (lb)	Mean Square	Comments
Main effects				
T	1	-17	2,211	
B	1	4	98	
S	1	-24	4,465	
V	1	95	71,631	Significant at 5 percent level
C	1	238	451,725	Significant at 0.1 percent level
Interactions				
TB	1	-28	6,441	
TS	1	-12	1,152	
BS	1	19	2,775	
CV	1	46	17,298	
TV	1	30	7,442	
BV	1	30	7,021	= 112,861, error = 11,286, df = 10
CS	1	-44	15,842	
SV	1	82	54,120	
BC	1	-8	528	
TC	1	5	242	
Treatments	(15)		42,866	Significant at 0.1 percent level
Lanes	1		66,795	Significant at 5 percent level
Error	15		11,890	
Total	31			

Additional factors: n = 32, $\bar{X}$ = 435 lb.

TABLE 12

KINEMATIC VISCOSITY AT 140 F OF ASPHALT RECOVERED FROM UNCOMPACTED MIXTURE

Source of Variation	Degrees of Freedom	Mean Effect (stokes)	Mean Square	Comments
Main effects				
T	1	-286	655,226	
B	1	-268	655,226	
S	1	3,508	98,445,009	Significant at 0.1 percent level
V	1	1,243	12,354,177	Significant at 1 percent level
C	1	-100	80,300	
Interactions				
TB	1	-457	1,673,077	= 9,493,316, error = 949,332, df = 10
TS	1	-347	965,008	
BS	1	-300	718,500	
CV	1	428	1,463,332	
TV	1	124	122,884	
BV	1	284	645,532	
CS	1	-36	10,117	
SV	1	671	3,597,232	
BC	1	-95	72,676	
TC	1	-168	224,958	
Treatments	(15)		8,106,787	Significant at 0.1 percent level
Replications	1		4,255	Significant at 1 percent level
Error	15		454	
Total	31			

Additional factors: n = 32, $\bar{X}$ = 3,079 stokes.

gives the results. The V and S are highly significant. The rubber produced an average increase in kinematic viscosity at 140 F of 3,508 stokes.

The results of the analysis of penetration of recovered asphalt are given in Table 13. Rubber solids produced a decrease of 11 points penetration in the original asphalt and 24 points in the recovered asphalt. The high-viscosity asphalt originally showed an average of 7 points higher but after mixing and recovery showed about 15 points lower than the low-viscosity asphalt.

TABLE 13

PENETRATION AT 77 F OF ASPHALT RECOVERED FROM UNCOMPACTED MIXTURE

Source of Variation	Degrees of Freedom	Mean Effect (points)	Mean Square	Comments
Main effects				
T	1	-6.9	385.03	
B	1	7.2	413.28	
S	1	-24.3	4,728.78	Significant at 0.1 percent level
V	1	-14.6	1,696.53	Significant at 1 percent level
C	1	3.4	94.53	
Interactions				
TB	1	5.8	270.28	= 1,189.55, error = 118.96, df = 10
TS	1	3.3	87.78	
BS	1	0.7	3.78	
CV	1	-3.1	75.03	
TV	1	1.8	26.28	
BV	1	0.1	0.03	
CS	1	6.4	331.53	
SV	1	4.7	175.78	
BC	1	0.7	3.78	
TC	1	-5.2	215.28	
Treatments	(15)		567.18	Significant at 0.1 percent level
Replications	1		7.06	Significant at 0.1 percent level
Error	15		0.90	
Total	31			

Additional factors: n = 32, $\bar{X}$ = 82 points.

Low-temperature ductility (39.2 F) was measured on the original and recovered asphalt. The results of the analysis are given in Table 14. Rubber solids significantly affect the low-temperature ductility. Average results for the original and recovered asphalt are as follows:

Original	Recovered
+S = 57 + 52/2 = 83 cm	+S = 27 + 33/2 = 43 cm
-S = 57 - 52/2 = 31 cm	-S = 21 - 33/2 = 11 cm

Viscosity showed a high significance in low-temperature ductility before mixing (V = 89 cm); the high-viscosity asphalt averaged 89 cm higher than the low-viscosity asphalt. However, after mixing and recovery there was no significant difference between the 2 asphalts.

Deflection Analysis—Deflection basins were determined by means of a Dynaflect, which has been described in other publications (2, 4, 5). Deflection measurements were taken on the natural ground, subgrade, base course, and surface course.

Ten repetitions were obtained on the natural ground. The magnitude of the basin for each layer is shown in Figure 7. The maximum deflection shows a definite weakness in surface of the natural ground due to lack of compaction.

Deflections were made in each test section after it was completely constructed and compacted. The height of the subgrade was approximately 3 ft above the natural ground. If the subgrade was constructed uniformly, deflection among test sections would not significantly differ. An analysis of variance was made by using the maximum deflection (sensor 1) for subgrade deflections. There was significant difference in deflection among test sections. Further analysis showed that the test sections to be overlaid with asphaltic concrete containing 3 percent rubber solids have significantly less deflection than those to be overlaid with asphaltic concrete without rubber solids. This effect will be taken into account in further analysis. None of the other factors is affected by the nonuniform subgrade deflections.

The deflection results correlate well with densities obtained on the subgrade: least squares regression $Y = 3.13 - 0.02X$, where Y = Dynaflect maximum deflection $\times 10^{-3}$ in. and X = dry density determined by depth probe in lb/cu ft; standard error of the

TABLE 14

DUCTILITY AT 39.2 F OF ASPHALT RECOVERED FROM UNCOMPACTED MIXTURE

Source of Variation	Degrees of Freedom	Mean Effect (cm)	Mean Square	Comments
Main effects				
T	1	16.6	2,192.87	Significant at 5 percent level
B	1	-4.6	172.05	
S	1	33.1	8,761.57	Significant at 0.1 percent level
V	1	0.9	6.94	
C	1	4.0	152.69	
Interactions				
TB	1	5.1	207.57	Significant at 5 percent level = 2,709.61, error = 271.0, df = 10
TS	1	15.0	1,807.51	
BS	1	-6.0	291.01	
CV	1	-2.5	49.75	
TV	1	2.1	34.24	
BV	1	-1.9	28.13	
CS	1	5.2	217.88	
SV	1	-0.6	2.82	
BC	1	0.2	0.20	
TC	1	3.0	70.51	
Treatments	(15)		933.00	Significant at 0.1 percent level
Replications	1		130.00	
Error	15		115.80	
Total	31			

Additional factors: n = 32, $\bar{X}$ = 27.3 cm.

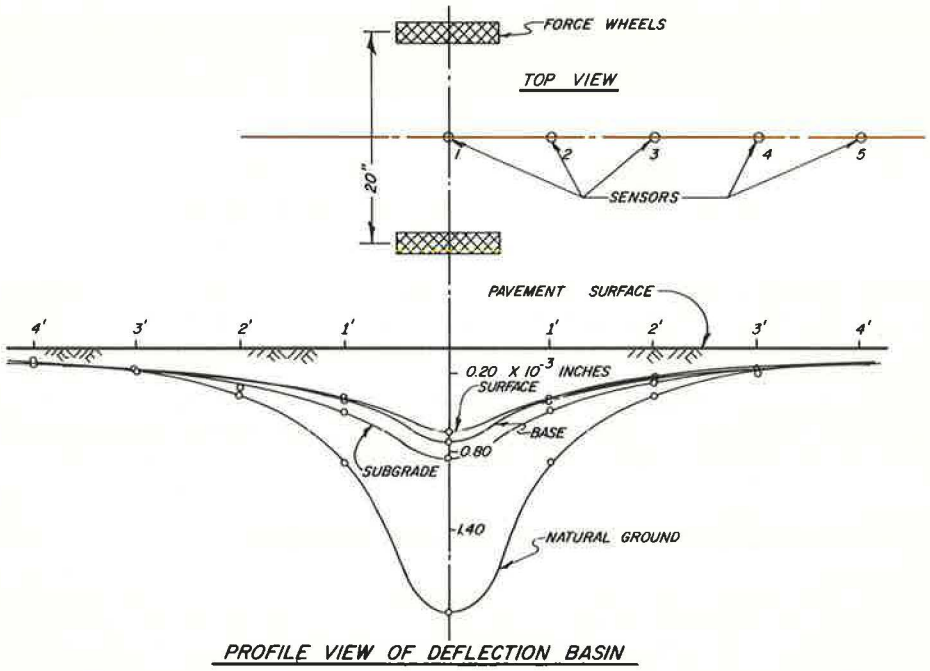

Figure 7. Average pavement deflection for various layers.

estimate $S_{y.x}$ = 0.45; and coefficient of correlation = 0.90. The greater the dry density of the subgrade, the less is the deflection. This is in line with theory. These differences in subgrade densities and deflections may significantly affect overall results obtained from the test sections and must be considered in future analysis.

The base gravel course was laid in 2 thicknesses: 2 and 4 in. Deflection readings were taken on the base course just before the asphaltic concrete surface was laid. An analysis of variance was then run on the deflection results. The only highly significant factor affecting deflection is the thickness of base course, which is the expected result.

Maximum deflections on the surface course are given in Table 15. The thickness of surface is highly significant in affecting deflections. The deflection basins of +T and -T surfaces are shown in Figure 8. The sections with 6-in. surfaces show significantly less deflection (25 percent) than sections with 3-in. surfaces. The effect of B also shows that the 4-in. base sections deflect 8 percent less than the 2-in. base sections. A correlation of the Dynaflect and Benkelman beam deflections has been made. The approximate beam deflection may be determined as follows: Benkelman beam deflection (in.) = 25 x Dynaflect maximum deflection x 10^{-3}. Therefore, the average (1-month period) is as follows:

+T = 0.652 x 10^{-3} - 0.188 x 10^{-3}/2 x 25 = 0.014 in. (Benkelman beam deflection)
-T = 0.019 in. (Benkelman beam deflection)

EVALUATION PROGRAM

The experiment is scheduled to extend 2 years after construction. Some failures of the pavements are expected within this period. If the design thickness is cut in half on certain sections, the failure rate is expected to accelerate. There are 7 time periods when extensive testing will be performed following construction: 2 weeks (initial), 3 months, 6 months, 9 months, 12 months, 18 months, and 24 months. At each of these periods, the tests and measurements will include the following: roughness, density,

TABLE 15

MAXIMUM DEFLECTION (ADJUSTED) ON ASPHALTIC CONCRETE SURFACE 1 MONTH AFTER CONSTRUCTION

Source of Variation	Degrees of Freedom	Mean Effect x 10^{-3} (in.)	Mean Square	Comments
Main effects				
T	1	-0.188	1.693	Significant at 0.1 percent level
B	1	-0.053	0.136	Significant at 5 percent level
S	1	0.019	0.017	
V	1	-0.912	0.006	
C	1	-0.026	0.031	
Interactions				
TB	1	0.020	0.020	
TS	1	-0.029	0.039	
BS	1	0.004	0.001	
CV	1	0.020	0.019	
TV	1	0.034	0.054	
BV	1	-0.024	0.027	= 0.194, error = 0.019, df = 10
CS	1	0.004	0.001	
SV	1	-0.025	0.030	
BC	1	0.008	0.003	
TC	1	0.002	0	
Treatments	(15)		0.138	Significant at 0.1 percent level
Lanes	1		1.005	Significant at 0.1 percent level
Centerline distance	1		0.145	Significant at 0.1 percent level
Position	2		0	
Error	172		0.005	
Total	191			

Additional factors: n = 192, $\bar{X}$ = 0.652 in. x 10^{-3}.

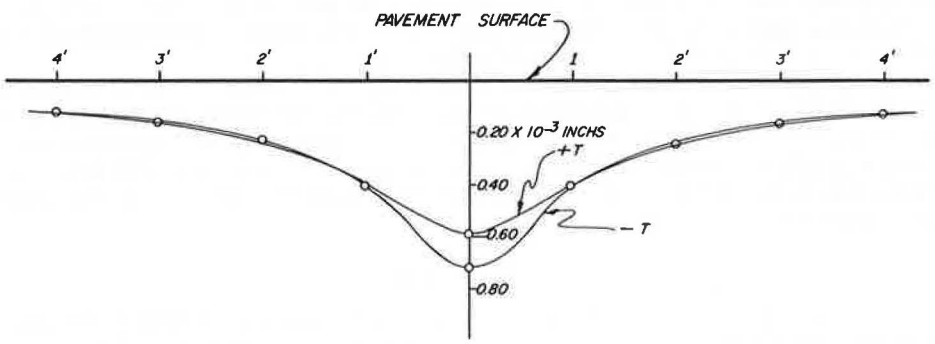

Figure 8. Average pavement deflection for surface course.

asphalt properties, stability of cores, deflection of pavement, thermorheologic properties, condition, visual observations, and skid resistance. Time trends of all these variables will be reported as they develop. An attempt will also be made to characterize the material properties of the 3 layers of the pavement. Through a comparison of the expected deflections and actual deflections, suitable design procedures will be developed.

CONCLUSIONS

Factor T had a highly significant effect on the magnitude of deflection. Pavements 5.7 in. thick had 25 percent less deflection than those 3 in. thick. The required pavement thicknesses were obtained as the analysis showed T as the only significant factor with +T = 5.7 in. and -T = 3 in.

The level of factor B had a significant effect on pavement deflections. The pavements underlaid with 4 in. of gravel base deflected 8 percent less than those underlaid with 2.2 in. of gravel base.

The proper thickness of B was achieved. The thick bases averaged 4.0 in., and the thin bases averaged 2.2 in.

The +S mixtures produced slightly denser pavements (1.8 lb/cu ft), greater air voids (1.2 percent), lower penetration (24 points), greater viscosities (3,508 stokes at 140 F), and greater ductilities (33 cm at 39.2 F) as determined from asphalt properties recovered from the mixtures. The mix design indicated that +S mixtures could take a greater asphalt content (up to ½ percent) without decreasing the stability or increasing the flow. The Marshall briquettes showed that rubber increased the stability by 385 lb.

V had a significant effect on the stability of the mix briquettes. The high-viscosity samples averaged 295 lb greater than the low-viscosity samples. The +V mixtures also had a stability 95 lb greater than that of the -V mixtures. V showed a highly significant effect on the viscosities measured on the asphalt samples taken from the storage tank and recovered from mix samples.

The +C mixtures showed a greater pavement density (4.6 lb/cu ft), less air voids (5.3 percent), and greater stability of cores (238 lb). The rich pavements averaged 6.48 percent, and the lean pavements averaged 5.24 percent asphalt.

The construction of the base course and surface course appears to have met specifications and the experimental design in every case. The resulting material variation also seems reasonable.

The construction of the subgrade shows a wide range of densities and soil properties. This may affect the results obtained from the experiment and must be considered in the future. Deflections on the surface course still reflect the nonuniformity of the subgrade. A good relationship was established between density of the subgrade and Dynaflect deflections.

The procedure for adding rubber latex directly to the continuous mix pugmill has given good dispersion of rubber solids throughout the pavement. There were no additional problems encountered in construction. The rubberized pavements were compacted about 50 F hotter than the nonrubberized pavements.

The test sections provide good sources for sampling and testing to determine the effects of the factors and any interactions between them. The test sections are also good sources from which to obtain valuable data related to pavement performance and design. The design provides a sound method of analysis and one that offers a definite basis to determine which factors and interactions are significant in affecting pavement performance and design.

ACKNOWLEDGMENT

This research project is administered by the Utah State Department of Highways in cooperation with the Bureau of Public Roads, Federal Highway Administration, U.S. Department of Transportation, and the International Institute of Synthetic Rubber Producers, Inc. The authors express appreciation and thanks to the Institute for considerable preliminary work that resulted in the experimental design and for continuing technical support and to the Utah highway department personnel including G. M. Tuckett, W. R. Delis, C. C. Sy, W. B. Betenson, M. L. Wiley, C. Briggs, G. Peterson, D. J. Black, and the drafting and secretarial staff of the Materials and Tests Division.

REFERENCES

1. Fisher, Ronald A. The Design of Experiments. Hafner Publishing Co., New York, 1966.
2. Pace, G. M. Evaluation of the Dynaflect for the Non-Destructive Testing of Portland Cement Concrete Pavements. Ohio River Division Laboratories, Corps of Engineers, U.S. Dept. of the Army, Aug. 1967.
3. Snedecor, G. W., and Cochran, W. G. Statistical Methods. Iowa State Univ. Press, Ames, 6th ed., 1967.

4. Swift, G. Dynaflect: Theory and Practice. Lane-Wells Highway Products, Technical memorandum, Nov. 1, 1965.
5. Zube, E., Forsyth, R. A., and Tueller, D. O. Evaluation of the Lane-Wells Dynaflect. Materials and Research Dept., California Div. of Highways, Oct. 1968.

Initial Evaluation of the Effect of Synthetic Rubber Additives on the Thermorheological Properties of Asphalt Mixtures

J. E. FITZGERALD and JAMES S. LAI, Civil Engineering Department, College of Engineering, University of Utah

This paper presents the results of the initial investigation of linear viscoelasticity property and the other related mechanical properties of 8 different kinds of asphalt mixtures (6.1 percent and 5.0 percent asphalt content by weight, high and low viscosity, with and without added rubber). At 70 F the viscosity shows the most significant effect where mixtures with low-viscosity asphalt (as measured at 77 F) yield high creep compliance, low ultimate compressive strength, and low ultimate tensile strength. Mixtures with high-asphalt content yield modulus, high creep compliance for the high viscosity mixtures. At 20 F, asphalt content and high viscosity contribute to the high ultimate compressive strength and high ultimate strain. Also, at 20 F, high viscosity and viscosity-asphalt content interaction contribute to the high creep compliance. The findings also indicate that the assumption of linear viscoelastic behavior of the asphalt mixtures is approximately held. Rubber additives do not show significant effect on creep compliances, ultimate compressive strengths and strains, and tensile strengths of the asphalt mixtures at the initial period.

•IN RECENT YEARS substantial data were obtained (1, 2, 3) suggesting that stress-strain relationships of asphalt mixtures used in flexible pavements are time dependent under service loads. This led to the development of the linear viscoelastic analysis of flexible pavement systems (4, 5). Before such analytic work can be applied to the design of a flexible pavement system, we must understand and establish the constitutive relationships of the various materials comprising the pavement.

Obviously, the property of the mixtures is dependent on their composition, temperature, loading, loading rate, moisture, density, and time. Therefore, a complete constitutive equation is still far from a reality. At the present time the most that can be hoped for, from the practical point of view, is equations that relate the time-dependent strain to the applied stress and temperature of each kind of material (the variables, such as the composition, moisture, and density, will be treated as implicit parameters).

Pagen and Khosla (6) observed that both the modulus of elasticity and the unconfined compressive strength of asphalt mixtures at 77 and 104 F decrease with an increase in the percentage of asphalt. Heukelom (7) observed that the strength of asphalt concrete increases with the stiffness of the asphalt binder. Recently, Riley (8) also showed that the strength of the composite increases with the strength of matrix. Another interesting, but not unexpected, result predicted by Riley is that the strength of the composite should increase if the elastic modulus of the "rigid" particles is decreased to a value closer to that of the matrix. In a restricted sense, this phenomenological approach

Paper sponsored by Committee on Mechanical Properties of Bituminous Paving Mixtures.

should be able to lead to a quantitative as well as a qualitative description of the effect of these implicit parameters on the mechanical properties of the asphalt mixtures. This description should provide a means for the designer to effectively choose or design different mixtures with different mechanical properties such that an optimum design of the pavement structure can be reached.

The findings presented in this paper are obtained from part of a continuing research project investigating the effect of rubber additives in asphalts of different viscosities with respect to the thermorheological properties and other related mechanical properties of resultant asphalt concrete mixtures as obtained from actual test pavements. The preceding paper reported the findings of the other phase of the research project in which the effect of synthetic rubber additives on the physical behavior of mixtures is sought. The correlation between the mechanical properties and the physical properties is intended in the future.

SCOPE

This paper presents the results of the investigation into the effect of rubber additives in asphalts of different viscosities with respect to the thermorheological properties of resultant asphalt concrete mixtures. The samples used in this experiment were obtained from 8 test sections of the rubber-in-asphalt project. The particular test sections that were sampled were 3 in. thick. The mixture combinations obtained provide a basis for a complete factorial experiment with 3 factors at 2 levels each. The factors and their levels are given in Table 1.

Three factors at 2 levels each can be put together in $2^3 = 8$ different combinations, or treatments in the terminology of factorial experiments. Thus the 8 different combinations of these materials were obtained from the 8 corresponding test sections that were constructed by normal construction procedures and control. The details of the compositions of each test section are described in the Appendix. Within 2 weeks after construction and at specified time intervals (3, 6, 9, 12, 18, and 24 months), cores will be taken and several types of tests at several temperature levels will be conducted. A complete description of sample sizes and preparation of samples for testing is given in the Appendix. The types of tests included are unconfined compressive creep test, constant strain rate unconfined compressive test, and constant strain rate diametral test.

The mechanical properties of each type of mixture can be characterized from an analysis of the experimental results from these tests. This paper includes the results for each kind of mixture of creep compliance, ultimate compressive strength, ultimate compressive strain, and indirect tensile strength. The statistical method of variance analysis reveals the effect of the compositions on the properties mentioned earlier. In this paper, only the results and the analyses on the initial pavement cores (taken 2 weeks after construction) are presented. The effect of the sampling periods (the effect due to environmental conditions such as traffic loads and weather conditions) on the various mechanical properties of different kinds of mixtures will be sought in the future.

TABLE 1

FACTORS AND THEIR LEVELS

Factor	Symbol	Level	Value
Synthetic rubber solids in rubber-asphalt compound	+S	High	3 percent by weight of asphalt
	-S	Low	0 percent
Kinematic viscosity of asphalt	+V	High	85 to 100 penetration grade, 292 centistokes at 275 F, 1,326 stokes at 140 F
	-V	Low	85 to 100 penetration grade, 199 centistokes at 275 F, 719 stokes at 140 F
Rubber-asphalt compound in paving mixture	+C	Rich	1.1 × design percentage or 6.48 percent
	-C	Lean	0.9 × design percentage or 5.24 percent

THEORETICAL BACKGROUND

Linear Viscoelastic Theory

In linear viscoelastic theory, creep behavior can be described by the following heredity integral under a uniaxial stress state:

$$\epsilon(t) = \int_0^t J(t - \tau) \frac{\partial \sigma(\tau)}{\partial \tau} d\tau \tag{1}$$

where ϵ is the uniaxial strain, σ is the uniaxial stress, and J(t) is the uniaxial creep compliance. Equation 1 assumes that an isothermal condition exists. From Eq. 1, the time-dependent strain can be predicted under the application of the stress, provided that the creep compliance J is known.

One of the simplest ways of determining the creep compliance J(t) experimentally is by means of the constant stress creep tests. For given constant stress σ_0, Eq. 1 becomes

$$\epsilon(t) = J(t)\sigma_0$$

or

$$J(t) = \frac{\epsilon(t)}{\sigma_0} \tag{2}$$

In this equation $\epsilon(t)$ is the measured response quantity, and thus J(t) can be obtained from Eq. 2. The details of the experimental apparatus, procedures, and data analysis will be discussed in subsequent sections.

Time-Temperature Superposition Principle

At different temperatures, the creep compliance and relaxation modulus will be different in general from those determined at a reference temperature. This dependence on temperature as well as on time can be expressed by the following equation:

$$J = J(T, t) \tag{3}$$

where T is the temperature and t is the time. However, theoretical and experimental results indicated that for a certain class of material these 2 effects can be combined into a single parameter through the time-temperature superposition principle.

$$J(T, \xi) = J(T_0, t) \tag{4}$$

$$\xi = t/a_T \tag{5}$$

where ξ is the reduced time, a_T is the temperature shift factor, T_0 is the reference temperature, and t is the real time. This last relationship has been used by Schwarzl and Staverman (9) to define a material as "thermorheologically simple." Thus, the determination of a_T as a function of temperature T will provide the necessary information for determination of the reduced time ξ. With the relation of a_T versus T available, the creep and relaxation behavior at a very short or a very long time at a particular temperature T_0 can be obtained through this reduced-time concept. The method for determining a_T versus T by the shift along the time scale of the creep modulus curves at several temperatures will be discussed in detail in subsequent sections (see also, 13, Figs. 14 and 15).

For tests involving varying temperatures during loading, the definition given by Morland and Lee (14) for reduced time is

$$\xi = \int_0^t \frac{d\tau}{a_T} \tag{6}$$

The extent to which Eqs. 4, 5, and 6 hold for materials of interest to this program is part of our objective.

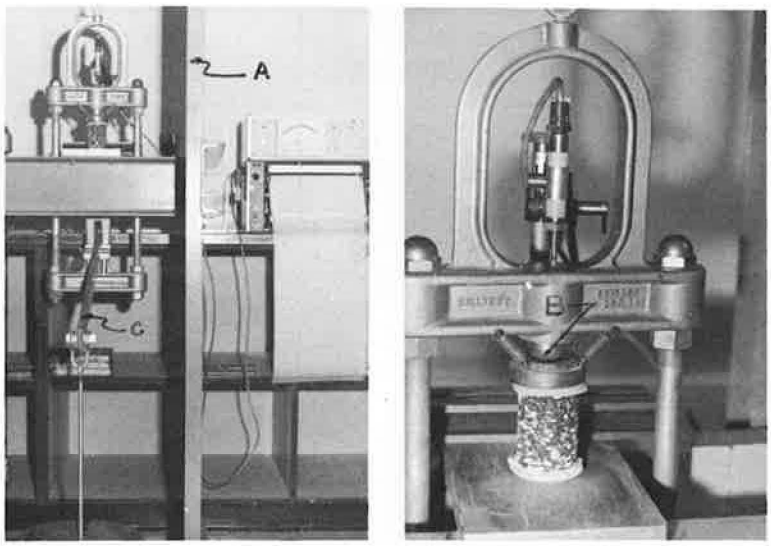

Figure 1. Basic equipment for unconfined compressive creep test.

Viscoelastic Theory of Circular Disc Under Diametral Loading

Consider a circular disc of diameter d and thickness h (where h < d) subjected to 2 equal compressive forces F applied along a vertical diameter as shown in Figure 1. The horizontal normal stress σ_x, vertical normal stress σ_y, and shear stress τ_{xy} produced at an arbitrary point p along the horizontal diameter are

$$\sigma_x(x, 0) = \frac{2F}{\pi dh}\left(\frac{d^2 - 4x^2}{d^2 + 4x^2}\right)^2$$

$$\sigma_y(x, 0) = \frac{2F}{\pi dh}\left[\frac{4d^4}{(d^2 + rx^2)^2} - 1\right] \tag{7}$$

$$\tau_{xy}(x, 0) = 0$$

where x is measured from the center of the disc. Although Eq. 7 was derived from linear elastic theory, Fitzgerald (13) has shown that for linear viscoclastic theory Eq. 7 is also valid so long as the stress-strain relationship is linear.

Equation 7 indicates that stress distribution along the horizontal axis is biaxial. The maximum stresses occur at center 0 and are

$$\sigma_x(0, 0) = \frac{2F}{\pi dh} \quad \text{(horizontal tension)}$$

$$\sigma_y(0, 0) = -\frac{6F}{\pi dh} \quad \text{(vertical compression)} \tag{8}$$

The ultimate biaxial tensile strength σ_T can be defined as

$$\sigma_T = \frac{2F\ \max}{\pi dh} \tag{9}$$

if the failure of the diametral samples occurs at the centerline and the failure is a ten-

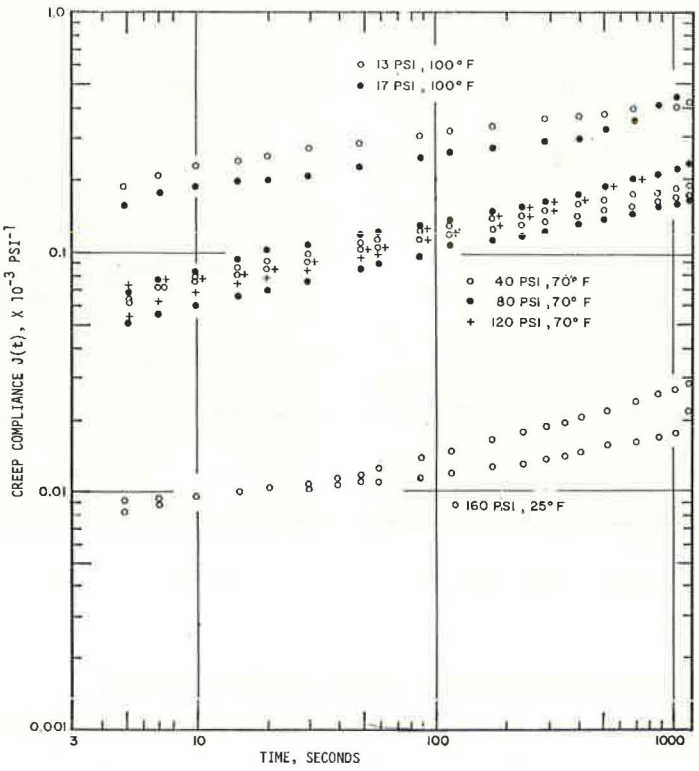

Figure 2. Constant stress creep tests on initial pavement cores from section 5.

sile failure (Fig. 2). Shear failure may also occur at the center when the ultimate shear stress, τ_{ult}, is reached with

$$\tau_{ult} = \frac{4F \text{ max}}{\pi dh}$$

In this case, the failure occurs at about 60 deg measured from the horizontal axis.

The theoretical derivation of Eq. 7 is based on the assumption that the material is isotropic and that the stress-strain relation is linear. Substantial evidence shows that the tension and compression properties of asphalt concrete are quite different. The theoretical analysis discussed here, using a common modulus for tension and compression, might introduce a significant error. Unfortunately, the analytic solution, which takes into account the difference of the tension and compression moduli, is quite complicated and has not yet been solved in closed form. (However, finite-element computer methods may be applicable.)

Another point that seems worth mentioning is that the failure criterion for asphalt concrete under biaxial stress state shall be carefully studied so that the failure of the diametral test can be understood.

EXPERIMENTAL APPARATUS AND PROCEDURES

Unconfined Compressive Creep Test and Diametral Creep Test

The basic test equipment, shown in Figure 1, for unconfined compressive creep test consists of a rigid frame (A), a loading head (B), a one to ten ratio loading lever

(C), and the deformation measuring devices. A linear variable differential transducer (LVDT) was used to measure the deformation of the specimen. The output from LVDT, which is directly related to the total deformation, could be automatically recorded on the strip-chart recorder.

When tests at either low or high temperatures were being performed, the equipment, except the strip-chart recorder, was moved into a 9- by 120-ft temperature- and humidity-controlled room. The temperature in this room could be controlled from -20 F up to 140 F with ±1 F fluctuation. In order to check the temperature in the specimen during the test, a separate temperature-sensing specimen with a pair of thermocouples embedded at its center was used. During the test, the temperature-sensing specimen and the testing specimen were put into the temperature-controlled room at the same time. Thus, the temperature in the testing specimen was checked indirectly by measuring the temperature in the temperature-sensing specimen. About 0.5 hour was required to attain a spatially uniform temperature distribution in the specimen.

Constant Strain Rate Test

An Instron universal tester with a temperature-conditioning chamber was used. Because this type of testing machine is fairly common, no detailed description of the machine will be given here. A special compressive cage was fixed in the grips of the tester such that under this setup the compression test could be performed.

When the constant deformation rate test was performed, the specimen was placed between the compressive cage and compressed at the predetermined rate until rupture occurred. The force versus the time was recorded automatically.

TEST RESULTS AND ANALYSIS

A series of different tests have been performed to determine the various mechanical properties of 8 different kinds of asphalt mixtures. The tests included in this paper are as follows:

1. Unconfined compressive creep tests at several temperature levels for determination of the creep compliances and the thermorheological properties;
2. Constant strain rate compression tests at several temperature levels for determination of the ultimate compressive strength; and
3. Constant strain rate diametral tests for determination of the failure under biaxial stress state and the indirect tensile strength.

Unconfined Compressive Creep Tests

In order to test the linearity of each mixture, 6 tests at 3 stress levels (about 40, 80, and 120 psi) were performed at room temperature (70 F) for 8 different kinds of mixtures. After that, 2 tests at 20 F with about 160 psi and 2 tests at 110 F with about 17 psi were performed. In each test the specimen was loaded for 24 min. The results of the creep compliances versus time (Eq. 2) were obtained. The typical creep compliances versus time are shown in Figure 3. If the material under consideration were truly a linear viscoelastic material, the result of the creep compliance versus time at different stresses (at the same temperature) should be the same. The experimental results indicate that the linearity is approximately held under the stress range and the time range as indicated. The results shown in Figure 2 and the rest of the test data obtained from the other kinds of mixtures indicate that each set of test data can be approximated by a straight line in the log-log plots. This implies that the creep compliances versus time can be represented by the following power law equation:

$$J(t) = At^n \tag{10}$$

where n is the slope of the straight line and A is the ordinate of the straight line at t = 1 sec. The results of the creep compliances of 8 different mixtures are given in Table 2.

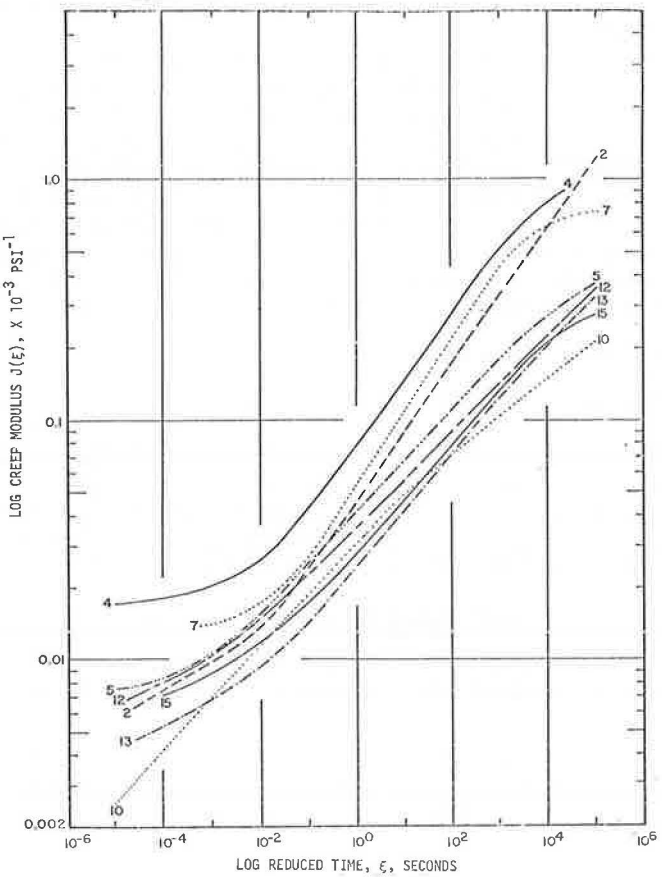

Figure 3. Master curves of unconfined compressive creep modulus at 70 F.

TABLE 2

CONSTANT STRESS CREEP COMPLIANCE

Section	25 F		70 F		100 F	
	A $\times 10^{-3}$ psi^{-1}	n	A $\times 10^{-3}$ psi^{-1}	n	A $\times 10^{-3}$ psi^{-1}	n
2	0.0065	0.13	0.05	0.32	0.28	0.24
4	0.014	0.10	0.12	0.21	0.25	0.21
5	0.066	0.16	0.047	0.20	0.14	0.16
7	0.011	0.18	0.07	0.28	0.34	0.12
10	0.0022	0.22	0.035	0.17	0.10	0.16
12	0.01	0.14	0.036	0.20	0.16	0.20
13	0.006	0.11	0.026	0.25	0.084	0.22
15	0.007	0.11	0.032	0.21	0.10	0.17

The master curves of the creep compliances versus reduced time were obtained by shifting the creep compliance versus time curves along the time axis, such that the creep compliance versus time curves for all temperatures formed a continuous curve. The amount of shift a_T of the creep compliance versus time curves at each temperature with respect to the reference temperature (70 F in the present analysis) was also obtained. The shift factor a_T versus temperature T for 8 mixtures is shown in Figure 4.

In order to investigate the effect of the mixtures (high and low viscosity of asphalt, with and without rubber) on the creep properties, the statistical method of variance analysis was employed to analyze the creep compliance at the reduced times of 10^{-4}, 10^{-0}, and 10^{+4} sec. The results of the variance analysis indicate that the most significant effect is from viscosity. Mixtures with high viscosity yielded high creep compliance at these 3 reduced times. This is shown in Figure 4 by comparing the master curves of test sections 4, 7, 5, and 2, which contained high-viscosity asphalt, with the other 4 sections, which contained low-viscosity asphalt.

The second significant effect is from the interaction between viscosity and asphalt content according to the variance analysis. However, the effect is more significant among the mixtures with high-viscosity asphalt where the high-asphalt content (sections 7 and 4) yielded high-creep compliances in comparison with the low-asphalt content (sections 5 and 2). The interaction has less effect among the mixtures with low-viscosity asphalt mixtures. Only at 10^{+4} sec, rubber and the interaction between rubber and viscosity are highly significant, where mixtures with rubber solids added yield low-creep compliances. The effect of the viscosity of the asphalt in the mixtures on

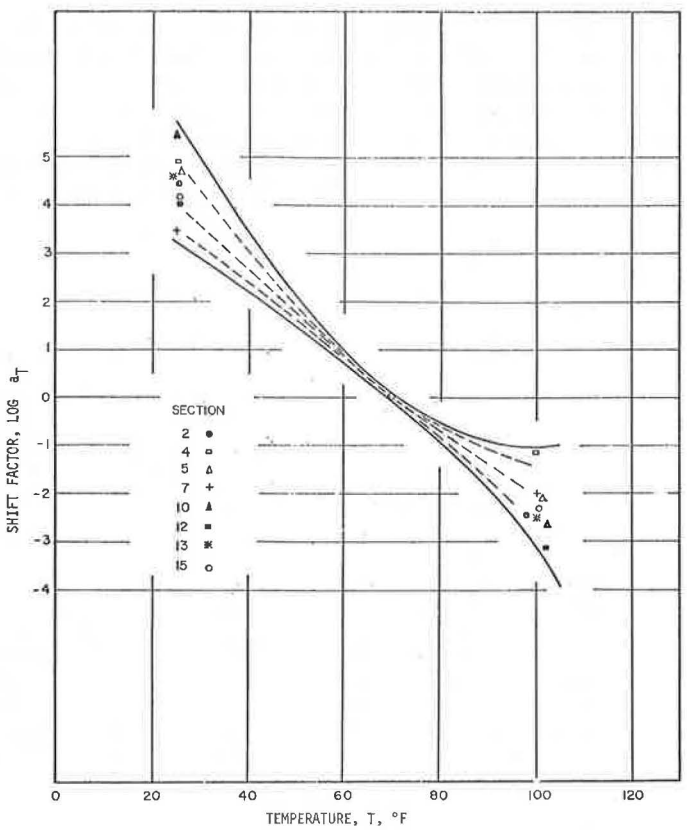

Figure 4. Shift factor versus temperature.

the creep compliances seems inconsistent with what has been found by Riley (8) where a stiffer binder (high-viscosity asphalt) resulted in a stiffer composite (asphalt concrete). The kinematic viscosity of the asphalt used was measured at 140 F. Perhaps the asphalt with high and low viscosity measured at 140 F may have low and high viscosity respectively at 70 F. Therefore, cannon-cone plate viscosity, penetration, and ductility measurements were conducted at 77 F and at 39.2 F. The results, given in the Appendix, do indicate that the asphalt with low kinematic viscosity measured at 140 F is greater at 77 F. Therefore, sections 10, 12, 13, and 15 actually are stiffer than sections 2, 4, 5, and 7 at room temperature. From now on, sections 10, 12, 13, and 15 are considered to have higher viscosity at room temperature.

Constant Strain Rate Unconfined Compression Tests

Initial pavement cores with 8 different asphalt mixtures were tested under the isothermal conditions at 4 temperatures: -20, 20, 70, and 110 F. All the tests were performed at 0.02 in./min constant rate except for the tests at 70 F, where 2 additional rates, 0.05 and 0.1 in./min were used. All samples were tested beyond the maximum compressive strength. The failure modes of the test samples after the stress reached the ultimate compressive strength were, in general, shear failure at 110 and 70 F and tensile failure at lower temperature (-20 F). At 20 F, both shear failure and tensile failure were observed.

The results of the ultimate compressive strength and strain of each test are given in Tables 3 and 4. Each value given in the tables is the average value from at least 2 identical tests. The temperature fluctuation during each test was within ±1 F. The results in Table 3 indicate that the increase of rate from 0.02 to 0.1 in./min results in an increase of the ultimate strength. The results in Table 4 indicate that the strength of the mixtures increases with decreasing temperature from 110 down to 20 F. Previous works of Vokac (12) and Pagen and Khosla (6) have shown that the exponential relationship exists between the ultimate compressive strength and temperatures. This relationship has also been observed in the present investigation, as shown in Figure 5. From 20 to -20 F the strengths do not show significant increases. In fact, the strength is decreasing in some cases because at -20 F the specimen is very brittle, and the failure is mainly due to the brittle fracture in which the strength is determined from the distribution of the flaw sizes in the sample. The ultimate compressive strain

TABLE 3

ULTIMATE UNCONFINED COMPRESSIVE STRENGTH AND STRAIN AT 70 F BY DEFORMATION RATE

Section	0.02 In./Min		0.05 In./Min		0.1 In./Min	
	Stress (psi)	Strain (in./in.)	Stress (psi)	Strain (in./in.)	Stress (psi)	Strain (in./in.)
2	155	0.0406	118	0.0213	171	0.0417
	157	0.0206	152	0.0301	199	0.0361
4	271	0.0358	205	0.0388	212	0.0408
	202	0.0456	170	0.0410	206	0.0392
5	236	0.0283	225	0.0342	251	0.0328
	237	0.0353	230	0.0292	244	0.0294
7	188	0.0387	216	0.0380	267	0.0407
	168	0.0352	214	0.0338	270	0.0394
10	255	0.0251	286	0.0292	293	0.0534
	184	0.0488	269	0.0463	349	0.0304
12	223	0.0327	202	0.0391	274	0.0258
	187	0.0220	241	0.0276	296	0.0341
13	196	0.0329	215	0.0352	268	0.0308
	177	0.0287	208	0.0283	237	0.0315
15	196	0.0222	243	0.0256	306	0.0280
	166	0.0228	269	0.0296	311	0.0300

TABLE 4

ULTIMATE UNCONFINED COMPRESSIVE STRENGTH AND STRAIN AT DEFORMATION RATE OF 0.02 IN./MIN BY TEMPERATURE

Section	-21 F		19 F		70 F		110 F	
	Stress (psi)	Strain (in./in.)	Stress (psi)	Strain (in./in.)	Stress (psi)	Strain (in./in.)	Stress (psi)	Strain (in./in.)
2	—	—	1,046	0.0443	155	0.0406	29.2	0.0228
	—	—	968	0.0482	157	0.0206	—	—
4	1,133	0.0360	1,166	0.0469	271	0.0358	40.5	0.0394
	1,940	0.0380	1,658	0.0583	202	0.0456	—	—
5	1,645	0.0726	1,340	0.0509	236	0.0283	38.6	0.0180
	—	—	1,440	0.0465	237	0.0353	18.4	0.0159
7	1,239	0.0579	1,700	0.0956	188	0.0387	32.8	0.0185
	1,745	0.0605	—	—	168	0.0352	27.2	0.0285
10	3,260	0.0702	1,290	0.0582	255	0.0251	40.8	0.0254
	—	—	1,140	0.0448	184	0.0488	42.9	0.0336
12	1,415	0.0745	1,140	0.0456	223	0.0327	34.8	0.0182
	1,295	0.0352	—	—	187	0.0220	33.8	0.0278
13	1,233	0.0329	1,308	0.0446	196	0.0329	34.9	0.0146
	—	—	—	—	177	0.0287	—	—
15	1,132	0.0734	809	0.0487	197	0.0222	39.6	0.0179
	944	0.0519	837	0.0677	166	0.0228	26.5	0.0356

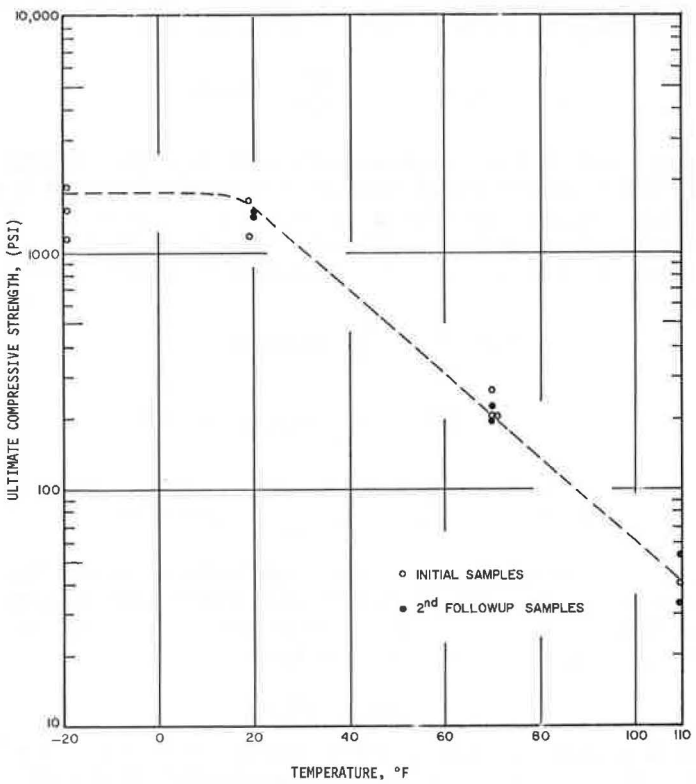

Figure 5. Ultimate compressive strength versus temperature—constant strain rate and unconfined compression.

observed in this investigation (Table 4) is also increasing with the decrease of temperature between 110 and 20 F, although the ductility of asphalt itself decreased with the decrease of temperature. Perhaps, among the very highly filled composite materials, ductility of the composite is not directly related to the ductility of the binder, especially for the asphalt mixture at high temperatures where the composite has about 0.02 ultimate strain, and the asphalt itself may have very large strains under tension and infinite strain under compression.

TABLE 5

MAXIMUM LOAD AND ULTIMATE TENSILE STRENGTH OF DIAMETRAL TESTS AT 70 F AND DEFORMATION RATE OF 0.02 IN./MIN

Section	Load (lb)	Tensile Strength (psi)	Section	Load (lb)	Tensile Strength (psi)
2	116	18.5	10	222	32.0
	108	17.0		225	34.6
4	108	18.5	12	203	29.2
	138	23.5		212	30.8
5	126	19.2	13	222	33.5
	170	28.0		192	30.0
7	142	24.1	15	139	21.0
	135	19.5		198	28.1

The effect of the composite on the ultimate compressive strength was analyzed through statistical methods. The results showed that at 20 F +C and +V contributed to the high ultimate strength; at 70 F the +V asphalt had greater strength than -V asphalt and the interaction of VC and SC was significant; and at 110 F none of the treatments was significant.

Constant Strain Rate Diametral Compression Tests

The diametral samples were tested at 70 F constant temperature at a constant deformation rate of 0.02 in./min until the samples failed. During the test, the failure was usually initiated at the center and was then gradually propagated toward both ends. The results of the maximum load at failure of each test are given in Table 5. The tensile stress along the vertical diameter from Eq. 9 is

$$\sigma_x(0,\ y) = \frac{2F}{\pi dh} \text{ (tension)}$$

With the maximum load, F max, obtained from each test, the ultimate tensile strength (one author called it "indirect tensile strength") was calculated and is given in Table 5. The ultimate tensile strength obtained in this way may not be equal to the ultimate tensile strength obtained from unconfined tensile test because the failure of the diametral test is initial from the center, which is subjected to the biaxial stresses

$$\sigma_x(0,\ 0) = \frac{2F}{\pi dh} \text{ (tension)}$$

$$\sigma_y(0,\ 0) = -\frac{6F}{\pi dh} \text{ (compression)}$$

where the failure is due not to σ_x alone but to both σ_x and σ_y. The failure criteria of the asphalt mixtures under multistresses are quite complicated and have not yet been established.

The statistical method of the variance analysis of the diametral test results indicates that the mixtures with high-viscosity asphalt show high-tensile strength. This is consistent with the findings in the preceding section where at 70 F the mixtures with high-viscosity asphalt show a high-compression strength.

CONCLUSIONS

1. The results of creep tests at different stress levels (Fig. 3 and Table 2) indicate that the linearity of the creep compliance is approximately held within the stress, strain, and time range used in this investigation. The creep compliance versus time can be represented by a power law (Eq. 10).

2. The effect of the compositions on the various properties is summarized as follows: At 70 F the viscosity shows the most significant effect where mixtures with low-viscosity asphalt (as measured at 77 F) yield high-creep compliance, low ultimate compressive strength, and low ultimate tensile strength. Mixtures with high-asphalt content yield high-creep compliance for the high-viscosity mixtures. At 20 F high-asphalt content and high-viscosity contribute to the high ultimate compressive strength and high ultimate strain. Also, at 20 F high viscosity and viscosity and asphalt content interaction contribute to the high-creep compliance. At 110 F the results are inconclusive.
3. The ultimate compressive strength and strain increase with decreasing temperatures from 110 to 20 F. An exponential relationship between the strength and temperature is observed.

ACKNOWLEDGMENTS

This continuing research work has been carried out as part of a project sponsored by the Bureau of Public Roads, Federal Highway Administration, U.S. Department of Transportation, in cooperation with the Utah State Highway Department. The work at the University of Utah was performed under contract to the Utah State Highway Department. The field sampling was conducted by the Utah State Highway Department. The tests reported in this paper were performed by the personnel of the Utah State Highway Department at the University of Utah, Civil Engineering Department, under the supervision of the authors. Thanks are due Roger Cahoon for coordinating the project; John Goris and the staff of the Utah State Highway Department for performing the experiments; Dale Peterson, Michael Darter, and Roland Vokac for valuable discussions; and George Jones for cooperation and interest in this project.

REFERENCES

1. Secor, K. E., and Monismith, C. L. Viscoelastic Properties of Asphalt Concrete. HRB Proc., Vol. 41, 1962, pp. 299-320.
2. Pagen, C. A. An Analysis of Thermorheological Response of Bituminous Concrete. Ohio State Univ., Columbus, PhD dissertation, 1963.
3. Papazian, H. S. The Response of Linear Viscoelastic Materials in the Frequency Domain With Emphasis on Asphalt Concrete. Internat. Conf. on the Structural Design of Asphalt Pavements, Univ. of Michigan, Ann Arbor, 1962.
4. Pister, K. S., and Monismith, C. L. Analysis of Viscoelastic Flexible Pavements. HRB Bull. 269, 1960, pp. 1-15.
5. Pister, K. S. Viscoelastic Plate on a Viscoelastic Foundation. Jour. Eng. Mech. Div., ASCE, Vol. 87, Feb. 1961.
6. Pagen, C. A., and Khosla, V. K. Temperature-Dependent Strength Characteristic of Sand-Asphalt Mixtures. Jour. of Materials, Vol. 3, No. 3, 1968.
7. Heukelom, W. Observations on the Rheology and Fracture of Bitumens and Asphalt Mixes. Proc., Assn. of Asphalt Paving Technologists, Vol. 35, 1966.
8. Riley, V. R. A Strength Prediction of Aggregated Composites. Jour. Composite Materials, Vol. 3, Jan. 1969.
9. Schwarzl, F., and Staverman, A. J. Jour. Appl. Physics, Vol. 23, 1952.
10. Timoshenko, S., and Goodier, J. N. Theory of Elasticity. McGraw-Hill, New York, 1951.
11. Fitzgerald, J. E. A New Bi-Axial Test for Ductile Materials. Proc., JANAF Solid Propulsion Meeting, Dallas, Texas, July 1961.
12. Vokac, R. Compression Testing of Asphalt Paving Mixtures. ASTM, Proc., Vol. 36, Part II, 1936, and Vol. 37, Part II, 1937.
13. Fitzgerald, J. E. Analysis and Design of Solid Propellant Grains. Internat. Conf. on Mechanics and Chemistry of Solid Propellants, Proc., Pergammon Press, Jan. 1967.
14. Morland, L. W., and Lee, E. H. Stress Analysis for Linear Viscoelastic Materials With Temperature Variation. Society of Rheology, Trans., Vol. 4, 1960.

Appendix

SAMPLE PREPARATION AND MATERIAL COMPOSITION

The 2- and 4-in. diameter core samples were cut from the pavements by means of an Acker core drill; water was used for a coolant. The pavement was cut from the following locations in each test section:

Initial samples were cut from the shoulders of the roadway 2 weeks after compaction. Three-month samples were cut from the shoulders of the roadway. Six-month samples were cut from the inner wheelpaths. Half of the samples were cut from the northbound lane and half from the southbound lane.

The 2-in. diameter cores were first cooled to 10 F for a period of approximately 48 hours. This cooling period was introduced to harden the specimens in order to facilitate the cutting process. After cooling, the specimens were cut to a length of approximately 3 in. by means of a diamond saw. Prior to testing, the length of each specimen was measured to the nearest 0.001 in. and its average diameter determined from 4 measurements taken along the length of the specimen. The specimens

TABLE 6

MATERIAL COMPOSITION OF 8 TEST SECTIONS

Test Section	Percent Asphalt[a]	Percent Rubber Solids[b]	Kinematic Viscosity at 140 F[c] (stokes)
2	5.59	0	1,390
4	6.74	0	1,206
5	5.19	3.0	1,309
7	6.74	3.0	1,336
10	6.26	0	684
12	5.20	0	670
13	6.48	3.0	630
15	5.26	3.0	625

[a]By weight of mixture.
[b]By weight of asphalt cement.
[c]Of asphalt taken from storage tank.

TABLE 7

PHYSICAL PROPERTIES OF INITIAL PAVEMENT CORES FROM 8 TEST SECTIONS

Test Section	Percent Air Voids	Percent VMA	Density (lb/cu ft)
2	8.7	20.6	137.5
4	3.1	18.4	141.9
5	10.6	21.4	134.5
7	4.6	19.2	140.4
10	4.9	19.0	141.3
12	9.2	20.4	135.9
13	4.2	18.6	139.9
15	9.9	21.2	135.5

TABLE 8

PHYSICAL PROPERTIES OF ASPHALT TAKEN FROM STORAGE TANK AND RECOVERED FROM PAVEMENT MIXTURES

Test Section	Mixture	Storage Tank		Recovered	Storage Tank		Recovered
		Original	Rubberized		Original	Rubberized	
		Penetration at 77 F (points)			Ductility at 39.2 F (cm)		
12		99	—	107	8.5	—	4.2
15	+S-V-C	101	81	69	8.1	29.5	34.5
2	+V-S-C	104	—	89	31.5	—	10.0
5	+S+V-C	104	96	59	98.5	150+	67.5
10	+C-S-V	96	—	113	9.1	—	8.8
13	+S+C-V	98	86	85	9.8	32.0	70.0
4	+V+C-S	98	—	88	83.5	—	9.2
7	+S+V+C	105	87	73	76.8	150+	54.0
		Kinematic Viscosity at 140 F (stokes)			Cannon-Cone Viscosity at 77 F (kilopoises)		
12		670	—	1,080	802	—	713
15	+S-V-C	625	1,545	4,303	704	539	1,096
2	+V-S-C	1,390	—	1,688	505	—	574
5	+S+V-C	1,309	2,310	5,680	521	338	846
10	+C-S-V	684	—	963	732	—	436
13	+S+C-V	630	1,830	4,302	688	502	893
4	+V+C-S	1,206	—	1,445	600	—	546
7	+S+V+C	1,336	2,280	6,313	473	360	920

were then capped with a sulfur capping compound.

The cooling and cutting processes used on the 2-in. diameter cores were also used on the 4-in. diameter cores with the exception that the length of the specimens was cut to approximately 1 in. to provide a disc-shaped specimen for the diametral tests. Prior to testing, the average diameter of each specimen was determined from 2 measurements taken along the axis of applied load and 2 measurements taken along an axis perpendicular to the applied load. The average length was determined from 2 measurements taken along the same axis as the diameter-measure cuts.

TABLE 9

GRADATION OF AGGREGATES

Sieve	Percent Passing	Sieve	Percent Passing
3/4 in.	100.0	No. 8	49.9
1/2 in.	91.9	No. 16	39.1
3/8 in.	82.6	No. 50	22.1
No. 4	64.4	No. 200	7.6

Data on the composition of the material in the test sections are given in Tables 6, 7, 8, and 9.

Case Studies of Pavement Shrinkage Cracking as Feedback for a Design Subsystem

R. C. G. HAAS, University of Waterloo, and
W. A. PHANG, Ontario Department of Highways

Low-temperature shrinkage cracking of pavements in Ontario and in other provinces or states has serious implications with respect to accelerating losses in serviceability of these pavements. To date, most research efforts have concentrated on the causes of the problem with little attention to any practical design methodology. A number of flexible pavement sections in Ontario with widely varying degrees of cracking were examined. Previously developed laboratory techniques to determine the low-temperature properties of the bituminous layers were extended and modified. Relatively simple, reliable, and low-cost apparatus for this purpose was developed and appears to be usable for routine design. The case studies indicated that high cracking frequencies were associated with stiff bituminous surfaces at low temperatures and that cracking could be correlated with the predicted fracture temperature of the mixture. They also indicated that the most dominant variable affecting fracture susceptibility was asphalt source and that, in order to achieve a certain cracking frequency, a "hard" asphalt from one source could be equivalent to a "soft" asphalt from another source, depending on their low-temperature stiffness properties. The use of information from this study in refining a previously developed design subsystem for low-temperature response has been indicated.

•SHRINKAGE CRACKING of flexible pavements, due primarily to thermal effects, occurs in varying degrees in most parts of Canada and in much of the United States. That such fracture can markedly accelerate the loss in serviceability of a pavement is well known and documented. Studies initiated in Alberta in early 1963 (1, 2) and others, such as those in western Canada (3, 4, 5, 6), Wyoming (7, 8) and Connecticut (9), demonstrated the importance of this problem. The problem was also explicitly recognized in a symposium in 1966 (10) and as a first-priority road research need in Canada in 1965 (11). More recently, a project on developing a rational design system for heavy wheel loads has included shrinkage cracking as one of its major design subsystems (12). The economic importance of the shrinkage-cracking problem has not been detailed, but an approximate analysis (13) has indicated that the annual cost to Canadians is in the multimillion dollar range. Fracture in bituminous surfaces can occur from causes other than low-temperature shrinkage. These causes are not well understood. A summary of all external and internal factors that may be significant to low-temperature cracking has been presented elsewhere (14).

The objectives of the project were as follows:

1. To test with field samples the validity of previously developed laboratory techniques for evaluating low-temperature rheological behavior of bituminous materials;
2. To evaluate with these field samples the validity of these previously developed techniques in predicting fracture susceptibility;

Paper sponsored by Committee on Mechanical Properties of Bituminous Paving Mixtures.

3. To develop simple, low-cost apparatus and instrumentation for testing bituminous materials over a low-temperature and time range; and
4. To extend or refine a previously developed design subsystem for the response of flexible pavements at low temperatures and to use the results of this investigation as feedback information.

BEHAVIOR OF FLEXIBLE PAVEMENTS AT LOW TEMPERATURES

Thermal Stresses in Bituminous Surfaces

The calculation of thermal stresses in a bituminous surface can be approached in a rigorous or in an approximate manner.

A simple and approximate method for determining stresses has been used by Hills and Brien (15), Lamb (7), and others, and extended to a range of thermal and stiffness gradient conditions by Haas and Topper (16). They basically used an approximation of the following equation for an infinitely long, narrow, and completely restrained strip:

$$\sigma_x(T) = \alpha \int_{T_o}^{T_f} S(r, T)dT$$

where

$\sigma_x(T)$ = unit tensile stress in the longitudinal direction;
α = average coefficient of thermal contraction;
T_o = initial temperature;
T_f = final temperature; and
$S(r, T)$ = stiffness modulus, which varies with temperature and rate of loading.

The approximation involves the determination of stiffness modulus, either directly or indirectly as subsequently discussed, at the midpoint of small temperature intervals (using a loading time corresponding to the cooling time for the temperature interval). In effect, the integral is replaced by a summation.

Mechanisms of Shrinkage Fracture

The actual mechanisms of shrinkage fracture have received little attention except for a crack initiation and propagation hypothesis by Haas and Topper (16). They pointed out that an understanding of the fundamental mechanics of such fracture could have some practical implications. Their hypothesis covered only the condition of simple thermal shrinkage, but in a subsequent effort Haas and Anderson (14) have presented qualitative categories of other possible, pertinent conditions.

Observations from a recent, extensive field experiment in Manitoba (5, 6) have tended to support this theory in part. However, they have also indicated that a more complete phenomenological model of flexible pavement shrinkage cracking is required, especially to incorporate varying subgrade effects.

Low-Temperature Response of Bituminous Materials

The response of bituminous binders and bituminous mixtures over a time and temperature range has been investigated fairly extensively. The principle of time-temperature superposition has been found applicable and has been used for low-temperature work on both thin films of binder and on bituminous mixtures (17). This work demonstrated that the fracture temperature for a restrained, bituminous mixture could be calculated from its stiffness characteristics.

Relationships Between Binder and Mixture Stiffness

Because the stiffness of an asphalt mixture is a fundamental parameter in evaluating its low-temperature properties, predicting stiffness from the properties of the binder would be very useful.

Considerable work in this regard has been summarized by Heukelom and Klomp (18) and by Heukelom (19). They describe how the stiffness of the binder can be determined from van de Poel's nomograph, then related to mixture stiffness. This relationship has been developed for well-compacted mixtures with about 3 percent air voids. When the air voids are greater than 3 percent, a "corrected" mixture stiffness can be calculated according to van Draat and Sommer (20).

Because the stiffnesses of the asphalt and the mixture are related and because the fracture strength of the mixture is related to its stiffness, relating the tensile or fracture strength of the mixture directly to the stiffness of the asphalt should also be possible. Heukelom (19) has shown such a relationship for 2 types of mixtures, and certainly an agency, say, a highway department, should be able to develop these curves for its own materials. However, the estimates are approximate. Furthermore, the stiffness of some binders (those of a more "complicated" nature) can be in error if determined by the nomograph. To correct this, Heukelom (21) has recently developed a bitumen test data chart with a consistency scale for use with the nomograph. Kopvillem and Heukelom (22) have shown how it can be applied to determine the stiffness of some Canadian asphalts with high-wax contents.

EXPERIMENTAL PROGRAM

Purposes

The general purpose of the experimental program was to test the validity of previously developed laboratory techniques for predicting fracture susceptibility, as described elsewhere (13, 14, 17), to actual field evaluation. An attendant purpose was to develop simple, low-cost apparatus and instrumentation for design purposes. It was intended that the results be applicable to extending and refining a shrinkage fracture design subsystem.

Selection of Test Sections

Test sections were selected in consultation with the Ontario Department of Highways (DHO) and were based on geographic dispersion in the province, varying properties and conditions, and varying degrees of cracking. They represent a variety of experience that the Department has with this problem. Table 1 gives a list of the sections with some general descriptive information regarding year of construction, type of subgrade, and freezing index for the location. Table 2 gives a listing of more specific informa-

TABLE 1

GENERAL INFORMATION ON TEST SECTIONS

Test Section	Highway Number	Location	Average Crack Index[a]	Freezing Index (deg days)	Subgrade Type	Construction Dates
1	41	Napanee to Roblin	8	115	Clay	May 1953, base June 1953, surf
2	17	Agawa	1	265	Clean granular	Sept.-Oct. 1959, base May-July 1960, surf
3	17	Heyden to Haviland Bay	13	175	Clean granular, boulder, and rock fill	Oct. 1960, base June 1961, surf
4	17	Sault Ste. Marie to Heyden	5	165	Clean granular	Oct.-Nov. 1960 and May 1961, base May-June 1961, surf
5	7	Arkona				
		Section A	21	65	Clay	1960
		Section B	1			
		Section C	1			
6	9	Orangeville				
		Section A	23	145	Silty sand	Oct.-Nov. 1961
		Section B	6			
7	11	Val Albert	2	345	Clayey, silt, and sand fill	Oct. 1964
8	11	Val Albert Easterly	32	345	Deep sand fill	July 1964

[a]From DHO crack surveys in 1966 and 1967.

TABLE 2

COMPONENT PROPERTIES OF TEST SECTION

Test Section	Asphalt Cement				Lift Properties				Reccmpaction				Aggregate	Prime
	Supplier and Refinery	Penetration Grade	Penetration at 77 F	Viscosity at 275 F (centistokes)	Type	Thickness, (in.)	Voids (percent)	Asphalt Content (percent)	Stability (lb)	Flow	Voids (percent)	VMA (percent)		
1	1a	85 to 100			HL3	1½	7.2	5.8	2,916	11.9	5.5	19.1	Quarr. L.S.C. aggr. and scr. min. filler	Yes
					HL8	1½	7.1	5.0	2,872	12.7	4.8	16.8		
					HL8	1¼	7.7	4.9	2,774	12.9	4.3	16.2		
					Gr. A	8								
					Gr. B	18								
2	2a	150 to 200	161	256	HL4	1½	5.0	5.2	2,500	9.3	2.6		Granitic gravel	Yes
					HL4	1½	5.0	5.3	2,480	11.9	2.1			
					HL4	1⅛	6.8	4.9	2,210	9.7	2.9			
					Gr. A	9								
					Gr. B	31								
3	2b	85 to 100	96	211	HL4	1½	4.6	5.7	2,994	10.1	2.9		Granitic gravel	No
					HL4	1½	5.4	5.5	3,600	13.2	2.3			
					Gr. A	7								
					Gr. B	8								
4	2a	85 to 100	89	331	HL4	2	5.3	5.9	3,659	11.0	3.6	17.9	Granitic gravel	No
					HL4	1¾	8.7	4.9	3,438	10.1	6.3	18.0		
	1a	85 to 100	96	211	HL4	2	8.5	5.4	3,685	10.5	5.1	18.1		
					Gr. A	8								
					Gr. B	9								
5A	2c	85 to 100	95	205	HL3	1½	4.3	6.0	3,107	14.5	1.7	16.4	L.S. gravel	No
					HL6	2¼	4.2	5.2	2,582	13.2	2.3	15.1		
					Gr. A	4								
					Gr. B	18								
5B	1a	85 to 100	95	336	HL3	1½	3.5	6.3	3,200	14.2	2.0	17.4	L.S. gravel	No
					HL6	2¼	5.6	5.1	3,071	10.9	3.2	15.6		
					Gr. A	4								
					Gr. B	18								
5C	3a	85 to 100	95	427	HL3	1½	4.2	6.5	3,188	12.7	2.0	17.7	L.S. gravel	No
					HL6	2¼	5.4	5.3	2,562	9.7	3.1	16.0		
					Gr. A	4								
					Gr. B	18								
6A	2c	85 to 100	84	205	HL4	2	3.1	6.7	2,382	14.7	1.3	17.7	L.S. gravel	No
					Gr. A	9								
					Gr. B	12								
6B	2c	150 to 200	157	142	HL4	2	3.1	7.0	2,145	12.5	1.6	18.5	L.S. gravel	No
					Gr. A	9								
					Gr. B	12								
7	4a	150 to 200	153	223	HL4	2	6.5	5.0	2,600	10.6	3.2	15.4	Granitic gravel	No
					Gr. A	8								
					Gr. B	12								
8	4a	150 to 200	153	226	HL4	2	5.4	5.1	2,718	9.6	3.1	16.0	Granitic gravel	No
					Gr. A	8								
					Gr. B	37								

tion regarding the structural components and their properties. Many of these characteristics and their differences, as they relate to variable degrees of cracking, were largely responsible for the choice of test sections.

Some Characteristics of the Test Sections

There are several characteristics of the test sections and their components that bear some discussion. First, the range in cracking index is from very low at several sections to very high at Val Albert Easterly, Orangeville section A, and Arkona section A. The DHO cracking index is calculated as the number of full transverse cracks plus one half of the half transverse cracks per 500 ft of roadway length. Transverse cracks less than one-half width should not be included because they usually occur subsequent to the formation of half or full cracks. In other words, they are not a primary manifestation of the inability of the pavement to withstand shrinkage stresses. These high indexes occur over the full range of freezing indexes encountered (from 650- to 3,450-deg days), which would indicate that degree of cracking is not related to freezing index per se.

Second, the effect of asphalt supplier (and in turn the source) may be significant in some of these sections. In the Arkona section A, the cracking index was 21. The supplier for this section was 2c, and the suppliers for sections B and C respectively, with much lower crack frequencies, were 1a and 3a. Although 2c supplied a lower viscosity asphalt, the evidence is certainly not conclusive enough in itself to point to 2c as the "villain." However, it should be noted that 2c also supplied asphalt for the Orangeville section A, which had a similar high cracking frequency.

Third, for the Orangeville section B, 2c supplied a softer asphalt and the cracking index dropped markedly. This would support the use of softer asphalts to control cracking (23, 24, 25), but it should be emphasized that the softer asphalt came from the same source.

The fourth point involves the question of whether cracking in Arkona section A could similarly have been reduced if 2c had supplied a softer asphalt. Other works (14, 17, 6) have indicated that a hard asphalt from one source can have better low-temperature stiffness properties than a soft asphalt from another source.

Fifth, the sections at Val Albert and Val Albert Easterly represent a far different situation in crack patterns, even though the supplier, 4a, is the same for both. However, it may be noted that the Val Albert Easterly section has a far greater depth of granular B (i.e., 37 in. versus 12 in. for the other section), implying a difference in subgrade support conditions. Consequently, it is possible that the high cracking index is largely associated with the subgrade rather than with the asphalt source.

Testing Program

The testing program consisted of slow tension tests on surface samples from the test sections. Apparatus and techniques used in the tests were subsequently described. The intention was to produce data for the type of analysis referred to.

Samples were obtained by sawing blocks out of the test sections. Locations were random and individual specimens of bituminous mixture used ($1\frac{1}{2}$ by $1\frac{1}{2}$ by 3 in. long) in the testing program were sawed from the larger blocks. They were tested in tension over a time and temperature range, and again random selection was used for a particular test. Time was actually recorded at various stress levels, although the nominal strain rate was noted. Six specimens from each section were tested at varying strain rates and temperatures ranging from -30 to +50 F.

Experimental Equipment

The basic ideas and apparatus for low-temperature tension testing of asphalt mixtures and films were developed in a previous work (17). However, there were a number of aspects that required further development or modification, including the requirement for low-cost and reliable equipment applicable to design evaluations.

Figure 1 shows the experimental equipment that was developed. There are a number of unique features to this equipment, and they are described in detail in a forthcoming DHO report on this work.

Figure 1. Experiment equipment.

EXPERIMENTAL RESULTS AND THEIR SIGNIFICANCE

Stress-Strain-Stiffness-Time Relationships

Typical stress-strain curves for the various temperature levels are shown in Figure 2 for the Orangeville section B. Numerous data points were plotted to obtain such relationships and a computer program was written to tabulate data and to calculate stiffness.

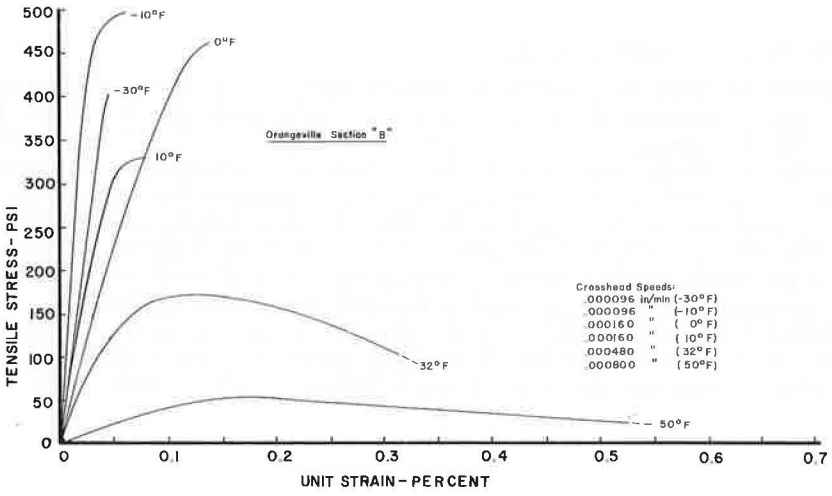

Figure 2. Stress-strain curves for various temperature levels.

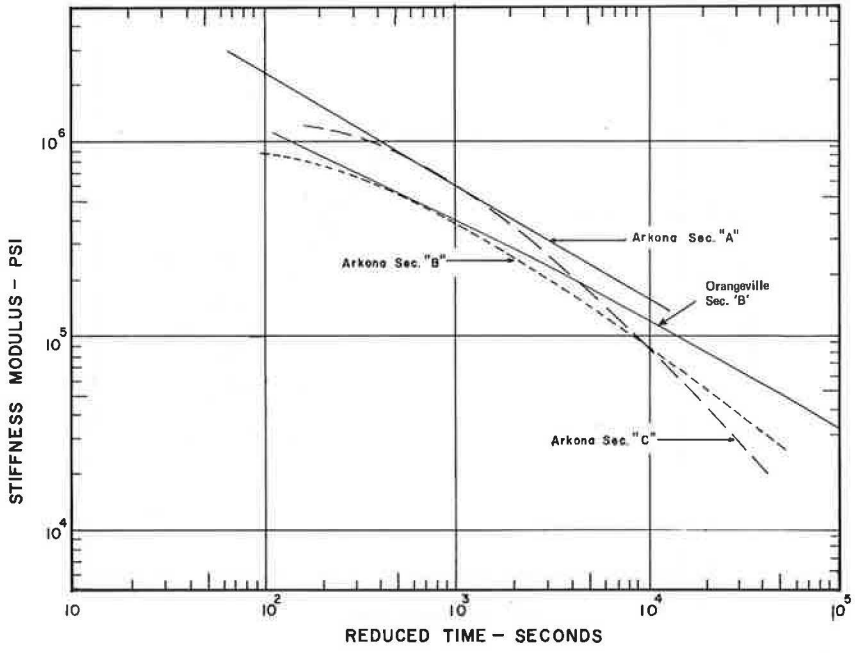

Figure 3. Master curves of stiffness modulus at 10 deg F.

Time was also recorded, which made it possible to plot stiffness modulus-time curves for each set of samples. From these relationships, it is possible to derive master curves of stiffness modulus versus reduced time by using the method of time-temperature superposition. A set of these is shown in Figure 3 for the 3 Arkona sections. Similar master curves were derived for all the other sections.

The shift factor relationships for the curves in Figure 3 are shown in Figure 4. Again, similar relationships were derived for the other sections. Figure 4 shows that extrapolation below the base temperature of 10 deg F would have produced erroneous results.

Estimating Thermally Induced Fracture

Procedures for predicting thermally induced fracture have been previously referred to in this paper. Although these methods are normally applicable to design, a major purpose of this investigation was to study the cracking characteristics of sections already in service. Consequently, estimates of fracture susceptibility of these sections were made. Of course, these estimates can only be made on the basis of the physical nature of the material (such as age) at the time of test and apply only to restrained samples. Furthermore, such procedures can evaluate only the surface; nevertheless, an analysis of the surface can be useful in tracing the cause of cracking, even where it may be subgrade associated (e.g., on the Val Albert Easterly section).

To estimate fracture susceptibility of a restrained bituminous sample requires master curves of stiffness modulus (Fig. 3) and the shift factor relationships (Fig. 4). A relationship between tensile strength and stiffness modulus is also required, and

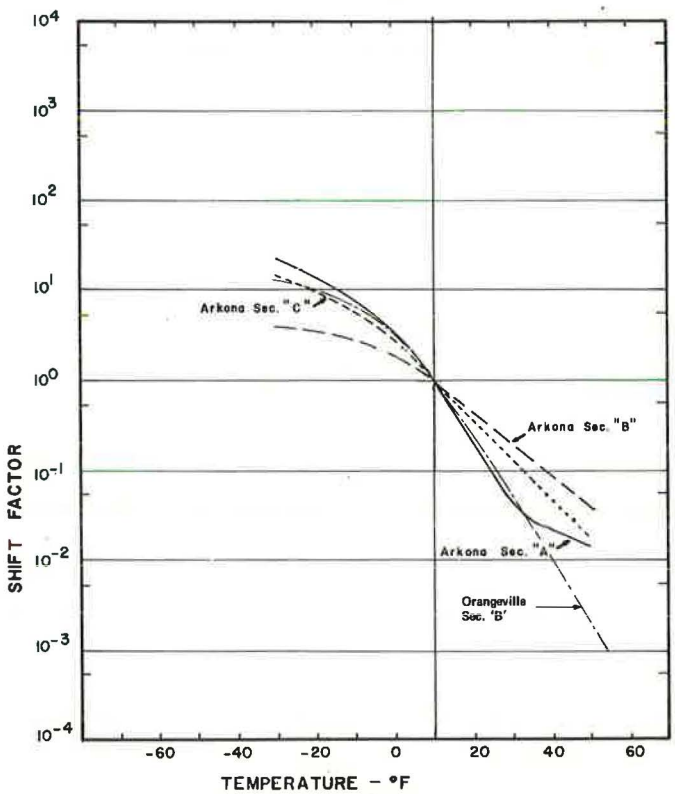

Figure 4. Shift factor relationships.

this has been derived for the test data, as shown in Figure 5. From these figures, thermally induced fracture as a function of temperature can be calculated for a selected cooling rate. An example is shown in Figure 6 for the Arkona sections. The point of thermal fracture, T_{FR}, is estimated as the intersection of the stress relationship and the tensile strength relationship (note that only the needed portion of the

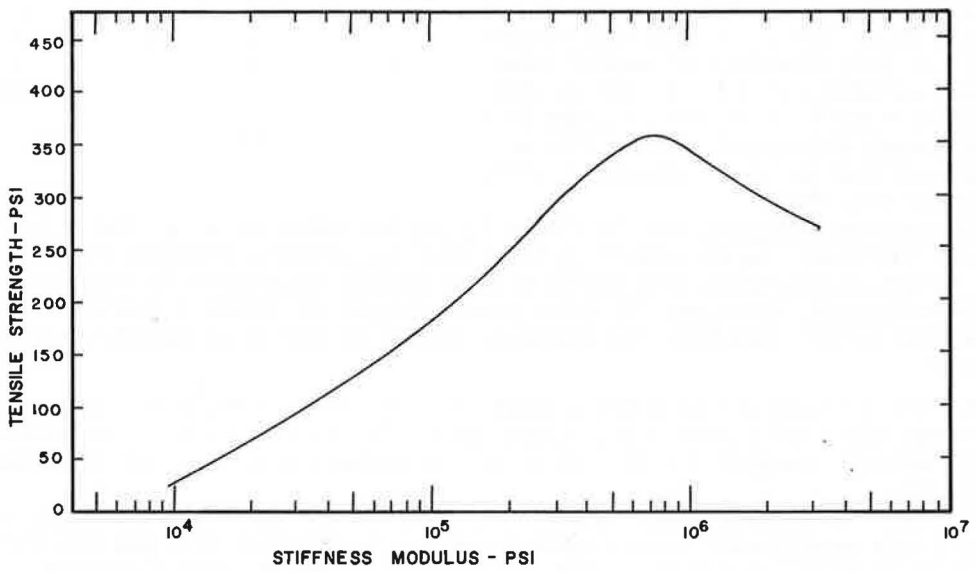

Figure 5. Tensile strength versus stiffness modulus.

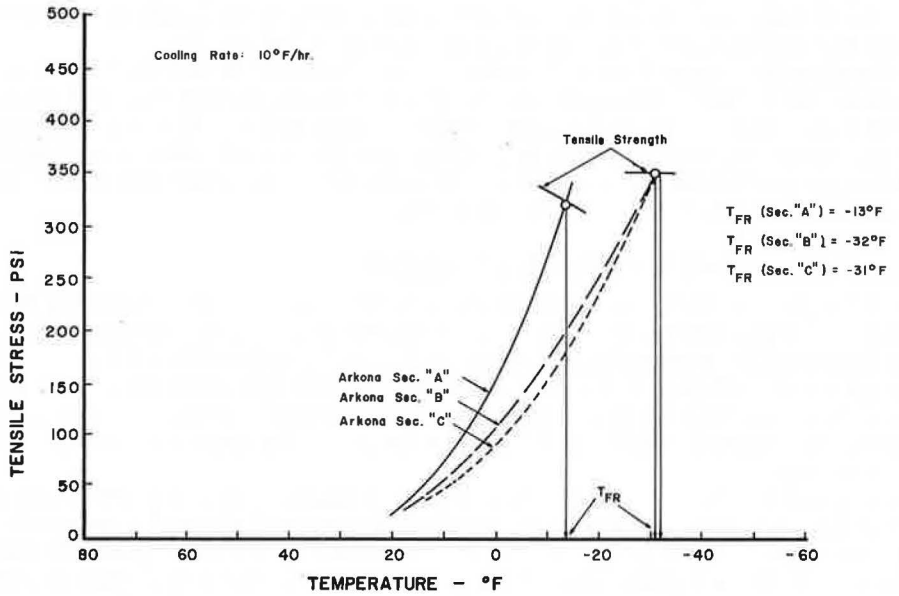

Figure 6. Estimate of thermally induced fracture.

strength relationship is shown in Figure 6). T_{FR} values were determined for all the sections and are given in Table 3.

TABLE 3

ESTIMATES OF THERMALLY INDUCED FRACTURE

Test Section	Estimate of Fracture Temperature[a] (deg F)	Test Section	Estimate of Fracture Temperature[a] (deg F)
1	-20	5B	-32
2	-38	5C	-31
3	-25	6A	- 6
4	-36	6B	-13
5A	-13	7	-30
		8	-28

[a]For a cooling rate of 10 F per hour.

Fracture Conditions and Section Variables

Although it was not possible to use a statistically designed experiment, the results of this investigation would strongly suggest that cracking frequency of asphalt pavements (or cracking index as measured by DHO) is in most cases related to the low-temperature stiffness of the mix. This is in turn reflected by the estimated fracture temperatures, T_{FR}.

Perhaps not so apparent are the causes behind the variations in T_{FR} and cracking index. These can only be postulated, but again some evidence, certainly not of a completely conclusive nature, is available in the descriptive features of the test sections (Tables 1 and 2). There are also other possibly important factors or descriptive features that are not available. Nevertheless, several aspects of the results are worthy of note.

1. The sections with fairly low cracking indexes, of 5 or less, generally have quite low T_{FR} values and appear to be primarily associated with mixtures of lower stiffness.
2. Asphalt suppliers 2a, 1a, and 3a were associated with the lower stiffness mixtures.
3. The Val Albert sections appear to contradict the first statement, but T_{FR} is very nearly equal for the mixes on both projects. Consequently, it is possible that some subgrade or other feature, rather than any variations in mixture stiffness, is responsible for the high cracking index at Val Albert Easterly.
4. The sections with cracking indexes greater than 5 generally had higher T_{FR} values (from -20 to -6 F). These were much stiffer mixes at low temperatures.
5. Arkona section A exhibits a much higher cracking index and T_{FR} than do sections B and C. Section A has supplier 2c's lower viscosity asphalt.
6. The Orangeville section A, with a cracking index of 23, which is very similar to the 21 for Arkona section A, has the same asphalt supplier, 2c.
7. Supplier 2c's asphalt was also used for the Orangeville section B but consisted of a softer, 150 to 200 penetration grade. The resultant mix was less stiff than that for section A. This would tend to support the contention that softer asphalts reduce cracking. However, this may only be strictly true for a single source or supplier. In fact, a hard asphalt from one supplier can actually give a less stiff mix at low temperatures than a soft asphalt from another supplier.

Cracking Index and Estimated Fracture Conditions

The data given in Table 3 indicate in a general manner that the estimated fracture temperature, T_{FR}, for the various sections seems to vary with cracking index. A plot of T_{FR} versus cracking index, shown in Figure 7, indicates that a linear relationship might exist, although there is considerable scatter (one point far off the line is the Val Albert Easterly section). A similar relationship, between cracking frequency and asphalt stiffness at -40 F and 10^4 sec loading time, has recently been presented by Young et al. (6).

Cursory examination of data shown in Figure 7 might suggest a rather weak relationship, and this is supported by a correlation coefficient of 0.53 for the regression line shown. However, age, location, subgrade, and other variables undoubtedly influence the scatter. If the one point representing the Val Albert Easterly section is removed (and this may be reasonable in that we strongly suspect a subgrade effect may be operative here), the correlation coefficient goes up to 0.81. This is a remarkably high

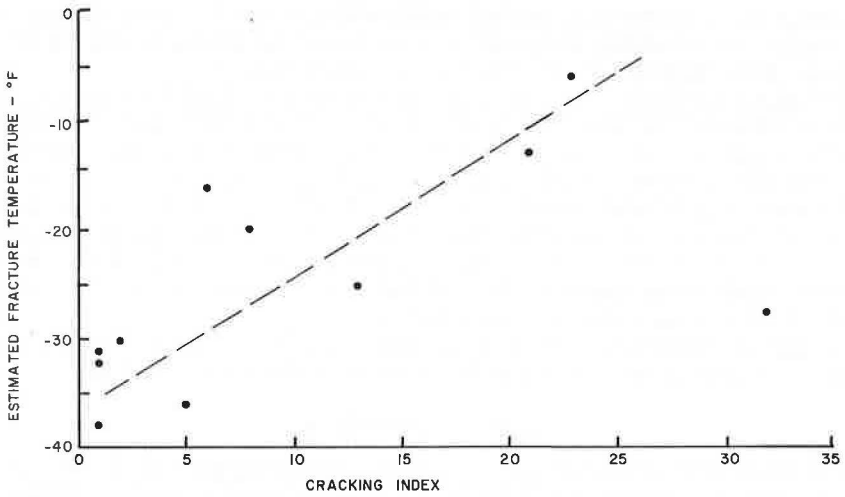

Figure 7. Estimated fracture temperature versus cracking index.

value considering the "mixture" of projects and variables that underlie this generalized relationship. Consequently, it is possible that for, say, a single subgrade class or age group the relationship would be better defined. If this were the case, and if stiffness properties or T_{FR} were determined for mixes in the design stage, it may be possible for an agency to develop a well-defined set of curves like those shown in Figure 7. In turn this could enable the agency to set specifications for low-temperature response of bituminous materials.

A DESIGN SUBSYSTEM

The principles of systems engineering can be used to structure a variety of engineering problems, including the process of pavement design and management as a whole (26, 17). For operational and organizational purposes, a series of component subsystems must be developed from this overall design and management process (14). This work also presented a tentative design subsystem and described the phases and components of the systems framework that was used. A forthcoming DHO report describing the investigation in detail demonstrates how case study results of this sort are used and outlines areas requiring additional study in order to refine the subsystem.

SUMMARY AND CONCLUSIONS

1. Thermal shrinkage cracking of asphalt pavements can originate in the bituminous layer, and perhaps does do so in most cases, but other causes of such fracture are also possible, including those associated with subgrade factors. Current knowledge about these cracking mechanisms is imperfect.
2. Techniques for determining the low-temperature stiffness of bituminous mixtures have been successfully adapted from previous laboratory investigations for the evaluation of field specimens from a number of Ontario highway projects. Relatively simple, reliable, and low-cost apparatus and instrumentation for this purpose has also been developed and is capable of being used for design.
3. The low-temperature stiffness values were extended over a time and temperature range by time-temperature superposition and used to calculate the probable fracture temperatures for the various field sections; we assumed that there were complete restraint conditions. It is subjectively apparent that the stiffer bituminous mixtures, with higher estimated fracture temperatures, exhibited much higher field-cracking frequencies than the sections with lower stiffness mixtures at low temperatures.

4. Although the field sections varied widely with respect to location, age, subgrade, soil type, and so on, cracking frequency can be correlated to the estimated fracture temperature. This finding has important design implications.

5. Although the evidence is again subjective, it appears that the dominant variable associated with low-temperature cracking frequency is asphalt source (or supplier). It also appears that for some cases, a relatively soft asphalt from one source (say, in the order of a 300 to 400 penetration grade) would be required to result in as low a cracking frequency as a hard asphalt (i.e., an 85 to 100 penetration grade) from another source. Only a pair of sections showed an exception to this observation. These varied widely in cracking frequency, but they had the same source of asphalt and exhibited the same mixture stiffness properties. We suspect that the high cracking frequency of the one section is associated with some subgrade factor.

6. Information from case studies of the type described in this paper can be used to extend and refine a previously developed but tentative design subsystem.

ACKNOWLEDGMENTS

The investigation on which this paper is based was sponsored and financially supported by the Ontario Department of Highways through the Ontario Joint Highway Research Programme. The Department's assistance is gratefully acknowledged as is the cooperation and advice of various members of its Research Branch.

REFERENCES

1. Shields, B. P., and Anderson, K. O. Some Aspects of Transverse Cracking in Asphalt Pavements. Proc., Canadian Tech. Asphalt Assn., 1964.
2. Anderson, K. O., Shields, B. P., and Dacyszyn, J. M. Cracking of Asphalt Pavements Due to Thermal Effects. Proc., Assn. Asphalt Paving Technologists, 1966.
3. Domaschuk, L., Skarsgard, P. S., and Christianson, R. H. Cracking of Asphalt Pavements Due to Thermal Contraction. Proc., Canadian Good Roads Assn., 1964.
4. Culley, R. W. Transverse Cracking of Flexible Pavements in Saskatchewan. Saskatchewan Dept. of Highways, Tech. Rept. 3, June 1966.
5. Deme, I., and Fisher, D. Ste. Anne Test Road, A Field Study of Transverse Crack Development in Asphalt Pavement. Proc., Canadian Tech. Asphalt Assn., 1968.
6. Young, F. D., Deme, I., Burgess, R. A., and Kopvillem, O. Ste. Anne Test Road: Construction Summary and Performance After Two Years Service. Paper presented to the Canadian Tech. Asphalt Assn., Edmonton, Nov. 1969.
7. Lamb, D. R., et al. Roadway Failure Study No. 1 Final Report. Natural Resources Research Institute, Univ. of Wyoming, Laramie, Hwy. Eng. Res. Publ. H-15, Aug. 1966.
8. Gietz, R. H., and Lamb, D. R. Age-Hardening of Asphalt Cement and Its Relationship to Lateral Cracking of Asphaltic Concrete. Proc., Assn. of Asphalt Paving Technologists, 1968.
9. Breen, J. H., and Stephens, J. E. Fatigue and Tensile Characteristics of Bituminous Pavements at Low Temperatures. School of Engineering, Univ. of Connecticut, Storrs, Rept. JHR 66-3, July 1966.
10. Nontraffic Load Associated Cracking of Asphalt Pavements. Proc., Assn. of Asphalt Paving Technologists, 1966, pp. 239-357.
11. Road Research Needs in Canada: 1965. Canadian Good Roads Assn., Tech. Publ. 27, May 1965.
12. Haas, R. C. G. Needs Analysis for Tasks to Develop a Design Subsystem for Shrinkage Fracture of Flexible Pavements. Paper prepared for Asphalt Inst. and Gulf Oil Canada Ltd., Aug. 1969.
13. Haas, R. C. G. The Low-Temperature Behaviour of Flexible Pavement Surfaces. Proc., Canadian Tech. Asphalt Assn., 1968.

14. Haas, R. C. G., and Anderson, K. O. A Design Subsystem for the Response of Flexible Pavements at Low Temperatures. Proc., Assn. of Asphalt Paving Technologists, 1969.
15. Hills, J. F., and Brien, D. The Fracture of Bitumens and Asphalt Mixes by Temperature Induced Stresses. Proc., Assn. of Asphalt Paving Technologists, Vol. 35, 1966, pp. 293-309.
16. Haas, R. C. G., and Topper, T. H. Thermal Fracture Phenomena in Bituminous Surfaces. HRB Spec. Rept. 101, 1969, pp. 136-153.
17. Haas, R. C. G. The Performance and Behaviour of Flexible Pavements at Low Temperatures. Univ. of Waterloo, Ontario, PhD thesis, June 1968.
18. Heukelom, W., and Klomp, J. G. Road Design and Dynamic Loading. Proc., Assn. of Asphalt Paving Technologists, Vol. 33, 1964.
19. Heukelom, W. Observations on the Rheology and Fracture of Bitumens and Asphalt Mixes. Proc., Assn. of Asphalt Paving Technologists, Vol. 35, 1966.
20. Van Draat, W. E. F., and Sommer, P. Ein Gerat zur Bestimmung der Dynamischen Elastizitattsmoduln von Asphalt. Strasse und Autobahn, Vol. 35, 1966.
21. Heukelom, W. A Bitumen Test Data Chart for Showing the Effect of Temperature on the Mechanical Behaviour of Asphaltic Bitumens. Jour. Inst. of Petroleum, Nov. 1969.
22. Kopvillem, O., and Heukelom, W. The Effect of Temperature on the Mechanical Behaviour of Some Canadian Asphalts as Shown by a Test Data Chart. Paper presented to Canadian Tech. Asphalt Assn., Edmonton, Nov. 1969.
23. McLeod, N. W. Softer Asphalt Cements Reduce Pavement Cracking. Paper presented at the 47th Annual Meeting of the Highway Research Board, Jan. 1968.
24. McLeod, N. W. Reduction in Transverse Pavement Cracking by Use of Softer Asphalt Cements. HRB Spec. Rept. 101, 1969, pp. 163-170.
25. McLeod, N. W. Transverse Pavement Cracking Related to Hardness of the Asphalt Cement. Proc., Canadian Tech. Asphalt Assn., 1968.
26. Hutchinson, B. G., and Haas, R. C. G. A Systems Analysis of the Highway Pavement Design Process. Highway Research Record 239, 1968, pp. 1-24.

Fatigue and Fracture of a Bituminous Paving Mixture

KAMRAN MAJIDZADEH, A. T. CHAN, and D. V. RAMSAMOOJ, Ohio State University

The fatigue behavior of simply supported sand-asphalt beams is examined by using experimental and analytical methods of fracture mechanics. The fatigue crack growth rates correlate well with the stress-intensity factor in accordance with Paris's law that states that $dc/dN = AK^4$, where dc/dN is the crack per cycle, A is a constant of a material, and K is the stress-intensity factor, which is dependent on the load, geometry, and boundary conditions. It is postulated that in a material such as a sand-asphalt mixture, which is abundantly endowed with flaws, fatigue damage is initiated at the first loading cycle, so that the fatgue life is the number of cycles of repeated loading to propagate a "starter flaw," c_o, into a crack of critical size, c_f. The starter flaw is a material's constant but is subject to statistical variation and is believed to be principally responsible for the statistical variation of fatigue life. The crack reaches the critical stress-intensity factor, K_c, which is a constant for a given material. K_c is the failure criterion for both static fracture and fatigue. A formula for fatigue life, N_f, is given. Methods for determining these constants are presented, and the fatigue lives, determined experimentally are compared with those predicted from the formula and show good agreement.

•MANY PAVEMENT DESIGNERS, in recent years, have expressed concern over the cracking of flexible pavements under repeated load applications. This type of distress, referred to as fatigue failure, appears in the form of alligator or map cracking, which is initially confined to localized zones and spreads at an increasing rate. Other types of pavement failure, such as rutting and shear failure, are also associated with cracking and may occur in conjunction with fatigue cracking. However, fatigue failure differs from other modes of pavement distress by the fact that it usually requires little or no permanent deformation or flow and is often of quasi-brittle type.

The phenomenon of fatigue failure is associated with the concept of damage or those changes in the material that lead to formation of macroscopic cracks and subsequent structural instability. The occurrence of fatigue failure is a result of 2 separate processes: damage initiation and damage growth (1, 2, 3, 4). The occurrence of these 2 processes in a material system results in a gradual weakening of the structural components. In order for the failure state to be reached, however, the damage should approach a critical level. In short, damage initiation and growth are necessary but not sufficient conditions for the occurrence of fatigue failure. In fact, damage growth in a material body can be arrested during the course of repeated loading before reaching the threshold of instability. The arrest of the damage can be attributed either to the inability of the applied load to furnish sufficient energy required for growth or to other changes that occur in the material body and boundary conditions and that alter the state of stress distribution in the structural component.

The processes of damage initiation and growth differ among various materials. Because of the presence of inherent flaws in certain alloys, plastic, polymers, and heterogeneous compositions such as asphaltic materials, damage can reasonably be expected

Paper sponsored by Committee on Mechanical Properties of Bituminous Paving Mixtures and presented at the 49th Annual Meeting.

to be initiated at the first few cycles of load application. The statistical distribution of such internal discontinuities, in fact, can account for statistical variations in the fatigue life (1, 2).

The process of damage growth has been discussed in various theories (4), but fundamentally it is related to the deformation occurring at the tip of discontinuities and is associated with the energy balance in these regions. The work of external forces in the regions of discontinuity is divided into stored elastic energy, the energy required for irreversible changes, such as viscous or plastic flow, in the material body, and the surface energy required to form a crack. The rate of crack growth then depends entirely on the energy balance, and the path it follows is governed by the minimum energy requirement.

During the cyclic deformation process, the tip of the zone of discontinuity blunts and resharpens resulting in crack growth through the body. This process continues until a crack of critical size has been reached, and the induced state of stress results in structural instability or terminal event of fracture.

The fatigue life, N_f, of a material or structural component can be represented by a parametric equation, such as

$$N_f = F\,[c_o,\ (A,\ n,\ K),\ K_c] \tag{1}$$

This equation expresses the fatigue life in terms of 3 sets of parameters. The parameter, c_o, is associated with the process of crack initiation and may be considered as the starter flaw in the tension face of the beam from which the crack will propagate. Its size is dependent on the material characteristics such as void content, statistical distribution of voids, and surface condition. This parameter cannot be directly measured and should be determined experimentally. It is believed to be principally responsible for the statistical variations in the service life of a mixture.

The second parameter set, (A, n, K), expresses the process of crack growth in the material system. A previous paper (4) pointed out that Paris's equation for rate of crack growth can be applied to bituminous mixtures. This equation is

$$dc/dN = AK^n \tag{2}$$

The constant, A, is a material constant and appears to be temperature dependent, and n has been found to be 4.0 as shown by Paris and Erdogan (5, 6). The parameter, K, is the stress-intensity factor at the crack tip affected by the applied load, geometry, support condition, and material stiffness.

The third parameter, K_c, describing the critical limit for damage, is the value of the stress-intensity factor at the start of instability, i.e., at the point where the crack will propagate spontaneously. K_c is determined from fracture tests and has been shown to be a constant of the material (7, 8, 9, 10).

These parameters are considered in this duscussion of the fatigue life of a paving mixture.

MATERIALS AND TESTING PROCEDURES

In this study a sand-asphalt mixture composed of a 60 to 70 penetration asphalt cement and a well-graded Ottawa sand mixture was utilized. The aggregate gradation is given in Table 1, and the characteristics of the asphalt cement and the specimen mixture used are given in Table 2. Six percent asphalt cement by weight of aggregate was used in the preparation of the specimen. Beam specimens of 1 by 1 by 12-in. were prepared by using a drop-hammer compaction assembly. The specimen density and void content are also given in Table 2.

The sand-asphalt beam specimens were subjected to both fatigue and fracture tests. Fracture bending tests were conducted on simply supported beams of 11-in. span loaded at midspan. Both unnotched and notched specimens were used in this investigation. Six notch depths were used ranging from $^5/_{32}$ to $^1/_2$ in. The fracture tests were conducted in stroke control by using an MTS testing machine (Fig. 1). The ramp loading function

TABLE 1

AGGREGATE GRADATION

Sieve Number	Percent Passing (samples)	ASTM Specification D1663-59T
16	100.0	85 to 100
30	88.0	70 to 95
50	64.2	45 to 75
100	30.1	20 to 40
200	15.7	9 to 20

TABLE 2

CHARACTERISTICS OF ASPHALT CEMENT AND SPECIMEN MIXTURE

Characteristics	Amount
Asphalt cement	
Test	60 to 70
Specific gravity	1.010
Softening point, ring and ball, deg F	123
Ductility at 77 F, cm	150+
Penetration	
100 grams, 5 sec, 77 F	63
200 grams, 60 sec, 39.4 F	23.5
Flash point, Cleveland open cup, deg F	455
Specimen mixture	
Asphalt cement, percent by weight of aggregate	6
Average density, grams/cm^3	2.052 ±0.011
Average air voids, percent	17.0 ±0.5

was used. At low temperatues the effect of rate of loading on the fracture test is not significant. Nevertheless, the rate of loading was selected so that it would be comparable to the average rate of loading in fatigue experiments, determined by approximating the sinusoidal curve with a triangular loading function.

The fatigue experiments were conducted at 0.5 cycles per second with a $P = P_o + P_1 \sin \omega t$ loading function. Nine different combinations of P_o and P_1 were selected to give a wide spectrum of fatigue loading. These tests were conducted on unnotched specimens. The results of fatigue response of notched specimens have been reported previously (4, 8). Although these experiments are being conducted at various temperatures, only the results of one temperature, 23 F, is presented in this paper.

ANALYSIS OF RESULTS

The fatigue life of a material can be expressed by

$$N_f = F\,[c_o,\ (A,\ n,\ K),\ K_c] \qquad (1)$$

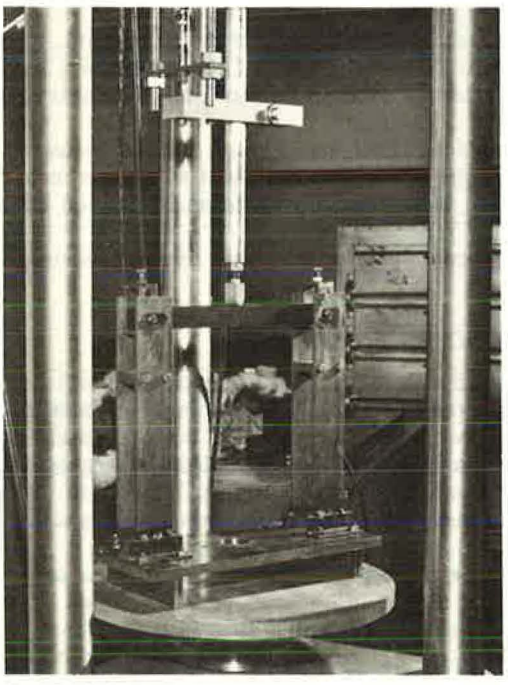

Figure 1. Specimen arrangements in testing frame.

where each parameter set describes different processes involved in the fatigue failure. In the following sections the methods for determining these parameters are discussed.

The Critical Stress Intensity Factor, K_c

At the terminal event of fracture, when the internal flaw has reached a critical size, the stress field in the vicinity of the crack tip is represented by a parameter, K_c, the critical stress-intensity factor. K_c is proportional to the critical strain energy release rate and Young's modulus. It is a material constant and is independent of the crack-to-beam depth ratio (c/d ratio) (7, 8, 9, 10). However, this parameter is affected by temperature and rate of loading.

K_c can be determined experimentally from fracture tests by using Winne and Wundt's equation (7):

$$K_c^2 = \sigma_n^2\, hf\,(cf/d) \qquad (2)$$

where

σ_n = nominal stress at the root of the notch = $M/[b(d-c)^2]$;
M = bending moment = P1/4;
P = load at fracture;
b = width of the beam;
d = depth of the beam;
c_f = crack depth at failure and is equal to the initial notch in the beam assuming that the crack just starts to propagate at the instant of failure;
h = d - c; and
f(c/d) = a function given by Winne and Wundt (7 Fig. 16).

The Parameters, A, n, and K, Describing the Crack Growth-Stress-Intensity Factor Relation

To determine the rate of crack growth requires that a direct measurement of the actual length of the crack be made. This is rather difficult to do in asphaltic materials and requires expensive equipment such as X-ray units. Other techniques such as the successive breaking of electrical circuits or ink staining give only qualitative or partial information (11). An indirect method, however, can be used to obtain the crack length from measurements of the compliance of the beam. The compliance, L, is defined as the inverse of the slope of the load-deflection diagram (Fig. 2). This method for obtaining the crack length is a recognized practice in experimental fracture mechanics (11, 12). The method is based on the fact that a beam will be weakened by the introduction of a crack or by the increase in length of an existing crack. The presence of the crack will cause a stress concentration in its vicinity resulting in an increase in the compliance of the beam. This increase in compliance is uniquely related to the increase in the crack depth, and this relation remains true regardless of the cause of the increase in the crack length, provided that the material behaves elastically and the changes in the material properties are negligible. In fact the relationship between the increase in compliance and the crack length is given by the equation (12)

$$\delta L/\delta c = (2/E)\,[(K/P)^2] \qquad (3)$$

where L is compliance, c is crack depth, P is load, E is Young's modulus, and K is a stress-intensity factor. In order to apply this technique for obtaining the crack growth, beams with notches of predetermined lengths were fabricated and tested so that a master curve of compliance versus crack length could be plotted. The artificial notch had the same effect on the compliance as a real crack of the same length. The results of the normalized compliance L/L_o versus crack length is shown in Figure 3. L_o is the compliance of the unnotched beam. The accuracy of this graph was checked

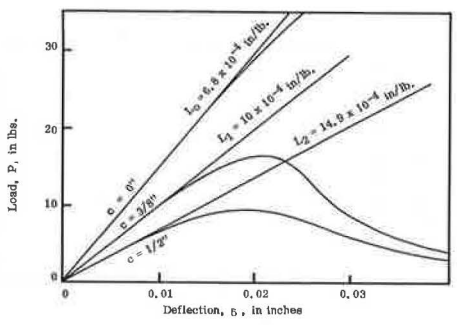

Figure 2. Load versus deflection and values of compliance.

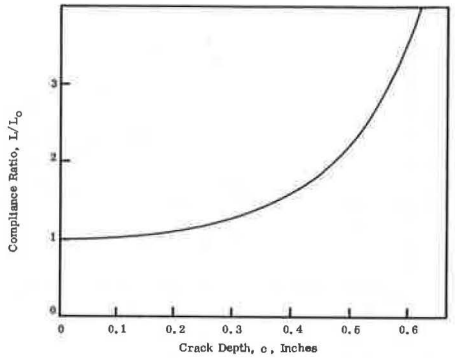

Figure 3. Normalized compliance versus crack depth from fracture tests.

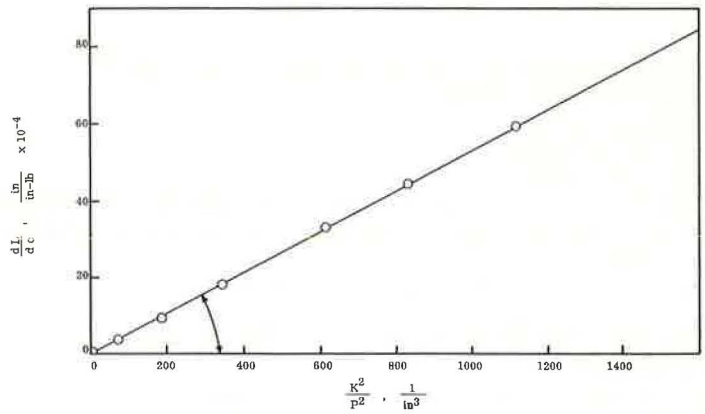

Figure 4. Relationship between dL/dc from fracture tests and theoretical K^2/P^2.

by differentiating it to obtain $\delta L/\delta c$ as a function of c. The values of $\delta L \delta c$ were then plotted versus the calculated values of K^2/P^2 from Winne and Wundt's formula (Fig. 4) and show a proportionality relation as indicated by the equation.

The fatigue tests were conducted on unnotched, simply supported beams loaded at midspan; the testing temperature was 23 F. During the test the load was maintained constant using the MTS in load control. The deflection increased as the test progressed, very slowly at first but with an exponential type of increase with the number of cycles. Figure 5 shows the normalized compliance versus the number of cycles. The only phenomenon that could account for the increase in the compliance was the increase in the crack depth at midspan.

Because the compliance and the crack depth are uniquely related, the crack depth at any stage of the fatigue process can be obtained as shown in Figure 5, where the crack depth after N cycles in the fatigue test corresponds to the crack depth at the point on the master curve where the compliance is the same as that on the fatigue curve. In this way it is possible to obtain the c-N curve for each fatigue test. Figure 6 shows a typical c-N curve.

By knowing the crack depth, c, at any cycle, N, one can calculate the stress-intensity factor, K, at any stage of the fatigue test. Similarly, K^2/P^2, which is expected to be proportional to the rate of

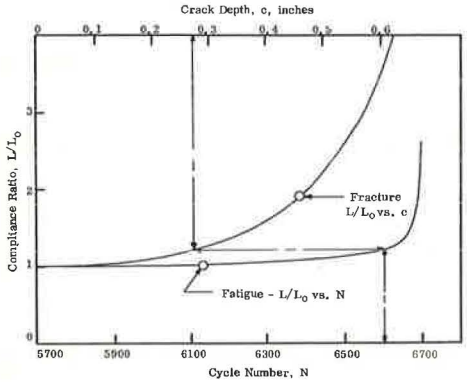

Figure 5. Normalized compliance versus number of cycles for fatigue test and normalized compliance versus crack depth for fracture test.

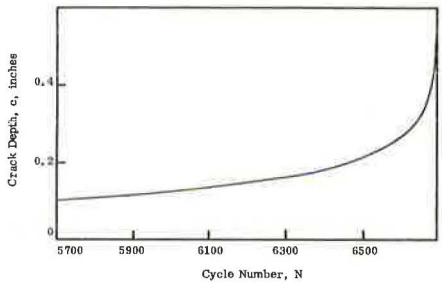

Figure 6. Crack depth versus number of cycles for fatigue test.

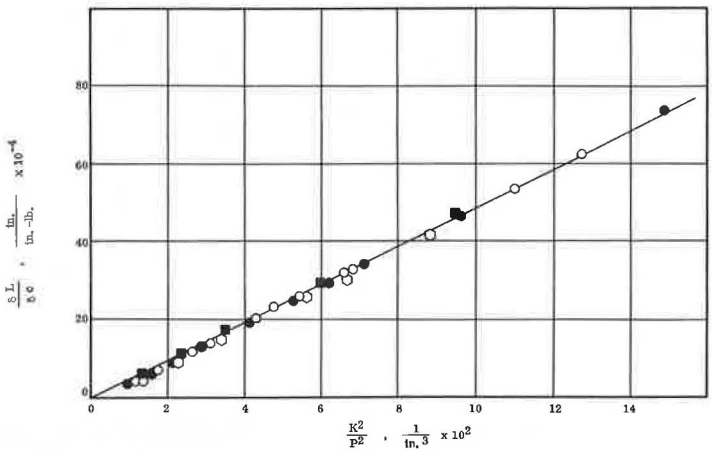

Figure 7. Relationship between $\delta L/\delta c$ from fracture tests and K^2/P^2 from fatigue tests.

change of compliance with crack depth, can be determined. The experimental values of $(\delta L/\delta c)$ versus calculated K^2/P^2 were plotted for a number of fatigue experiments, and a linear relationship between the two (Fig. 7) was indicated.

To determine the rate of crack growth-stress-intensity factor relation requires that the curve shown in Figure 6 be differentiated to obtain dc/dN versus c. Knowing c and the load P, one can calculate the stress-intensity, K. The (dc/dN) - K relationship is then plotted on a log-log scale in the search for a relationship of the form

$$dc/dN = AK^n \tag{4}$$

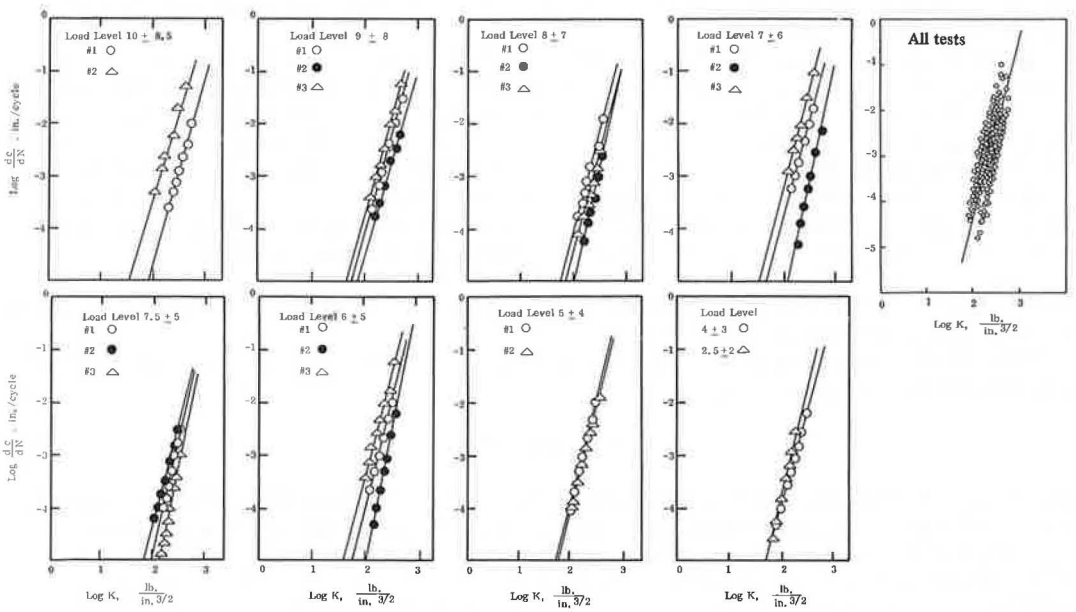

Figure 8. K versus dc/dN for different load levels and for all tests.

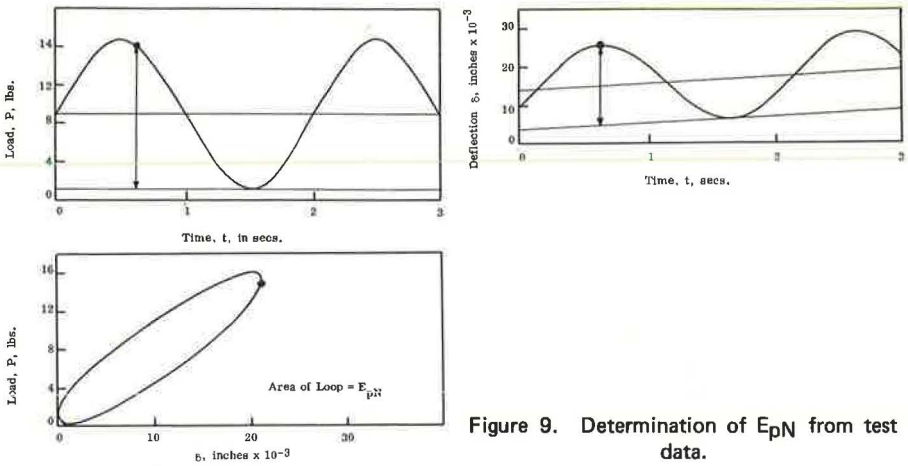

Figure 9. Determination of E_{pN} from test data.

The results for 9 stress levels and all levels combined are shown in Figure 8. From these graphs, the crack-growth relation is

$$dc/dN = 5 \times 10^{-3} K^4 \qquad (5)$$

which is in accordance with Paris's law.

It is also possible to correlate the rate of crack growth with the hysteresis energy loops obtained from the dynamic load-deflection diagrams at various stages of the fatigue process. The hysteresis loop in the Nth cycle, E_{pN}, measures the total energy dissipated in the Nth cycle by viscous, plastic, and surface work. This energy may be conveniently divided into 2 parts: one part is concerned with the energy dissipated in viscous and plastic deformation when no crack is present and the other is concerned with the viscous and plastic deformation in the zone of influence of the crack and the energy consumed in forming any new surfaces of crack that may develop during the particular cycle of loading.

During the first cycle of loading in an unnotched beam, it may be assumed that no increment of crack length occurs (because the rate of crack propagation at this stage is negligible) so that the hysteresis loop is a measure of the energy loss in the usual viscous and plastic deformation process. This initial loop will be called E_{p1}. If during the subsequent loading the crack does not propagate, the area of the hysteresis loop will remain constant. In most cases, however, the area of the hysteresis loop will increase over the initial value because of the formation of new crack surfaces and the intensification of the local stress field in the zone of influence of the crack. This increase in the hysteresis energy loop will be called E_p, and it is equal to $E_{pN} - E_{p1}$, where E_{pN}, the hysteresis loop in the Nthecycle, can be determined as shown in Figure 9, and E_{p1} is the hysteresis loop at N = 1.

The relationship between the part of the hysteresis loop, E_p, and the rate of crack growth, dc/dN, is given as (6)

$$E_p = T(dc/dN) \qquad (6)$$

where T is a constant. This relationship holds only if the size of the plastic zones at the crack tip is small in comparison to crack length and the specimen dimensions.

A plot of E_p versus dc/dN shows a linear relationship for all stress levels (Fig. 10). Thus the hysteresis loop is an indication of the rate at which the crack is propagating or the rate at which damage is progressing during fatigue.

In this study of the rate of crack growth, the indirect method of deducing the crack length from the compliance of the beam was used. Although it is considered to be a reliable technique in fracture mechanics, it is desirable that the rate of crack growth

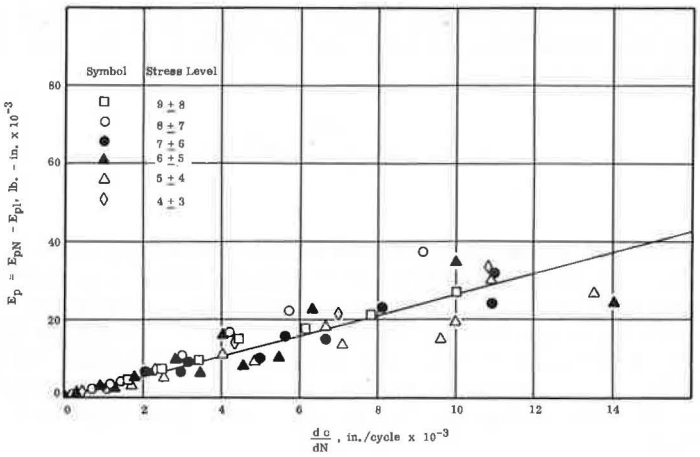

Figure 10. Relationship between hysteresis loops and dc/dN from fatigue tests.

be determined by direct experimental methods. Work is in progress at the present time to utilize direct observational techniques to measure crack depth during fatigue tests.

The Parameter, c_o, the Starter Flaw

From the crack-growth law, $dc/dN = AK^4$, the crack, c, at any stage is given by

$$c = c_f - \int_N^{N_f} AK^n \, dN \tag{7}$$

Because of the limits of experimental accuracy and the relative insensitivity of the L/L_o versus c curve from which the c-N curve is obtained, the crack-growth law could

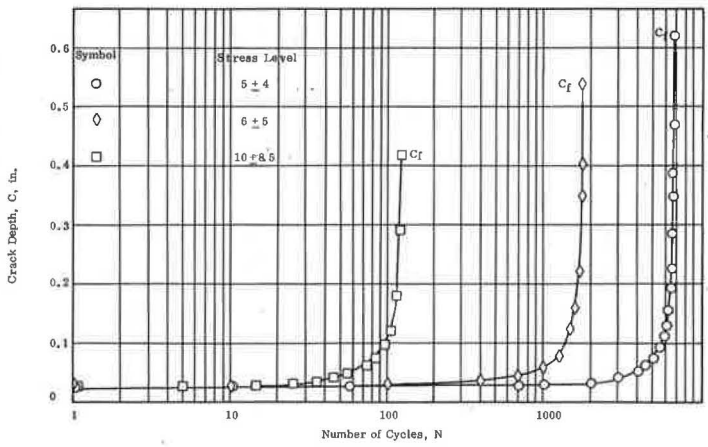

Figure 11. Crack depth versus number of cycles for 23 F from a computer solution of crack-growth law.

not be obtained experimentally for crack depths smaller than about 0.2 in. Assuming, however, that the law holds from the first loading cycle, then the "crack" depth at the first loading cycle is given by

$$c_o = c_f - \int_1^{N_f} AK^4 \, dN \tag{8}$$

where all the quantities on the right side are known. However, because K is a function of c, the solution of the integral is difficult; therefore, numerical methods utilizing computer programming were used. The crack depth, c_o, is referred to as the equivalent size of the most critical flaw or discontinuity that will propagate into a crack of engineering size. In this paper it is referred to as the starter flaw or the equivalent initial crack depth, c_o. Typical c-N curves extrapolated analytically to N = 1 are shown in Figure 11. The values obtained for c_o ranged from 0.007 to 0.13 in. with an average of 0.05 in.

PREDICTION OF FATIGUE LIFE

After the constants of the material, c_o, (A, n, K), and K_c, are determined, the fatigue life of a simply supported beam can be predicted for any stress level. In accordance with the foregoing concepts, the fatigue life is obviously the number of cycles for the starter flaw, c_o, to propagate into a crack of critical length, c_f. Thus the fatigue life, N_f, is given by

$$N_f = \int_{c_o}^{c_f} (1/AK^n) \, dc \tag{9}$$

where c_f can be obtained from

$$K_c^2 = \sigma_n^2 h \, f(c_f/d) \tag{10}$$

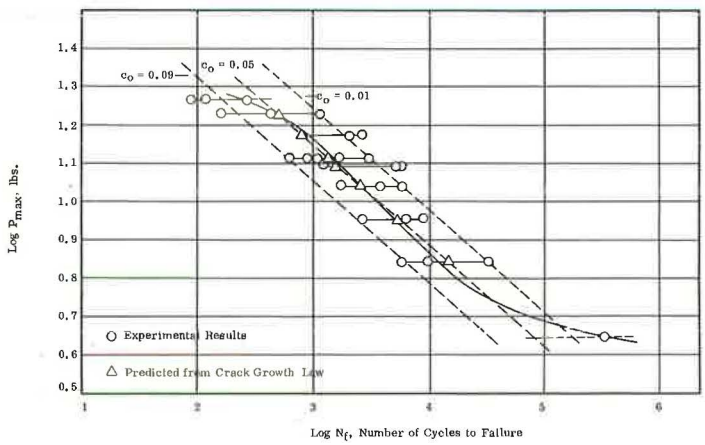

Figure 12. Relationship between P_{max} and N_f for 23 F.

Using the values

$c_o = 0.05$ in.,
$A = 5 \times 10^{-3}$,
$n = 4$, and
$K_c = 400$,

we calculated the fatigue lives from this equation by using numercial methods for evaluating the integral. Figure 12 shows the close agreement of the calculated values of the fatigue lives with those determined experimentally. Further research is being done to determine the variation of the constants of the materials at different temperatures and to study the applicability of the method in designing pavement systems.

SUMMARY AND CONCLUSIONS

In this paper the fatigue life of a bituminous paving mixture is expressed in terms of 3 parameter sets. These are K_c, the critical stress-intensity factor, which is the failure criterion; (A, n, K) that express the rate of crack growth; and c_o, the initial flaw size or starter flaw from which damage is initiated. The results presented indicate the following:

1. The rate of change of compliance (inverse slope of the load-deflection curve) with crack depth is in accordance with Irwin's equation, which is

$$dL/dc \propto K^2/P^2$$

where K is calculated from Winne and Wundt's equation.

2. The rate of crack growth follows Paris's law, $dc/dN = AK^n$, where A and n are material constants and $n = 4$.

3. The crack-growth law is used to analytically extrapolate the c-N curve to the point where $N = 1$ to obtain the starter flaw, c_o. This parameter is shown to be a constant of the material and is believed to be responsible for statistical variations in the fatigue life.

4. The fatigue life of bituminous paving mixtures may be predicted when all the constants of the material, such as c_o, (A, n, K), and K_c, and the variables load, geometry, and boundary conditions, which determine the stress-intensity factor, K, are known. The fatigue life may be expressed as

$$N_f = \int_{c_o}^{c_f} (1/AK^n)\,dc$$

where c_f is given by

$$K_c^2 = \sigma_n^2\, h\, f(c/d)$$

The comparison of experimentally observed fatigue lives and calculated values for simply supported beams is presented.

ACKNOWLEDGMENTS

The financial support for this study was provided by the Bureau of Public Roads, Federal Highway Administration, U. S. Department of Transportation. The opinions, findings, and conclusions expressed are those of the authors and not necessarily those of the Bureau of Public Roads.

REFERENCES

1. McEvily, A. J., Jr., Boettner, R. C., and Johnston, T. L. On the Formation and Growth of Fracture Cracks in Polymers. In Fatigue, an Interdisciplinary Approach, Proc., 10th Sagamore Army Mat. Res. Conf., Syracuse Univ. Press, N. Y., 1964.

2. McEvily, A.J., and Boettner, R.C. On Fatigue Crack Propagation in F.C.C. Metals. Acta Metallurgica, Vol. 11, 1963, p. 725.
3. Frost, N.E. The Growth of Fatigue Cracks. Proc., First Internat. Conf. on Fracture, Sendai, Japan, Vol. 3, 1965, p 1433.
4. Majidzadeh, K., Ramsamooj, D.V., and Fletcher, T.A. Analysis of Fatigue of Sand-Asphalt Mixtures. Paper presented at the annual meeting of Assn. of Asphalt Paving Technologists, 1969.
5. Paris, P., and Erdogan, F.J. A Critical Analysis of Crack Propagation Laws. Jour. Basic Engineering, Trans. ASME, Series D, Vol. 85, 1963, p. 528.
6. Paris, P.C. The Fracture Mechanic Approach to Fatigue. In Fatigue, an Interdisciplinary Approach, Proc., 10th Sagamore Army Mat. Res. Conf., Syracuse Univ. Press, N.Y., 1964.
7. Winne, D.H., and Wundt, B.M. Application of the Griffith-Irwin Theory of Crack Propagation to the Bursting Behavior of Discs, Including Analytical and Experimental Studies. Trans. ASME, Vol. 80, 1958, pp. 1643-1655.
8. Kauffmann, E.M. Analysis of Fracture Mechanics in Bituminous Materials. Ohio State Univ., Columbus, MS thesis, Dec. 1968.
9. Moavenzadeh, F. Asphalt Fracture. Proc., Assn. of Asphalt Paving Technologists, Vol. 36, 1967.
10. Bahgat, A.G., and Herrin, M. Brittle Fracture of Asphaltic Mixes. Paper presented at the annual meeting of the Assn. of Asphalt Paving Technologists, Feb. 1968.
11. Glucklich, J. Static and Fatigue Fractures of Portland Cement Mortar in Flexure. Proc., First Internat. Conf. on Fracture, Sendai, Japan, 1965.
12. Irwin, G.R. Fracture. In Encyclopedia of Physics, Vol. 6.

Effect of Particle Shape and Surface Texture on the Fatigue Behavior of Asphaltic Concrete

G. W. MAUPIN, JR., Virginia Highway Research Council

This paper reports a laboratory investigation of the effects of particle shape and particle surface texture on the fatigue behavior of an asphaltic surface mixture. The investigation was limited to one mixture tested in a constant-strain mode. Three aggregates were used in separate mixtures for the particle shape-fatigue comparisons: round gravel, limestone, an intermediate-shaped aggregate that was neither round nor slabby, and slabby slate. Two mixtures, one containing unetched limestone and the other etched limestone, were compared in the particle surface texture-fatigue study. Beams dimensioned to 2.5 by 3 by 14 in. were compacted from each mixture and tested in the laboratory. The fatigue life was defined by cracking of the beam surface and monitored by the resultant cracking of foil strips glued to the beam. The results of the constant-strain mode fatigue tests show that the mixture containing the slabby-shaped aggregates had a significantly shorter fatigue life than the mixture containing the rounded gravel. There was no significant difference between the fatigue life of the unetched limestone mixture and that of the etched limestone mixture. The data on rupture modulus versus number of cycles indicate that a linear relationship on a log-log plot existed for all mixtures containing aggregates with different shapes and surface textures. The curves are essentially parallel for all mixtures, and the unetched and etched limestone curves are essentially identical.

•FATIGUE IS A PHENOMENON by which the structure of a material is gradually weakened by repeated applications of stresses lower than its ultimate failure stress. On an asphaltic pavement, fatigue cracks and failures can be caused by moving wheel loads that produce alternating compressive and tensile flexural stresses on the upper and lower surfaces.

Fatigue cracks originally were not recognized as such but were considered to be mere "aging cracks" or pavement distress. In the last 2 decades researchers such as Hveem (1) have recognized fatigue failure caused by repeated flexing of asphaltic layers on highly resilient soil bases. Hveem's investigation, linking pavement failures, magnitude of deflection, and pavement stiffness, indicated that to be well designed a pavement must be capable of withstanding deflections or have sufficient stiffness to reduce the deflections to a permissible level.

Nijboer and Van Der Poel (2) also recognized there was a problem of fatigue failure in asphaltic pavements. They used a vibration machine to simulate road traffic on a test pavement, and measured deflections, strains, stresses, and stiffness moduli. They concluded that the observed pavement cracks were caused by bending stresses greater than the fatigue strength of the material. More recently, Kasianchuk, Monismith, and Garrison (3) developed a method in which a fatigue design subsystem is used to design the pavement structure against fatigue failure.

Paper sponsored by Committee on Mechanical Properties of Bituminous Paving Mixtures and presented at the 49th Annual Meeting.

The material variables that affect fatigue should be understood so that they may be considered when the asphaltic concrete components are selected. Some component variables that have been investigated are binder type (4, 5, 6, 7), binder hardness (8, 6), aggregate gradation (9), and aggregate type (10). The effect of aggregate type on fatigue behavior has not been investigated extensively. Because aggregates used in asphaltic mixes vary from site to site, depending on surface geology and general availability, it is important that the effects of aggregate types and characteristics on the serviceability of asphaltic concrete be understood.

This paper reports a limited laboratory investigation of the effect of aggregate shape and surface texture on the fatigue behavior of asphaltic concrete. In the investigation, beam specimens composed of asphaltic concrete containing aggregates with distinct shape and surface characteristics were tested in a constant-strain mode, the method of test believed to best describe the behavior of Virginia pavements showing fatigue distress.

APPROACH

The 3 aggregates selected for the shape study were (a) gravel, rounded, (b) an impure limestone, intermediate between the shape of slate and gravel, and (c) slate, flat and slabby. The 2 aggregates selected for comparison in the surface texture investigation were unetched impure limestone and etched impure limestone from the same source, the latter of which yielded a rough surface texture. The asphalt content selected was that yielding maximum flexural strength of the asphaltic concrete because this was thought to produce the most fatigue-susceptible mixture in the region of optimum asphalt content.

Each mix was tested in a constant-strain mode at its predetermined asphalt content, and the fatigue life was determined. The fatigue lives were compared statistically to determine if significant differences existed. Also, the static flexural strength was determined at several intervals between zero number of cycles and number of cycles yielding fatigue life to gain an indication of the progressive fatigue breakdown.

MATERIALS

The aggregates used in the investigation are shown in Figures 1, 2, and 3; their physical properties are given in Table 1. The flakiness index, given in Table 1, is a measure of the flatness and slabbiness of the aggregate with higher numbers indicating a flatter, slabbier aggregate.

A rough texture aggregate was obtained by soaking the limestone in 0.5 N HCl solution for 20 min. The 20-min etching time was selected because it produced surface

Figure 1. Coarse portion (⅜ to ½ in.) of aggregates used in particle-shape comparison.

Figure 2. Unetched limestone (5x magnification).

Figure 3. Etched limestone (4x magnification).

impurity protrusions that did not break off when the aggregate was mixed and handled.

An 85 to 100 penetration asphaltic cement having an average absolute viscosity of 1,405 poises at 140 F was used as the binder. All aggregates were separated and recombined to yield the desired gradations (Table 2). Table 2 also gives the gradations of the aggregates recovered from several of the beams after the binder was extracted; these data indicate that negligible breakup occurred during mixing and compaction of all the materials.

TABLE 1

PHYSICAL PROPERTIES OF AGGREGATE

Aggregate	Flakiness Index		Specific Gravity	Absorption (percent)	L.A. Loss (percent)	
	3/8 to 1/4 in.	1/4 in. to No. 4			B	C
Gravel	1.0	2.8	2.60	1.18	34.8	38.6
Limestone	30.2	30.3	2.72	0.60	23.5	30.1
Slate	56.1	57.4	2.79	0.40	23.9	21.7

TABLE 2

GRADATIONS OF ASPHALTIC MIXTURES BEFORE AND AFTER COMPACTION

Sieve	Percent Passing			
	Before Compaction	Gravel After Compaction	Limestone After Compaction	Slate After Compaction
1/2 in.	100	100	100	100
3/8 in.	90	90	89	88
No. 4	60	61	63	63
No. 8	45	47	48	47
No. 30	22.5	24	26	24
No. 50	14.5	15	18	17
No. 100	9	10	13	12
No. 200	5	6	9	9

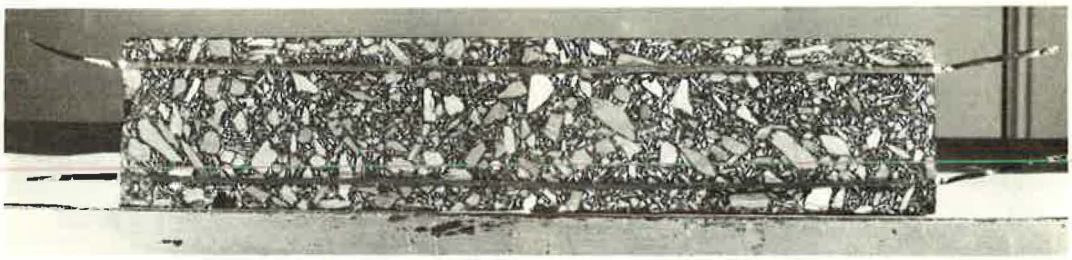

Figure 4. Aluminum foil strips on bottom of beam.

TESTING

The test specimens, 3 by 3 by 14 in. beams, were compacted on a modified California kneading compactor similar to the one used by Monismith (9). The beams were compacted in 3 equal layers with the application of 2 leveling passes, 2 passes at 181 psi foot pressure, and 2 passes at 250 psi foot pressure to each layer.

After the specimens had cooled to room temperature, the density and air void content were determined. Approximately $\frac{1}{4}$ in. was sawed from both the top and bottom of each beam to yield 2.5 by 3 by 14 in. specimens. The beams were sawed in order to eliminate surface texture effects and to decrease fatigue variability within a mix. They were allowed to age one week from the compaction date before testing.

Prior to fatigue testing, a $\frac{1}{8}$ in. aluminum foil strip was glued $\frac{1}{2}$ in. from each side on the bottom of each beam (Fig. 4). When the fatigue crack formed, both aluminum strips were broken; the machine stopped automatically, and the fatigue life was recorded.

In order to obtain the proper asphalt content for comparison of different mixes in the fatigue tests, the maximum flexural strength (modulus of rupture) was determined at 5 asphalt contents for each mixture. The beams, simply supported at the ends, were deflected at the center point at the rate of 0.5 in. per minute. A proving ring was used to record the maximum load applied, and the modulus of rupture was determined from the load data by the flexure formula, Mc/I, where M is the maximum moment in the beam, c is half the height of the beam, and I is the moment of inertia. The asphalt content that yielded the greatest modulus of rupture was selected.

The constant-deflection fatigue tests were performed on the apparatus shown in Figure 5. The beam was simply supported and loaded at the center point, with care being taken to provide sufficient bearing area to prevent deformation of the beam under load repetition. The beam was sandwiched between $\frac{1}{8}$ in. aluminum sheets and $\frac{1}{16}$ in. neoprene sheets to help distribute the load and also to allow longitudinal movement under the flexing action.

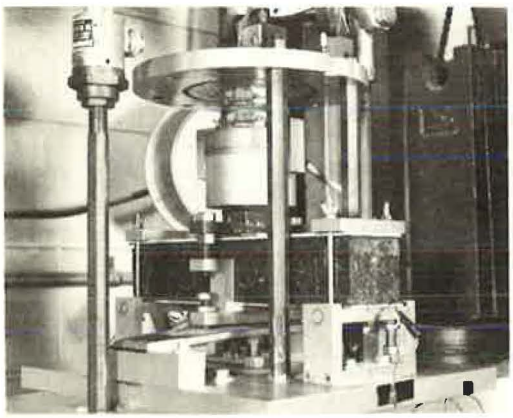

Figure 5. Constant-deflection flexural fatigue testing device.

The load was transferred directly through a yoke surrounding the asphaltic beam to a 13 in. leaf spring beneath, and only the load necessary to deflect the beam was transferred from the yoke to the beam. The yoke was used around the beam to prevent compaction due to transferring the load directly through the beam to the spring. A stop was installed under the spring to limit the deflection to the desired amount, although the load was usually decreased as the beam weakened.

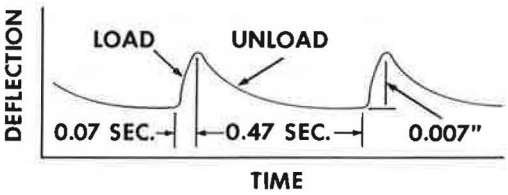

Figure 6. Deflection time-curve.

The load mechanism consisted of an air cylinder activated by a dc solenoid valve. The air pressure entering the cylinder could be regulated to obtain the desired load. The deflection was set at 0.007 in. for each beam and checked with a LVDT unit connected to the load shaft. A typical section from the recorder chart is shown in Figure 6; the load time was 0.07 sec, and the unload time was 0.47 sec.

After the beams had failed, they were tested in simple flexure to determine the flexural strength (modulus of rupture) and breakdown caused by cycle repetition. Also the modulus of rupture was obtained on beams subjected to an intermediate number of cycles to get enough points to plot a curve.

DISCUSSION OF RESULTS

Asphalt Content

The asphalt contents indicated by the maximum flexural strength were 5.0, 6.0, 5.5, and 5.75 percent for gravel, slate, unetched impure limestone, and etched impure limestone respectively. These results seemed reasonable because the rougher and more irregular aggregates required more asphalt than did the smooth aggregate (gravel).

Influence of Particle Shape

The average fatigue lives were 208,299 for gravel, 103,958 for unetched impure limestone, and 52,728 for slate (Table 3). An analysis of variance indicated that there was a significant difference at a 90 percent confidence level between the gravel and slate, the aggregates with round and flat shapes respectively. The flexural strength tests also revealed that the slate produced a mixture that was 20 percent stiffer than the gravel mixture. These results are logical because it is generally agreed that fatigue life decreases

TABLE 3

FATIGUE LIFE AND STRENGTH DATA

Material	No. of Specimens	No. of Cycles	Fatigue Life Standard Deviation (cycles)	Modulus of Rupture (psi)	Modulus of Rupture Standard Deviation (psi)
Gravel	4	208,299[a]	129,899	123	14
	4	156,226	—	109	7
	4	104,150	—	117	26
	4	52,075	—	122	18
	4	0	—	178	13
Unetched limestone	7	103,958[a]	57,151	111	20
	4	92,506	—	96	19
	4	61,671	—	107	15
	4	30,855	—	95	5
	4	0	—	137	22
Etched limestone	8	108,470[a]	106,823	104	12
	4	88,852	—	106	10
	4	54,235	—	85	19
	4	27,118	—	97	14
	4	5,424	—	94	10
	4	0	—	125	7
Slate	4	52,728[a]	28,562	146	13
	4	39,546	—	124	70
	4	26,364	—	131	56
	4	13,182	—	134	16
	4	0	—	214	11

[a]Average fatigue life.

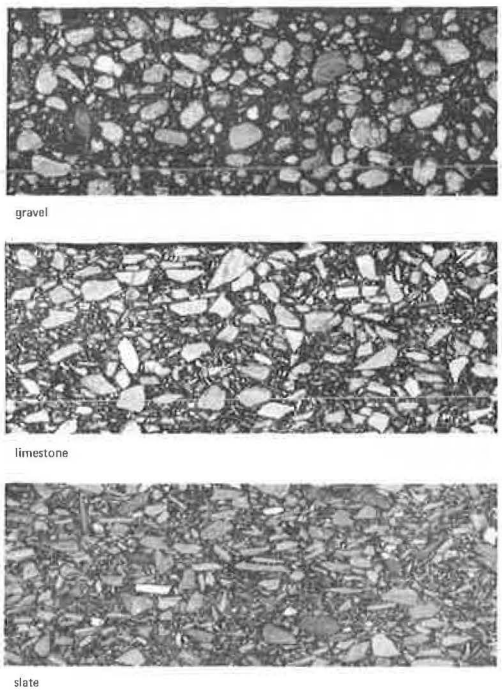

Figure 7. Sawed cross sections of beams.

when stiffness increases for fatigue tests in the constant-strain mode (11).

Sawed cross sections of all mixtures revealed that the slate particles had an interlocking structure but the gravel particles were "floating" in the bitumen-fines matrix (Fig. 7). Thus equal strains in both mixtures would tend to produce higher stresses in the bitumen between the interlocked particles (slate mixture), and the fatigue life would be lower.

The results indicate that the gravel mixture had a longer fatigue life than the crushed slate mixture, but Monismith (10) found that a crushed stone mixture had a longer fatigue life than a gravel mixture. This seeming disagreement of results can possibly be explained by the fact that the crushed stone mixture tested by Monismith had considerably more air voids than the gravel mixture, resulting in a more flexible mix and increased fatigue life. The mixes in the present study had approximately equal quantities of air voids.

The plot of the strength (modulus of rupture) versus strain repetitions for the 3 mixtures on a log-log scale reveals a parallel linear relationship (Fig. 8). If the specimens had been tested past the crack formation stage, the strength probably would have decreased at a much faster rate, which would have resulted in a nonlinear curve after crack formation.

Careful examination of the points (average of 4 or more individual measurements) on each curve leaves the impression that there was a slight increase of strength at failure.

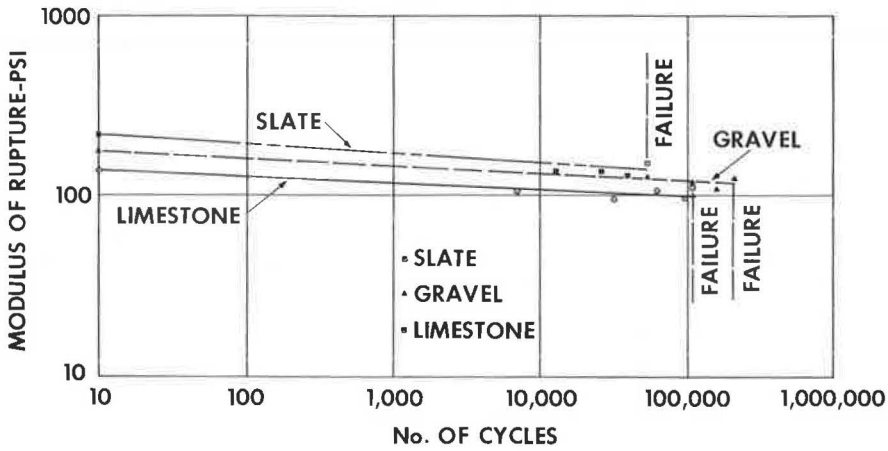

Figure 8. Strength-fatigue curves for asphaltic mixtures containing different shaped aggregates.

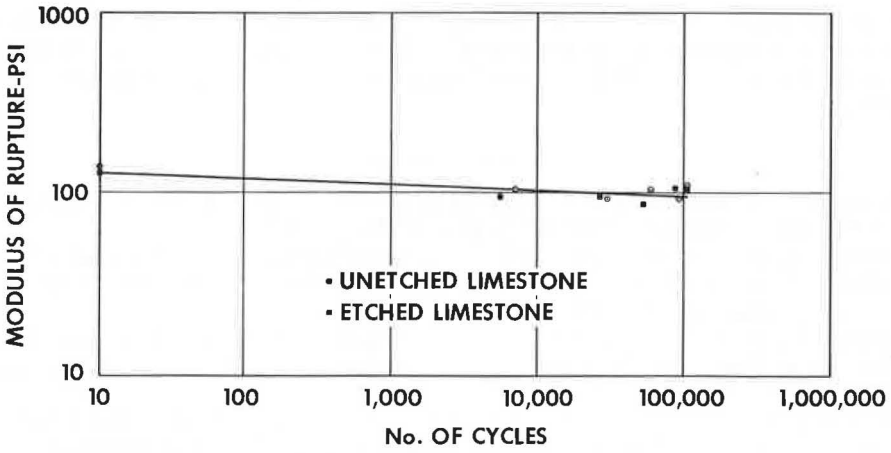

Figure 9. Strength-fatigue curves for asphaltic mixtures containing etched and unetched limestone.

Variability caused some beams to fail before the average number of cycles to failure. This means that some of the beams tested to give intermediate points on the curve failed before reaching the specified number of cycles. Because the strength decreases at a faster rate after failure, those specimens cycled past failure lowered the average strength value of the intermediate points below the linear value and produced an apparent rise in strength of the failure specimens.

Influence of Particle Surface Texture

The fatigue lives of the unetched and etched impure limestones were 103,958 and 108,470 cycles respectively. There was no statistical difference in the 2 values; therefore, it appears that a slight increase in surface roughness (etched) does not affect the fatigue life significantly. Jimenez and Gallaway (8) observed a difference between the fatigue life of a mixture made with rough textured aggregates and that of a mixture made with smooth aggregates. The degree of roughness of the aggregates was not well defined, and the test used was a constant-stress type; therefore, the results cannot be compared to those of this investigation. This does point out, however, that a sufficiently rough aggregate surface texture can have an effect on fatigue life.

Also the flexural strength (modulus of rupture) versus strain repetitions are essentially identical (Fig. 9). The variability of the fatigue results of the etched limestone was extremely high; however, this variability could have been caused by the irregular nature of the material.

SUMMARY

Although this investigation was rather limited, it yielded a good indication that particle shape can significantly affect the fatigue life of an asphaltic mixture in the constant-strain mode test. The mixture containing slabby particles had a significantly shorter fatigue life than the mixture containing equidimensional rounded particles. Examination of the matrix displayed in the cross sections of the sawed beams confirmed that lower stresses would be developed in the gravel beams than in the slate beams, which would result in a longer fatigue life for the gravel mixes. The slabby particle mixture also had a higher stiffness than the gravel mixture, which is indicative of a lower fatigue life for a constant-strain test (11).

The fatigue lives of the unetched limestone and etched limestone (rough surface texture) asphaltic mixtures were not significantly different.

A linear relationship exists between the logarithm of flexural strength (modulus of rupture) and the logarithm of the number of cycles of constant deflection for all materials tested. These relationships were essentially parallel (i.e., the slopes were equivalent).

REFERENCES

1. Hveem, F. N. Pavement Deflections and Fatigue Failures. Design and Testing of Flexible Pavement, HRB Bull. 114, 1955, pp. 43-87.
2. Nijboer, L. W., and Van Der Poel, C. A Study of Vibration Phenomena in Asphaltic Road Constructions. Proc., Assn. of Asphalt Paving Technologists, Vol. 22, 1953, pp. 197-237.
3. Kasianchuk, D. A., Monismith, C. L., and Garrison, W. A. Asphalt Concrete Pavement Design—A Subsystem to Consider the Fatigue Mode of Distress. Highway Research Record 291, 1969, pp. 159-172.
4. Monismith, C. L. Effects of Temperature on the Flexibility Characteristics of Asphaltic Paving Mixtures. Symposium on Road and Paving Materials, American Society for Testing and Materials, Philadelphia, STP 277, 1960, pp. 89-108.
5. Monismith, C. L. Asphalt Mixture Behavior in Repeated Flexure. California Div. of Highways and Univ. of California, IER Rept. TE-64-2, 1964.
6. Monismith, C. L. Asphalt Mixture Behavior in Repeated Flexure. California Div. of Highways and Univ. of California, IER Rept. TE-63-2, 1963.
7. Gregg, L. E., and Alcoke, W. H. Investigations of Rubber Additives in Asphalt Paving Mixtures. Proc., Assn. of Asphalt Paving Technologists, Vol. 23, 1954, pp. 28-60.
8. Jimenez, R. A., and Gallaway, B. M. Preliminary Report of an Apparatus for the Testing of Asphaltic Concrete Diaphragms. Proc., Assn. of Asphalt Paving Technologists, Vol. 31, 1962, pp. 477-498.
9. Monismith, C. L. Flexibility Characteristics of Asphaltic Paving Mixtures. Proc., Assn. of Asphalt Paving Technologists, Vol. 27, 1958, pp. 74-106.
10. Monismith, C. L. Asphalt Mixture Behavior in Repeated Flexure. California Div. of Highways, Rept. TE-65-9, Nov. 1965.
11. Finn, F. N. Factors Involved in the Design of Asphaltic Pavement Surfaces. NCHRP Rept. 39, 1967.

Time and Load Independent Properties of Bituminous Mixtures

S. A. SWAMI, West Virginia Institute of Technology; and
W. H. GOETZ and M. E. HARR, Purdue University

This paper presents a new approach to characterize the time-dependent behavior of asphaltic concrete by a transfer function that is derived from the frequency response of the material, using sinusoidal loading tests. The ratio of the Laplace transform of the output to the Laplace transform of the input to any system is defined as the transfer function of the system between the input and the output. The transfer function is a function of the complex variable $s = j\omega$, where ω is the frequency of the input and j is the imaginary unit. In this study asphaltic concrete was treated as a damped, linear system in which the applied force f(t) was the input and the resulting displacement x(t) was the output. Both the input and output were functions of time. By varying the frequency of the input, the output-input magnitude ratio was obtained for each frequency, and its plot against log frequency yielded the frequency spectrum. Also, the time lag between the output and the input was noted from which the phase angle was calculated. A simple geometric technique to obtain the transfer function directly from the frequency spectrum was used in this investigation. This technique was applied to the results of the test specimens of asphaltic concrete cut from laboratory compacted beams of 2 different compositions tested at 3 temperatures. It is shown that the transfer function for bituminous concrete thus derived from a dynamic test can be used to predict the displacement of the test specimen subjected to a static load by treating the latter as a step function of time and through the use of Laplace inverse transform. The excellent agreement between the calculated and measured values of the displacements indicates that the transfer function represents a material property that is independent of load input. The concept of transfer function makes it possible to represent the time-dependent behavior of asphaltic concrete by a fourth order linear differential equation with constant coefficients without assuming any spring-dashpot model. The coefficients can be computed from the roots of the denominator and numerator of the transfer function.

•THEORETICAL DEVELOPMENTS in the stress-displacement behavior of asphaltic concrete in a pavement structure are very restricted in their applicability to represent actual field conditions because of the complexity of asphaltic concrete as a structural material and the complicated interaction with the other structural layers. A rigorous theoretical solution to a typical boundary value problem in pavement mechanics must satisfy the equations of equilibrium (or motion), compatibility equations (or some other form of conservation equation), boundary conditions, and initial conditions. The development of such a solution requires the use of some form of stress-displacement-time relation for the material, and it is this aspect that specifies the solution for a particular

Paper sponsored by Committee on Mechanical Properties of Bituminous Paving Mixtures and presented at the 49th Annual Meeting.

medium. At present, there are no satisfactory constitutive relations available for pavement materials, both asphaltic concrete and soils, and this is perhaps the greatest impediment to realistic theoretical solutions of the response of pavement systems to applied loads, dynamic or static.

Having the ultimate objective to design such layered pavement structures, the theory of linear viscoelasticity has been widely used for the evaluation of pavement components as well as for understanding their response to varied loading conditions. Layered systems were not, however, analyzed using time-dependent (viscoelastic) material properties until after the development of the correspondence principle for isotropic media in 1955 by Lee (1) and shortly thereafter the extension by Biot (2) to include anisotropic media. Stress and strain for linear viscoelastic materials can be related by either differential or integral linear operators. The differential operator form of the stress-strain law is most commonly used and, as Biot (3) has pointed out, may be visualized as a combination of springs and dashpots. More general methods of viscoelastic stress analysis have been described by Lee (4) and Lee and Rogers (5).

Pister and Monismith (6) have applied the basic differential equation for the 3-element model to the solution of a viscoelastic beam on an elastic foundation. Pister (7) has considered the solution of a viscoelastic plate on a viscoelastic foundation. Other literature (8, 9, 10) also exists in limited quantity dealing with viscoelastic slabs or foundations in various ways. Harr (11) used a 2-element model to show the influence of vehicle speed on pavement deflection. The usefulness of these methods is restricted to the extent of the realistic representation of the viscoelastic characteristics of the materials of the pavement structure in the numerical analysis.

The study of viscoelastic characteristics of bituminous mixtures has been the object of many research workers, and here again spring-dashpot models have been generally made use of. By using a Burger's model, Wood and Goetz (12) found that the behavior of a sheet asphalt mixture obeyed the laws of linear viscoelasticity for limited stresses and small deformations. Secor and Monismith (13) observed that the 4-element model, suggested by Kuhn and Rigden (14), was capable of representing the displacement of an asphaltic concrete only to a limited extent.

Dynamic tests, such as those employing sinusoidal loading, have been used to study the viscoelastic response of asphaltic concrete by some investigators (15, 16, 17). They have attempted to characterize the viscoelastic response by using the phase angle and the complex elastic modulus, obtained from the input-output traces of the dynamic tests. However, these parameters are not easily adaptable for numerical analysis. Besides, they are functions of the input load, which seriously limits the ability of these parameters to truly represent the load response characteristics of the material.

This motivated the authors to search for a parameter or parameters or a function that can represent the viscoelastic response of the material under any load and that, at the same time, is independent of the type and magnitude of the input load. Such a function should necessarily be time-dependent and should be used as the material characteristic for both static and dynamic loads. A study of the literature reveals that transfer functions are frequently used to characterize a dynamic system in electrical and mechanical engineering problems (18, 19, 20, 21, 22, 23). While serving as a link between the time-dependent input and output of the system, the transfer function completely describes its dynamic response. Hence, it was attempted to investigate the feasibility of applying the concept of transfer functions to describe the response of bituminous mixtures to dynamic and static loads. This paper presents a method of obtaining the transfer function for a given bituminous concrete from laboratory tests and studies the extent to which this function can represent the viscoelastic characteristics of the material. Effects of mix type, temperature, and anisotropy on the transfer function were studied with a view to providing insight into this function. It is hoped that this insight may facilitate the development of more refined methods for the structural design of pavements.

It is assumed in this investigation that asphaltic concrete behaves as a linear system. Although it has been recognized that the behavior of this material is nonlinear, particularly at higher stress levels and at higher temperatures, the investigations of Busching, Goetz, and Harr (24) and others (15, 25) have established the validity of this assumption for small displacements normally encountered in bituminous mixtures.

CONCEPT OF TRANSFER FUNCTION

Figure 1. The transfer function.

The ratio of an operational output (Laplace transform of the output) of a dynamical system to the operational input (Laplace transform of the input) is called the transfer function between the operational input and its corresponding output. The transfer function is shown schematically in Figure 1. It is by definition a function of the complex variable s.

If a rigid body is subjected to a dynamical force f(t), then the force and the resulting displacement x(t) can be considered as the input and output respectively for the dynamic system. The transfer function between the operational force and the operational displacement is given by

$$G(s) = \frac{\bar{x}(s)}{\bar{f}(s)} \tag{1}$$

where $G(s)$ = the transfer function,
$\bar{x}(s)$ = Laplace transform of the output, $\mathcal{L}[x(t)]$, and
$\bar{f}(s)$ = Laplace transform of the input, $\mathcal{L}[f(t)]$.

Solving for $\bar{x}(s)$,

$$\bar{x}(s) = G(s)\bar{f}(s) \tag{2}$$

The inverse transform of $\bar{x}(s)$ is x(t) and is

$$x(t) = \mathcal{L}^{-1}\left[G(s)\bar{f}(s)\right] \tag{3}$$

Equation 3 shows that, once the transfer function G(s) is known for any system, the displacement x(t) can be evaluated for that system for another given input force f(t).

In general, the transfer function G(s) is a ratio of 2 polynomials in s, such as

$$G(s) = \frac{N(s)}{D(s)} = \frac{(s - a_1)(s - a_2) \ldots (s - a_n)}{(s - b_1)(s - b_2) \ldots (s - b_m)} \tag{4}$$

where a_i's and b_i's are the roots or zeros of the numerator N(s) and denominator D(s) of G(s) respectively. The b_i's are also called the poles of G(s) because the transfer function becomes infinite when evaluated at a zero of its denominator. That is,

$$G(b_i) = \infty \tag{5}$$

Substituting for G(s) in Eq. 2, $\bar{x}(s)$ can be rewritten as

$$\bar{x}(s) = \frac{\bar{f}(s)(s - a_1)(s - a_2) \ldots (s - a_n)}{(s - b_1)(s - b_2) \ldots (s - b_m)} \tag{6}$$

Equation 6 can be expanded in m partial fractions for the m roots of D(s) as

$$\bar{x}(s) = \frac{C_1}{(s - b_1)} + \frac{C_2}{(s - b_2)} + \ldots + \frac{C_m}{(s - b_m)} \tag{7}$$

which is an identity in s where C_1, C_2, ..., C_m are constants independent of s. Using the Laplace inverse transform, the final solution for x(t) is obtained from Eq. 7 as

$$x(t) = C_1 e^{b_1 t} + C_2 e^{b_2 t} + \ldots + C_m e^{b_m t} \tag{8}$$

From this discussion it is obvious that once the transfer function for a system is known, the displacement x(t) of the system for a given force input f(t) can be evaluated theoretically.

DETERMINATION OF THE TRANSFER FUNCTION

The experimental basis to determine the transfer function for a test specimen is the frequency spectrum, which, in turn, may be obtained from sinusoidal input-output data of the test specimen (23). The plot of the amplification (that is, the ratio of the output magnitude to the input magnitude) against the test frequency is the frequency spectrum, and for convenience the magnitude of the amplification is plotted in decibels ($R_{db} = 20 \log_{10} R$). The frequency spectrum is approximated with a series of connected straight lines so as to form asymptotes to the curve (Fig. 2). The intersections of the asymptotes determine the corner frequencies. The modified transfer function is then obtained (26) as a function of the slopes of the asymptotes and their corner frequencies as

$$G(j\omega) \cong A(j\omega + \omega_1)^{\frac{k_1}{6}} (j\omega + \omega_2)^{\frac{k_2-k_1}{6}} (j\omega + \omega_3)^{\frac{k_3-k_2}{6}} \ldots (j\omega + \omega_n)^{\frac{k_n-k_{n-1}}{6}} \tag{9}$$

The modified transfer function is the vector amplification or simply the ratio of the magnitude of the output to that of the input and is a function of the input frequency. By substituting $s = j\omega$ in Eq. 9, the transfer function for the system is obtained.

$$G(s) \cong A(s + \omega_1)^{\frac{k_1}{6}} (s + \omega_2)^{\frac{k_2-k_1}{6}} (s + \omega_3)^{\frac{k_3-k_2}{6}} \ldots (s + \omega_n)^{\frac{k_n-k_{n-1}}{6}} \tag{10}$$

The constant A can easily be determined from any one experimental frequency in the frequency spectrum by calculating the absolute value of the transfer function from Eq. 9 at that frequency and equating it to the corresponding amplification value in the frequency spectrum.

In approximating the frequency spectrum, the slopes of the asymptotes are generally taken to be 6 decibels per octave for greater ease of determination, although straight

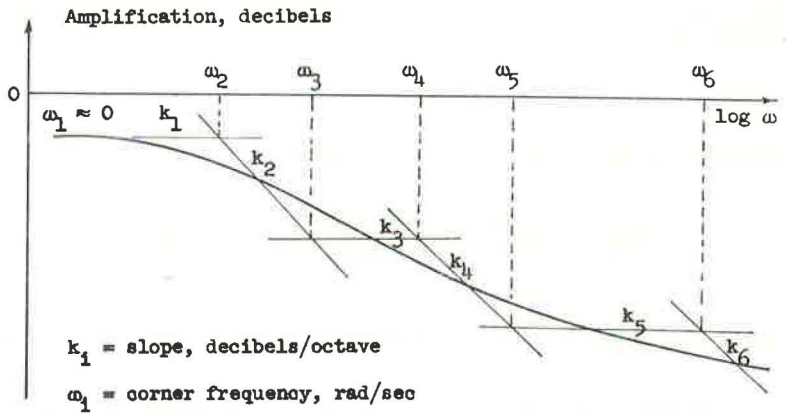

Figure 2. Asymptotic approximation of a frequency spectrum.

lines of any slope may be used. (An octave is defined as the frequency range for which the ratio of the upper bound frequency to the lower bound frequency is 2 to 1; that is, $\omega_i < \omega < 2\omega_i$ is an octave.) The closer the approximation is to the actual frequency spectrum curve, the better will be the approximation of the transfer function being sought.

EXPERIMENTAL INVESTIGATION

The experimental phase of this study had as an objective the development and use of accurate techniques for obtaining all of the data required in the determination of the transfer function from a frequency spectrum. The core of the technique lies in devising a system that can apply a sinusoidal force input of a desired magnitude and frequency and that can simultaneously measure the displacement output.

An MTS electronic function generator coupled with a loading frame that was fitted

Figure 3. Function generator.

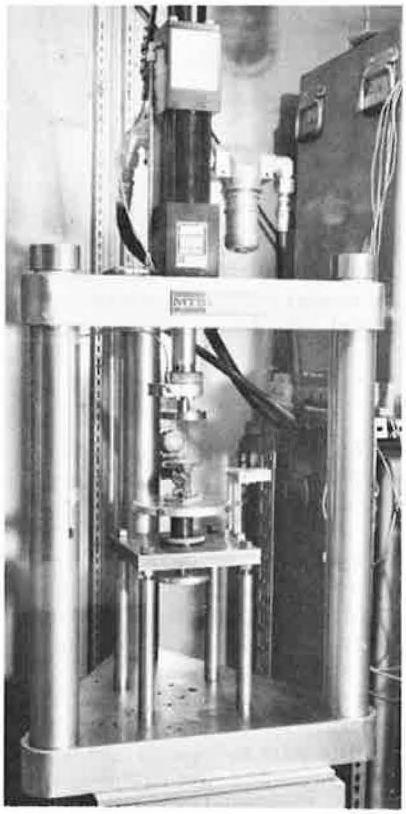

Figure 4. Loading frame.

Figure 5. Specimen in position for testing.

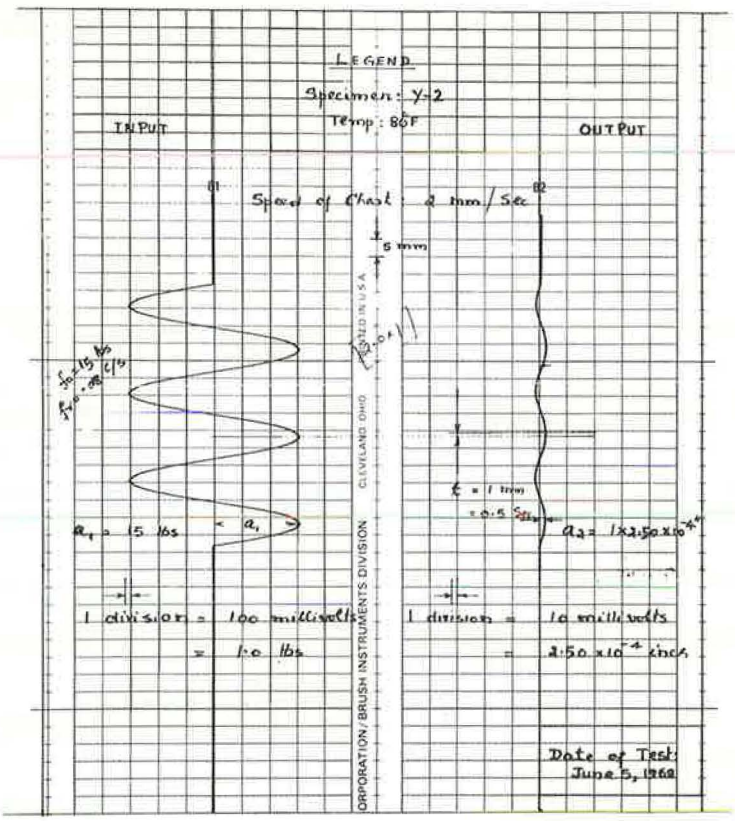

Figure 6. Typical traces of a sinusoidal loading test.

with an electronically controlled hydraulic actuator was used for this purpose (Figs. 3 and 4). The loading frame was installed in a constant temperature room that facilitated carrying out the tests at the desired temperatures. A 2-channel Brush recorder that was attached to the function generator recorded the input and output of the test specimen simultaneously.

Dynamic Tests

The function generator was used to apply sinusoidal force inputs to the asphaltic concrete specimen by suitable manipulation of the controls. The magnitudes of the force varied from 2.5 to 15 lb and the frequencies varied from 0.0016 to 1.6 cycles per second.

Because in a sine test the specimen is alternatively in compression and in tension, the method of mounting the specimen in the test assembly was of paramount importance. Two aluminum plates, 2 by 2 by $\frac{3}{8}$ in. in size, were glued to the specimen top and bottom respectively, using commercially available Eastman 910 adhesive. The plates, in turn, were connected to the top and bottom platens by screws and nuts. The top platen was rigidly fixed to the moving ram of the hydraulic actuator while the bottom platen was fixed to the loading deck (Fig. 5). Remotely controlled and commanded by the electronic console of the function generator, the hydraulic ram moves up and down at the preset sine force and frequency. Thus the specimen was subjected to the desired sinusoidal force input that was recorded by the left channel of the Brush recorder. The corresponding displacement of the specimen was sensed by the LVDT in the actuator

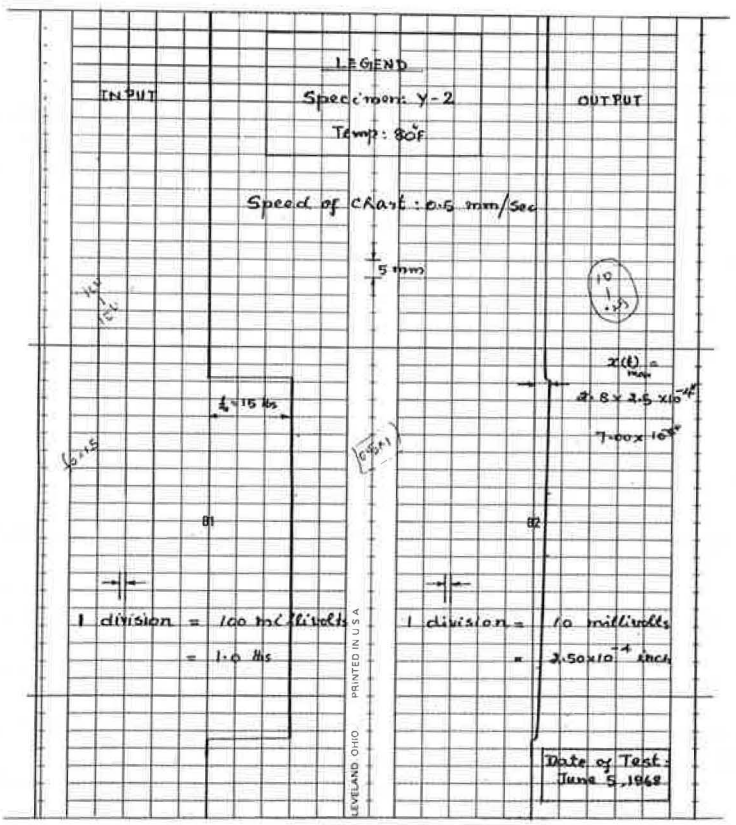

Figure 7. Typical traces of a static compression test.

and was simultaneously recorded as the output in the right channel of the recorder. Figure 6 shows the 2 traces thus obtained in a typical dynamic test.

Static Tests

The same test assembly that was used for the dynamic tests was used for the static tests. When the function generator is set for a combination of a ramp function and a high frequency, the actuator applies a static compressive force of desired magnitude. As before, the left and right channels recorded the input and output respectively. The 2 traces of a typical static compression test are shown in Figure 7.

Materials and Preparations of Specimens

Two different gradings, one with a maximum size of the No. 4 sieve and the other the $\frac{3}{8}$-in. sieve, were used in this investigation. The bituminous mixes prepared on the basis of these gradings were designated as mix 1 and mix 2 respectively. A 60 to 70 penetration asphalt cement was used. The mix was compacted into beams 2 by $2\frac{1}{2}$ by 12 in., from which test specimens 1 by 1 by 2 in. were cut along the x, y, and z axes of the beam, x being the longest axis and z the vertical axis. The specimens were designated as x-1, y-1, z-1, x-2, y-2 and z-2, the letter denoting the axis along which it was cut and the numeral the mix. The details of obtaining the specimens are given in another report (26).

DISCUSSION OF RESULTS

Frequency Response of Asphaltic Concrete

In most of the dynamic tests a magnitude of 10 lb was employed for the sinusoidal load input for frequencies covering 3 decades, varying from 0.01 radians per sec to 10.0 radians per sec (rad/sec). These were observed to be respectively the slowest and the fastest frequencies to which the test specimens were responsive. The input magnitude and the output displacement were recorded in pounds and inches respectively. Also, both of them were recorded in millivolts (mv).

The ratio of the output to the input expressed in decibels (also referred to as amplification or gain) plotted against log frequency gives the desired frequency spectrum. The phase lag or simply the phase angle for each frequency was also computed from

$$\phi = \omega t \tag{11}$$

where ϕ = the phase angle in radians,
ω = the test frequency in rad/sec, and
t = time lag between input and output in seconds.

The phase angle is also plotted against log frequency. The 2 plots together represent the frequency response of the test specimen completely.

Table 1 shows typical test results for a dynamic test, and Figure 8 gives the frequency response for the same test. It is seen that the displacement of the specimen is largest at the slowest frequency and is least at the fastest frequency. Thus the gain continuously falls with increase in frequency, and this indicates the overdamped nature of the test specimen.

The phase angle increases with increase in frequency in the first decade of test and then decreases so that a bell-shaped curve results when phase angle is plotted against frequency. The peak has, in general, been observed to occur in the region of 0.05 to 0.1 rad/sec. These results substantiate the observations of Pagen and others who have studied the dynamic response of bituminous concrete in sinusoidal testing (15, 16, 17).

Form of the Transfer Function

Table 2 shows a set of typical transfer functions obtained for the specimens tested at 80 F, from which it is seen that the transfer function derived for each individual case

TABLE 1

RESULTS OF A TYPICAL SINUSOIDAL TEST OF SPECIMEN Z-1 AT TEST TEMPERATURE 80 F

ω	a_1	a_2	$R = \frac{a_2}{a_1}$	R_{db}	t	ϕ	
						rad	deg
0.025	1000	22.0	0.0220	-33.1520	15.30	0.382	21.8
0.050	1000	19.5	0.0195	-34.4240	8.32	0.416	23.9
0.100	1000	17.0	0.0170	-35.3920	4.15	0.415	23.8
0.250	1000	11.0	0.0110	-39.1720	1.50	0.375	21.5
0.500	1000	9.0	0.0090	-40.9160	0.68	0.340	19.5
1.000	1000	8.0	0.0080	-41.9380	0.311	0.311	17.8
2.500	1000	6.5	0.0065	-43.7420	0.110	0.271	15.5
5.000	1000	5.0	0.0050	-46.0200	0.046	0.230	13.2
10.000	1000	4.0	0.0040	-47.9580	0.021	0.210	12.0

Note: ω = input frequency, rad/sec,
a_1 = input magnitude, mv,
a_2 = output magnitude, mv,
$R = a_2/a_1$,
R_{db} = R expressed in decibels = $20 \log_{10} R$,
t = time lag between input and output, sec, and
ϕ = phase lag between input and output = ωt radians.

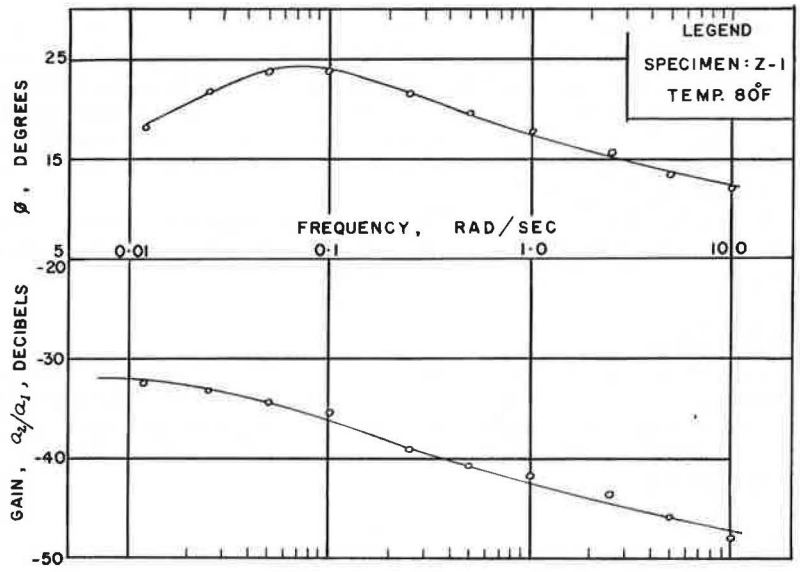

Figure 8. Typical frequency response curve.

is of the form

$$G(s) = \frac{A(s + a_1)(s + a_2)(s + a_3)}{(s + b_1)(s + b_2)(s + b_3)(s + b_4)} \qquad (12)$$

where A is a constant and a_i's and b_i's are the corner frequencies previously defined and obtained in the process of approximating the frequency spectrum with asymptotes. The significant feature of this form of the transfer function is that the factors in both the numerator and denominator are to first power. It may be recalled that this is due to the geometric procedure followed in approximating the frequency spectrum with asymptotes of slopes of 6 decibels per octave. It was also mentioned that any slope can be used, in which case it is obvious from Eq. 10 that the transfer function may contain fraction powered or higher powered terms in either the numerator or the denominator or both. This form is not desirable because the resulting transfer function will be too difficult or even impossible to handle through Laplace transforms.

From the procedure followed in approximating the frequency spectrum with asymptotes, it is obvious that the number of factors in the numerator and denominator of the transfer function in Eq. 12 depends on the number of asymptotes used to approximate the frequency spectrum. It was found from the analysis of the experimental results that the transfer function obtained using 8 asymptotes was accurate enough for practical purposes.

TABLE 2

TRANSFER FUNCTIONS AT 80 F

Specimen	Transfer Function
z-1	$G(s) = \frac{(0.05)(s + 0.025)(s + 0.2)(s + 2)}{(s + 0.02)(s + 0.1)(s + 1)(s + 10)}$
x-1	$G(s) = \frac{(0.0415)(s + 0.028)(s + 0.17)(s + 1.8)}{(s + 0.02)(s + 0.1)(s + 1)(s + 10)}$
y-1	$G(s) = \frac{(0.04)(s + 0.025)(s + 0.16)(s + 2.3)}{(s + 0.02)(s + 0.1)(s + 1)(s + 10)}$
z-2	$G(s) = \frac{(0.04)(s + 0.025)(s + 0.16)(s + 2.3)}{(s + 0.02)(s + 0.1)(s + 1)(s + 10)}$
x-2	$G(s) = \frac{(0.0415)(s + 0.028)(s + 0.17)(s + 1.8)}{(s + 0.02)(s + 0.1)(s + 1)(s + 10)}$
y-2	$G(s) = \frac{(0.0415)(s + 0.028)(s + 0.17)(s + 1.8)}{(s + 0.02)(s + 0.1)(s + 1)(s + 10)}$

Effect of Mix Type on Transfer Function

The 2 different bituminous mixes studied in this investigation were quite dissimilar in their aggregate gradings

and in their binder contents, namely, 5.0 and 3.5 percent by weight of aggregate for mix 1 and mix 2, respectively. However, it is apparent from Figure 9 that there was no appreciable difference in the transfer functions of the specimens, irrespective of their composition or orientation when tested at any one temperature. Even though the grading and asphalt content were different for the 2 mixes, their density-void ratio characteristics were similar, namely 142.6 lb/cu ft and 6.5 percent for mix 1 and 142.0 lb/cu ft and 8.5 percent for mix 2.

It can be anticipated that density will have a marked influence on the response to loading of a given mix and hence on its transfer function. However, more work is necessary to study the effect of this and other mix variables.

Effect of Specimen Orientation

It was pointed out earlier that for each mix 3 specimens were cut along 3 mutual perpendicular directions, designated x, y, and z. Figure 9 shows that there is not much difference in the transfer functions of the differently oriented specimens of either mix at any one temperature. This suggests that effect of anisotropy, if any, is not reflected in the transfer function.

Effect of Temperature

The experiments in the present investigation were conducted at 70, 80, and 90 F. By examining the absolute value curves in Figure 9, it is readily seen that temperature plays an important role in the transfer function of any specimen. Asphalt cement being thermoplastic, the asphaltic concrete specimen will yield increased displacements for increases in temperature at a given stress level. This results in a decrease in viscosity of the binder in the asphaltic concrete as temperature increases. Thus the output-input ratio for a constant input at any frequency will increase with decrease in viscosity or increase in temperature. This is precisely what is shown by the curves.

Examination of the transfer functions revealed that, for a given specimen, the various factors in the numerator and denominator do not seem to vary much with change in temperature, but that the coefficient A varies appreciably. It would be of interest to study this change in A with reference to the viscosity of asphalt cement or the asphalt cement-filler matrix.

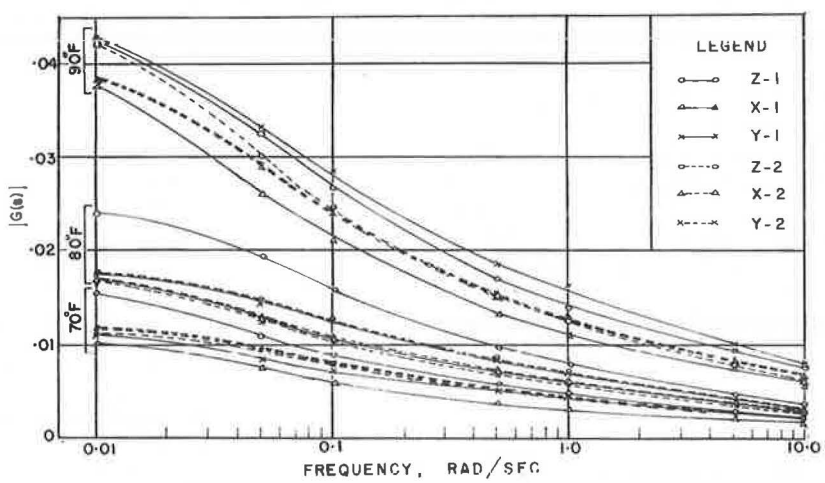

Figure 9. Curves of $|G(s)|$ versus frequency.

Effect of Specimen Size on Transfer Function

Frequency-response tests were conducted on 3 different-sized specimens with constant height-width ratio using mix 1 at 90 F. They were cut along the same direction in the compacted beam. The large, medium, and small sizes were $1\frac{1}{4}$ by $1\frac{1}{4}$ by $2\frac{1}{2}$ in., 1 by 1 by 2 in., and $\frac{3}{4}$ by $\frac{3}{4}$ by $1\frac{1}{2}$ in. respectively. Analysis of their test results showed that the frequency spectrums for the 3 specimens are nearly the same and that they can be approximated by one single transfer function, which shows that the transfer function for the mix is independent of the specimen size.

In the light of this observation, it appears that the transfer function can be used to represent the dynamic characteristics of a viscoelastic material in much the same way as the elastic modulus represents the stress-strain characteristics of an elastic material. In other words, for a given viscoelastic material such as a bituminous concrete, there is only one transfer function for a given temperature.

Prediction of Displacements for Sinusoidal Loads

It was seen earlier that, once the transfer function of a system is known, it can be used to predict the output of the system for any other given input that is a function of time. After the transfer functions for the asphaltic concrete test specimens under investigation were determined, attempts were made to predict the output displacement of the specimens when subjected to a sinusoidal input of known magnitude, other than the one used to determine the transfer function. Each specimen was tested under 3 sinusoidal inputs of known magnitude, other than the one used to determine the transfer function. Each specimen was tested under 3 sinusoidal inputs at each of the 3 temperatures used previously.

From Eq. 3, the solution for the output displacement of a dynamic system with a transfer function G(s) for a sinusoidal load input of $f(t) = f_o \sin \omega t$ is given by

$$x(t) = f_o \, |G(s)| \, \sin(\omega t + \phi) \tag{13}$$

where f_o = magnitude of the input,
ω = frequency of the input, and
ϕ = phase angle between output and input.

In Eq. 13, x(t) is a maximum when $\sin(\omega t + \phi) = 1$, so that

$$x(t)_{max} = f_o \, |G(s)| \tag{14}$$

Experimentally, it is convenient to measure $x(t)_{max}$ at the peak of the sinusoidal displacement output. Thus, the calculated displacement from Eq. 14 can be compared with the measured displacement for a given magnitude and frequency.

It was mentioned elsewhere that in the experimental setup of this investigation, the input was recorded in pounds and millivolts and the output was recorded in inches and millivolts. Thus the output-input ratio can be either dimensionless or in units of inches per pound. The frequency spectrum and the transfer function analyses were obtained as dimensionless quantities. In applying units to Eq. 14, an experimental constant K needs to be introduced and it becomes

$$x(t)_{max} = K f_o \, |G(s)| \tag{15}$$

From the sensitivity control values of the recorder, K was calculated and found to be

$$K = 25 \times 10^{-4} \text{ in./lb} \tag{16}$$

The calculated and measured values for the maximum displacement for all the specimens tested at 80 F are given in Table 3. In all cases the magnitude of the sinusoidal

TABLE 3

CALCULATED AND MEASURED DISPLACEMENTS AT 80 F

Specimen	Sine Load Input				Constant Load Input		
	f_o (lb)	ω (rad/sec)	x(t) Calculated (in. x 10^{-4})	x(t) Measured (in. x 10^{-4})	f_o (lb)	x(t) Calculated (in. x 10^{-4})	x(t) Measured (in. x 10^{-4})
z-1	5	0.05	2.37	2.25	5	3.13	2.50
	5	0.50	1.20	1.25	10	6.26	5.00
	5	5.00	0.58	0.50	15	9.39	10.00
x-1	5	0.05	1.59	1.25	5	2.23	2.00
	5	0.50	0.87	0.75	10	4.46	3.75
	5	5.00	0.50	0.50	15	6.69	5.50
y-1	15	0.05	5.32	5.00	5	2.30	2.25
	15	0.50	3.18	3.00	10	4.60	4.00
	15	5.00	1.43	1.75	15	6.90	8.75
z-2	15	0.05	5.32	5.00	5	2.30	2.25
	15	0.50	3.18	3.00	10	4.60	4.50
	15	5.00	1.43	1.50	15	6.90	6.50
x-2	15	0.05	4.76	5.00	5	2.23	1.25
	15	0.50	2.62	2.50	10	4.46	4.00
	15	5.00	1.50	1.75	15	6.69	9.50
y-2	15	0.05	4.76	4.75	5	2.23	2.25
	15	0.50	2.62	2.50	10	4.46	4.00
	15	5.00	1.50	1.50	15	6.69	7.00

input was kept the same and only the frequency was varied. Comparison of the calculated and the measured displacement values clearly indicates the close agreement between these values in all cases. Besides proving the efficacy of the transfer function as a displacement predicting tool for viscoelastic materials, this also shows that the bituminous concrete behaves as a linear system at the levels of stress considered in the tests.

Prediction of Displacements for Static Loads

The transfer function can be used to predict the time-dependent displacements of a system subjected to a step function input, and, mathematically, a static load can be represented by a step function. For the transfer function given by Eq. 12, the solution for the displacement under a static load can be shown as

$$x(t) = C_1 e^{b_1 t} + C_2 e^{b_2 t} + C_3 e^{b_3 t} + C_4 e^{b_4 t} + C_5 \tag{17}$$

where C_i is a constant independent of t for the system and b_i is the root of the denominator of the transfer function that is observed to be negative in the case of the experimentally derived transfer functions.

Two boundary conditions are applicable to Eq. 17: (a) when $t = 0$ and (b) when $t = \infty$.

When $t = 0$,

$$x(t) = 0 \tag{18}$$

that is

$$C_5 = C_1 + C_2 + C_3 + C_4 \tag{19}$$

When $t = \infty$,

$$x(t) = C_5 \tag{20}$$

When a constant load is applied to a viscoelastic material, the displacement approaches a constant value after a certain time depending on the nature of the material. In the laboratory, for the bituminous concrete specimens tested, this time was observed to be in the order of a few minutes. Hence, the second boundary condition can be applied to this steady displacement value in the test; that is, Eq. 20 can be used to calculate the displacement. The limitations of using Eq. 20 are recognized in that in a test t does not reach infinity and hence the measured value will be slightly lower than the calculated value.

In order to get the calculated displacement in proper units, Eq. 20 should be multiplied by the experimental constant K, described in the previous section so that

$$x(t) = K C_5 \tag{21}$$

where $K = 25 \times 10^{-4}$ in./lb. C_5 has the units of pound.

The calculated and measured values of the displacement at 80 F for the specimens, each under 3 different constant loads, are given in Table 3. Comparison of the calculated and the measured displacement values clearly indicates the close agreement between the two in almost all cases. This observation is very significant and it brings to focus the following points:

1. The mathematical theory of transfer functions is applicable to viscoelastic materials in general and to bituminous concrete in particular;
2. The techniques developed to derive the transfer function in this investigation are sound; and
3. The transfer function serves as a connecting link between the responses of the material tested under dynamic and static loads.

Differential Equation From Transfer Function

Once the transfer function is known for a given system, the differential equation for the system behavior can be written using the Laplace inverse transform. For bituminous concrete, the transfer function was seen to be of form

$$G(s) = \frac{A(s + a_1)(s + a_2)(s + a_3)}{(s + b_1)(s + b_2)(s + b_3)(s + b_4)} \tag{12}$$

From definition

$$G(s) = \frac{\bar{x}(s)}{\bar{f}(s)} \tag{1}$$

From Eqs. 1 and 12,

$$\frac{\bar{x}(s)}{\bar{f}(s)} = \frac{A(s + a_1)(s + a_2)(s + a_3)}{(s + b_1)(s + b_2)(s + b_3)(s + b_4)} \tag{22}$$

Rewriting,

$$\bar{x}(s)(s + b_1)(s + b_2)(s + b_3)(s + b_4) = A\,\bar{f}(s)(s + a_1)(s + a_2)(s + a_3) \tag{23}$$

Multiplying and rearranging the terms,

$$\bar{x}(s)\left[s^4 + B_1 s^3 + B_2 s^2 + B_3 s + B_4\right] = A\,\bar{f}(s)\left[s^3 + B_5 s^2 + B_6 s + B_7\right] \tag{24}$$

where $B_1 = b_1 + b_2 + b_3 + b_4$, (25)

$B_2 = b_1b_2 + b_2b_3 + b_3b_4 + b_4b_1 + b_4b_2 + b_3b_1$, (26)

$B_3 = b_1b_2b_3 + b_2b_3b_4 + b_3b_4b_1 + b_4b_1b_2$, (27)

$B_4 = b_1b_2b_3b_4$, (28)

$B_5 = a_1 + a_2 + a_3$, (29)

$B_6 = a_1a_2 + a_2a_3 + a_3a_1$, and (30)

$B_7 = a_1a_2a_3$. (31)

Rewriting Eq. 24,

$$s^4\bar{x}(s) + B_1s^3\bar{x}(s) + B_2s^2\bar{x}(s) + B_3s\bar{x}(s) + B_4\bar{x}(s)$$

$$= A\left[s^3\bar{f}(s) + B_5s^2\bar{f}(s) + B_6s\bar{f}(s) + B_7\bar{f}(s)\right] \quad (32)$$

Applying the Laplace inverse transform,

$$\frac{d^4x(t)}{dt^4} + B_1\frac{d^3x(t)}{dt^3} + B_2\frac{d^2x(t)}{dt^2} + B_3\frac{dx(t)}{dt} + B_4x(t)$$

$$= A\left[\frac{d^3f(t)}{dt^3} + B_5\frac{d^2f(t)}{dt^2} + B_6\frac{df(t)}{dt} + B_7f(t)\right] \quad (33)$$

Equation 33 is a fourth order linear differential equation that has constant coefficients and that describes the dynamics of the bituminous concrete. The input (force) and the output (displacement) are the equation's 2 variables that are functions of time. The constants, B_i's, are easily determined from the roots of the denominator, b_i's, and from those of the numerator, a_i's, of the transfer function, using Eqs. 25 through 31.

It is of significance to note here that these roots of the differential equation are obtained as the corner frequencies directly from the frequency spectrum for the material under test, and no assumption whatsoever has been made in deriving the equation.

CONCLUSIONS

Based on the results and within the limitations of this investigation, the following conclusions are enumerated:

1. The viscoelastic or time-dependent characteristics of an asphaltic concrete can be represented by a transfer function G(s) that is a function of the complex variable s. The transfer function is unique for the material at a given temperature. It is possible to obtain this function experimentally from a series of sinusoidal load tests on the material.
2. The transfer function for an asphaltic concrete is of the form

$$G(s) = \frac{A(s + a_1)(s + a_2)(s + a_3)}{(s + b_1)(s + b_2)(s + b_3)(s + b_4)} \quad (12)$$

where A is a constant, and a_i's and b_i's are roots of the numerator and denominator respectively.

3. The roots of the denominator of G(s), namely b_1, b_2, b_3, and b_4, are negative, real, and distinct, thus indicating that bituminous concrete behaves as an overdamped system.
4. Parameters obtained in the transfer function for bituminous concrete are believed to be better indicators of material performance than those commonly used, such as Young's modulus and Poisson's ratio, which change with rate and time of loading.

5. Temperature is the one single factor that has the greatest effect on the transfer function of asphaltic concrete. Increase in temperature increases the value of the constant A in the transfer function equation.

6. The transfer function is a powerful tool useful in predicting the displacement of asphaltic concrete under an applied load, dynamic or static. By treating the static load as a step function of time, the resulting displacement can be calculated by means of the transfer function derived experimentally from the dynamic test. The excellent agreement between the calculated and measured values of the displacement in this investigation validates the concept that the transfer function represents a material property that is independent of the type of load input.

7. Through the use of the transfer function and without assuming any spring-dashpot model, it is possible to represent the time-dependent behavior of asphaltic concrete by a fourth order linear differential equation with constant coefficients. The coefficients can be computed from the roots of the denominator and numerator of the transfer function.

ACKNOWLEDGMENTS

The authors acknowledge the assistance of the Bureau of Public Roads, Federal Highway Administration, U. S. Department of Transportation, who supported the investigation with the Indiana State Highway Commission. Laboratory testing and experimental techniques were carried out in the Bituminous Materials Laboratory of the Joint Highway Research Project at Purdue University, Lafayette, Indiana.

REFERENCES

1. Lee, E. H. Stress Analysis in Viscoelastic Bodies. Quarterly of Applied Mathematics, July 1955.
2. Biot, M. A. Dynamics of Viscoelastic Anisotropic Media. Proc., Fourth Midwestern Conference on Solid Mechanics, Sept. 1955.
3. Biot, M. A. Theory of Stress-Strain Relations in Anisotropic Viscoelasticity and Relaxation Phenomena. Jour. of Applied Physics, Vol. 25, No. 11, Nov. 1954.
4. Lee, E. H. Viscoelastic Stress Analysis. In Structural Mechanics, Proc., First Symposium on Naval Structural Mechanics, Pergamon Press, New York, 1960.
5. Lee, E. H., and Rogers, T. G. Solution of Viscoelastic Analysis Problems Using Measured Creep or Relaxation Functions. Jour. of Applied Mechanics, Vol. 30, No. 1, March 1963.
6. Pister, K. S., and Monismith, C. L. Analysis of Viscoelastic Flexible Pavements. HRB Bull. 269, 1960, pp. 1-15.
7. Pister, K. S. Viscoelastic Plate on a Viscoelastic Foundation. Jour. of Engineering Mechanics Div., ASCE, Vol. 87, Proc. Paper EM1, Feb. 1961.
8. Pister, K. S., and Williams, M. L. Bending of Plates on a Viscoelastic Foundation. Jour. of Engineering Mechanics Div., ASCE, Vol. 86, Proc. Paper EM5, Oct. 1960.
9. Reissner, E. A Note on Deflections of Plates on Viscoelastic Foundation. Trans., ASME, Vol. 25, No. 1, March 1958.
10. Hoskin, B. C., and Lee, E. H. Flexible Surfaces on Viscoelastic Subgrades. Jour. of Engineering Mechanics Div., ASCE, Vol. 85, Proc. Paper EM4, Oct. 1959.
11. Harr, M. E. Influence of Vehicle Speed on Pavement Deflection. HRB Proc., Vol. 41, 1962, pp. 77-82.
12. Wood, L. E., and Goetz, W. H. Rheological Characteristics of a Sand-Asphalt Mixture. Proc., Assn. Asphalt Paving Technologists, Vol. 28, 1959.
13. Secor, K. E., and Monismith, C. L. Analysis of Triaxial Test Data on Asphalt Concrete Using Viscoelastic Principles. HRB Proc., Vol. 40, 1961, pp. 295-314.
14. Kuhn, S. H., and Rigden, P. J. Measurement of Viscoelastic Properties of Bitumens Under Dynamic Loading. HRB Proc., Vol. 38, 1959, pp. 431-463.
15. Papazian, H. S. The Response of Linear Viscoelastic Materials in the Frequency Domain with Emphasis on Asphaltic Concrete. Proc. , Internat. Conference on the Structural Design of Asphalt Pavements, Univ. of Michigan, Ann Arbor, 1962.

16. Pagen, C. A. Rheological Response of Bituminous Concrete. Highway Research Record 67, 1965, pp. 1-26.
17. Kallas, B. F., and Riley, J. C. Mechanical Properties of Asphalt Pavement Materials. Proc., Second Internat. Conference on the Structural Design of Asphalt Pavements, Univ. of Michigan, Ann Arbor, 1967.
18. Truxal, J. C. Control System Synthesis. McGraw-Hill, New York, 1955.
19. Nixon, F. E. Principles of Automatic Controls. Prentice Hall, 1960.
20. Goldberg, J. H. Automatic Controls: Principles of Systems Dynamics. Allyn and Bacon, Boston, 1964.
21. Tsien, H. S. Engineering Cybernetics. McGraw-Hill, New York, 1954.
22. Etkin, B. Dynamics of Flight. John Wiley and Sons, New York, 1959.
23. Crafton, P. A. Shock and Vibration in Linear Systems. Harper and Brothers, 1961.
24. Busching, H. W., Goetz, W. H., and Harr, M. E. Stress-Deformation Behavior of Anisotropic Bituminous Mixtures. Proc., Assn. Asphalt Paving Technologists, Vol. 36, 1967.
25. Lister, N. W., and Jones, R. The Behavior of Flexible Pavements Under Moving Wheel Loads. Proc., Second Internat. Conference on the Structural Design of Asphalt Pavements, Univ. of Michigan, Ann Arbor, 1967.
26. Swami, S. A. The Response of Bituminous Mixtures to Dynamic and Static Loads Using Transfer Functions. Purdue Univ., Lafayette, Indiana, PhD dissertation, Jan. 1969.

Long-Term Compaction of Asphalt Concrete Pavements

JON A. EPPS, BOB M. GALLAWAY, and WILLIAM W. SCOTT, JR.,
Texas Transportation Institute, Texas A&M University

Fifteen field test sites were selected in Texas in an attempt to define more accurately the influence of material properties, mix design, weather conditions, and traffic on the long-term density gain of pavements. Asphalt cores obtained from these test sections over a 2-year period indicate that the majority of these mixes were compacted to an air void content within 2 to 3 percentage points of each other regardless of the compactive effort employed, and the resulting densities after 2 years of service are within a range of 1 or 2 percentage points of each other regardless of the position of the core with respect to the wheelpaths of the traffic. Samples of field mixtures were compacted in the laboratory by use of the Texas gyratory compactor, and these results are compared with the density obtained in the field. These results show that 85 percent of the samples did not obtain 95 percent of the laboratory density during construction. After one week of traffic, approximately 50 percent of the test sections had reached 95 percent of laboratory density, and after 4 months, 80 percent had reached 95 percent laboratory compaction. Two years of service resulted in all except two of the test site pavements reaching greater than 95 percent relative compaction, and only 20 percent reached 100 percent relative compaction.

•THE IMPORTANCE of proper compaction of asphalt pavements has been recognized for many years. Investigators have shown that bituminous pavement stability, durability, tensile strength, fatigue resistance, stiffness, and flexibility are strongly influenced by density.

To ensure adequate compaction, several agencies specify "in-place" density requirements. These in-place requirements are commonly expressed as a percentage of a standard laboratory compaction density. Although laboratory tests are intended to give the engineer needed information about the density of the surfacing material as it ultimately appears on the roadway, there is evidence that an increasing number of bituminous concrete pavements in Texas as well as other states are not stabilizing at a density equal to that obtained in the laboratory design of a companion paving mixture.

The reasons for this unpredictable behavior are probably many and complex. In an attempt to define more adequately the variables that may affect the long-term density of a pavement, 15 test sites were selected throughout Texas, and compaction data were collected over a 3-year span, covering a maximum life span of 2 years for any individual pavement. The results of this study are presented herein.

TEST PROGRAM

The test program may be conveniently separated into field and laboratory phases, as discussed in the following sections.

Paper sponsored by Committee on Construction Practices—Flexible Pavement.

Field Testing Program

The field work included site selection, preparation and placing of the test section, and regular sampling of test sections.

Fifteen test sites were selected in 6 highway districts. The selection of the test sites was based on contract work in progress, traffic volume, climatic conditions, materials, pavement type (flexible or rigid), and construction type (new or overlay). In addition, the grade line was approximately level; there was no ingress or egress from the test sections; and all tests sites were on tangents.

Each test section was 600 ft in length and 1 traffic lane in width. The sections were further subdivided into subsections A, B, and C with each part or subdivision receiving a different amount of construction compaction as follows:

Subsection A—half the roller passes subsection B,
Subsection B—normal rolling procedure for a given project, and
Subsection C—double the roller passes of subsection B.

TABLE 1: COMPACTION PROCEDURE

Test Section	AGGREGATES: Aggregate	Source	Grading (Plant): +#4	-#4	-#40	-#200	Maximum Size (100% pass)	ASPHALTS: Asphalt Source	Asphalt Type	Asphalt Content, Percent: Design	Extraction	Original Viscosity: mega-poise 77°	stokes X10³ 140°	stokes 275°	Original Penetration at 77°F, dmm
Childress US 287 25-42-9	Siliceous CRS - 65% Fines - 35%	Local - Tucker Pit	36%	64%	16.6%	1.2%	1/2	01	AC-20	5.0	5.26	2.2	2.410	3.9	65
Matador US 70 25-145-8	CRS - 18.9% Int. - 23.2% Fine - 21.1% Sand - 36.8%	Local - Campbell Pit	45.5%	54.5%	23.1%	6.1%	7/8	01	AC-20	5.0	5.4	2.7	3.151	4.08	61.5
Sherman SH 5 1-47-3	3/8 crushed LS. - 65% Field Sand - 25% Conc. Sand - 10%	Crushers Inc. Bill Rldenour	43%	57%	25.5%	2.2%	1/2	09	AC-20	5.8	6.5	1.59	2.597	5.14	75
Cooper SH 24 1-136-3	L.S.S. - 18.1% Field Sand - 21.9% Pea Gravel - 55.2%	Bridgeport, Tex. Local - Backus Pit Van Pit Seegeville	38%	62%	31.1%	2.4%	1/2	03	AC-20	4.8	4.6	2.06	3.02	5.10	69.2
Cumby IH 30 1-9-13	L.S.S. - 18.1% Field Sand - 21.9% Pea Gravel - 55.2%	Bridgeport, Tex. Local - Backus Pit Van Pit Seegeville	39%	61%	27.5%	3.9%	1/2	03	AC-20	5.1	5.1	2.28	3.10	5.19	68.8
Clifton SH 6 9-258-7	D Rock - 32% Fine Sand - 28.3% Conc. Filler - 35%		41.8%	58.2%	19%	3.4%	1/2	01	AC-10	4.7	5.6	2.0	2.788	3.98	55
Waco US 84 9-55-8	Flex Base with one Course Surf Treat	Neilson Pit	41.7%	58.3%	21.7%	2.7%	1/2	09	85-100	4.8	4.95	0.87	2.28	5.12	75
Robinson US 77 9-209-1	River Gravel - 65% Field Sand - 20% Conc Sand - 15%	Neelleys Pit Simons Pit	49.2%	50.8%	22.1%	7.2%	1/2	03	AC-20	4.5	4.71	1.5	2.89	6.41	74
Milano SH 36 17-185-4	RSA - 70% RSA - 30% Rock Asphalt	Alcoa Uvalde Rockdale	5.4%	94.6%	18.4%	6.9%	3/8	06	AC-20	6.75	6.77	3.6	3.349	4.32	39
Bryan Spur 308 17-599-1	RSA - 75% L.S. screen - 20% Field Sand - 5%	Alcoa - Rockdale Georgetown	1.3%	98.7%	22.8%	4.3%	3/8	06	AC-20	6.2	6.1	2.16	3.188	4.55	45
Tamina IH 45 12-110-4	Iron Ore - 70% L. S. - 30%	Iron Ore Champion Pit (I-A)	44.8%	55.2%	26.0%	3.4%	1/2	06	AC-10	4.6	4.41	.77	1.672	3.1	85
Conroe FM 1485 12-1062-35	Iron Ore Field Sand	Gaylord Construction Company	42.0%	58.0%	26.1%	2.7%	1/2	11	AC-20	4.75	5.2	1.8	3.888	5.12	53
Baytown Spur 330 12-508-7	Limestone - 33% Sand Coarse - 30% Sand Fine - 37%		46.0%	54%	28.6%	3.5%	1/2	11	85-100	5.2	5.4	.72	1.529	3.41	72
Orange SH 12 20-499-3	L.S. - 35% Vido Field S. - 24% Helm's Screening- 41	Tex. Const. Mat. Burnet & Eagle Smith Pit-Vidor	35.7%	64.3%	25.9%	2.3%	1/2	05	AC-20	5.0	5.2	5.4	4.186	5.15	37
Bridge City IH 87 20-306-3	L. S. - 35% Vidov F. S. - 24% Helm's Scr. - 41%	Tex. Const. Mat. Burnet & Eagle Smith Pit-Vidor	32.4%	67.6%	27.6%	3.3%	1/2 1/2	05	AC-20	5.0	5.3	5.4	4.186	5.15	37

It was believed that this range of roller passes would span the range of compactive efforts encountered in practice. Compaction procedures are given in Table 1.

In order to obtain samples, aluminum foil was placed on the surface to be paved. A single 4-in. diameter core was removed from each prepared location according to the following schedule:

1 day	18 cores at 3 subdivisions = 54 samples
1 week	18 cores at 3 subdivisions = 54 samples
1 month	9 cores at 3 subdivisions = 27 samples
4 months	9 cores at 3 subdivisions = 27 samples
1 year	9 cores at 3 subdivisions = 27 samples
2 years	9 cores at 3 subdivisions = 27 samples

Total number of samples per test site = 216

The sequence of coring proceeded against the traffic flow.

TABLE 2: AGGREGATES AND ASPHALTS

Test Section	Compaction Equipment: Breakdown Rolling — Passes/Section A	B	C	Type Roller/Size	Compaction Equipment: Intermediate Rolling — Passes/Section A	B	C	Type Roller/Size	Compaction Equipment: Final Rolling — Passes/Section A	B	C	Type Roller/Size	Temperature, °F: Air	Breakdown	Final Roll	Field Initial Density (1 Day) Section B PWP
Childress US 287 25-42-9	4	3	6	3 wheel tandem, 12 ton; 5'-4' diameter	4	4	4	2 wheel tandem, 10 ton; 5'-4' diameter	14	14	14	Pneumatic, 25ton 60 psi	51	145	125	8.69
Matador US 70 25-145-8	11	11	11	3 wheel, 10 ton	5	11	21	Tandem 10 ton	7	13	25	Pneumatic, 25 ton 75 psi	63	225	145	7.68
Sherman SH 5 1-47-3	6	12	24	3 wheel 10 ton	5	5	9	Tandem 8 ton	10	20	40	Pneumatic, 12 ton 70 psi	80	200	135	8.26
Cooper SH 24 1-136-3	3	5	9	3 wheel 10 ton	3	5	9	Tandem 10 ton; 4' diameter	1	4	7	Pneumatic	82	155	75	10.85
Cumby IH 30 1-9-13	3	7	13	3 wheel 10 ton	3	5	9	Tandem 8 ton	3	5	9	Pneumatic, 22.3ton 102 psi	46	205	100	5.51
Clifton SH 6 9-258-7	3	3	6	3 wheel 10 ton, 60"-42" diameter	4	8	16	Pneumatic 16.3ton 75 psi	3	7	14	Tandem, 8.8ton, 60"-48" diameter	96	220	150	9.89
Waco US 84 9-55-8	4	3	9	Tandem, 8 ton, 54" diameter	4	4	4	Tandem, 8 ton, 54" diameter	15	15	15	Pneumatic, 8 ton, 44-52 psi	101	180	135	7.39
Robinson US 77 9-209-1	3	3	7	3 wheel, 10 ton, 60"-42" diameter	4	4	4	Tandem 8 ton, 54"-42" diameter	12	12	18	Penumatic, 25 ton, 60 psi	98	160	130	8.53
Milano SH 36 17-185-4	3	3	7	3 wheel, 10 ton, 60"-30" diameter	3	3	3	Tandem, 8 ton, 54" diameter	3	7	13	Penumatic, 25 ton, 60 psi	95	160	145	20.79
Bryan Spur 308 17-599-1	3	6	12	3 wheel, 10 ton, 60" diameter	3	3	3	Tandem, 8 ton, 54" diameter	4	4	8	Penumatic, 12 ton, 75 psi	95	170	135	18.76
Tamina IH 45 12-110-4	3	7	4	3 wheel, 10 ton, 42"-66" diameter	6	6	24	Penumatic, 10 ton 85 psi	2	2	2	Tandem, 10 ton, 54" diameter	97	185	145	12.72
Conroe FM 1485 12-1062-35	3	7	14	3 wheel, 10 ton, 60" diameter	10	10	20	Pneumatic, 25 ton 65-70 psi	3	3	6	Tandem, 8 ton, 60" diameter	95	155	135	12.34
Baytown Spur 330 12-508-7	3	6	12	3 wheel, 10 ton, 60" diameter	NONE				3	3	3	Tandem, 8 ton, 54" diameter	108	180	100	25.88
Orange SH 12 20-499-3	5	7	13	3 wheel, 10 ton, 5'-3' diameter	NONE				3	5	11	Tandem, 12 ton, 4 1/2' - 3 1/2'	90	200	170	10.02
Bridge City IH 87 20-306-3	5	9	15		NONE				5	7	11	Tandem, 8 ton, 5'-4'	85	200	165	13.83

Laboratory Testing Program

Samples of uncompacted asphalt mix were obtained from each test site in the field. These loose samples were compacted by using the gyratory compactor according to the procedures of the Texas Highway Department (1). Percentage of air voids, stability, and cohesiometer values were obtained from the compacted samples and are reported elsewhere (2).

MATERIALS

Different asphalts, aggregates, and aggregate grading were used at the 15 test sites.

Aggregates

Table 2 gives the type, source, grading, and maximum sizes of aggregates used in this study. Aggregate types included siliceous materials used on the Childress project, rock asphalt used on the Milano project (rockdale slag aggregate plus asphalt rock), iron ore aggregate used on the Tamina and Conroe projects, slag used on the Milano and Bryan project, and limestone, which was the predominant type of aggregate.

Asphalts

The asphalt source, type, content, viscosity, and penetration for the various test sites are given in Table 2. The viscosity and penetration of the asphalts recovered after service for various lengths of time were obtained and are reported elsewhere (2).

RESULTS

Variation in pavement densities with time has been studied by various groups including Kenis (3), Bright et al. (4), Palmer and Thomas (5), Campen et al. (6), Gallaway (7), and Pauls and Halstead (8). These and other studies have suggested that the following factors influence the long-term density of the pavement.

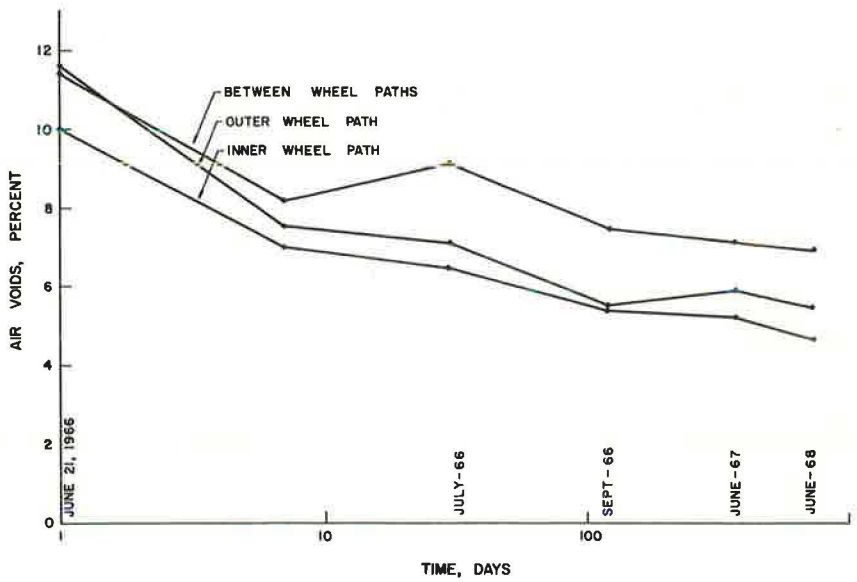

Figure 1. Pavement densification with time at various locations in the pavement, Orange test section.

1. Degree of initial compaction
2. Material properties
   a. Aggregate absorption
   b. Aggregate surface characteristics
   c. Aggregate gradation
   d. Asphalt temperature-viscosity relationship
   e. Asphalt susceptibility to hardening
3. Mix design
   a. Asphalt content (film thickness)
   b. Voids in mineral aggregate
4. Weather conditions
   a. Air temperature variations (daily and seasonally)
   b. Date of construction
5. Traffic
   a. Amount
   b. Type
   c. Distribution throughout the year
   d. Distribution throughout the day
   e. Distribution in lanes
6. Pavement thickness

Results selected from the 15 test sites (see reference 2 for complete data) in this study are shown in Figures 1 through 4. Figures 1 and 2 show air void contents for normal compactive efforts between the wheelpaths as well as the inner and outer wheelpath. Figures 3 and 4 show air void contents at the inner wheelpath for the 3 compactive efforts. As suggested previously the results shown in Figures 1 through 4 are dependent on several factors discussed in the following sections.

Initial Compaction

The initial density of the pavement is dependent on the compactibility of the mix or the ease with which it can be compacted, the type of compaction equipment, the rolling

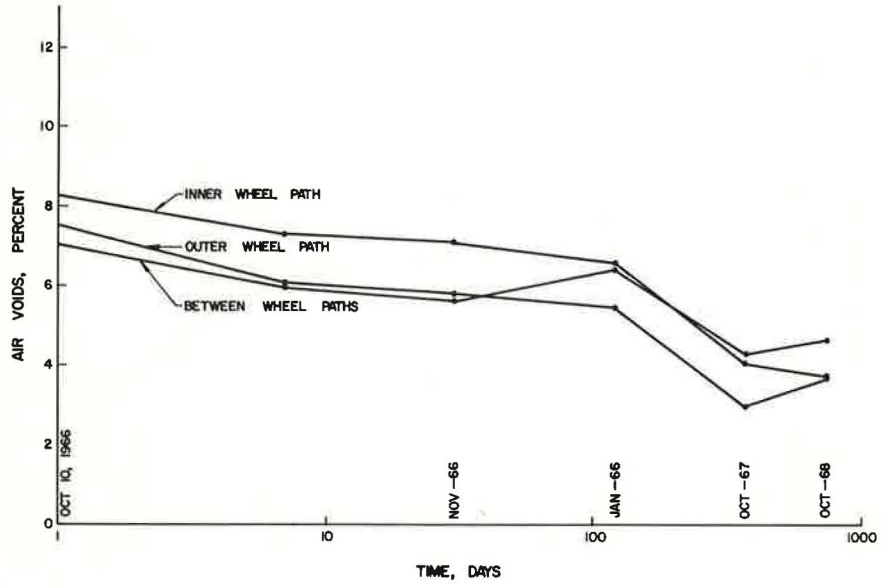

Figure 2. Pavement densification with time at various locations in the pavement, Sherman test section.

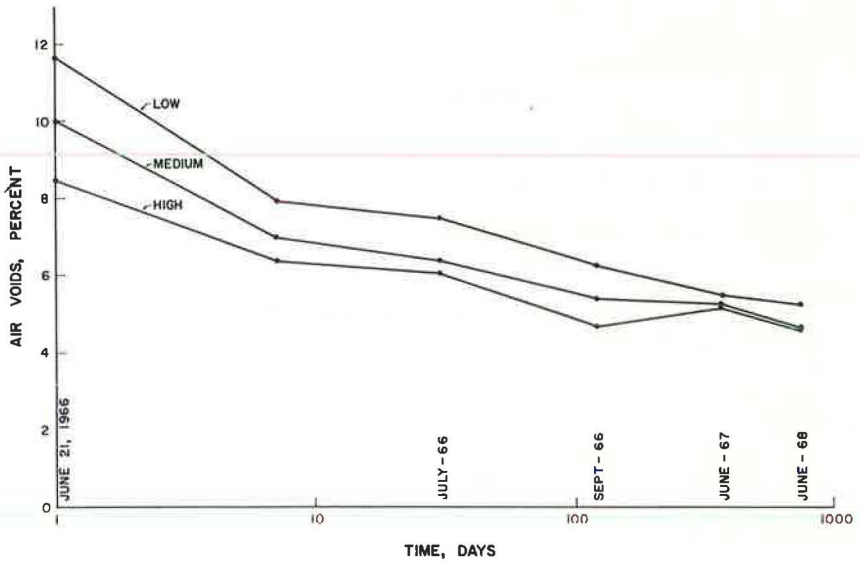

Figure 3. Pavement densification with time for various compactive efforts, inner wheel path, Orange test section.

sequence and procedure, and the timing of the compaction processes. Furthermore, the compactibility of a mix is dependent on material properties, mix design, subgrade support, thickness of lift, temperature of the surface and the mix, weather conditions during placement, and moisture in the mix. All of these factors must be considered if the relative compactibility of a mix is to be determined.

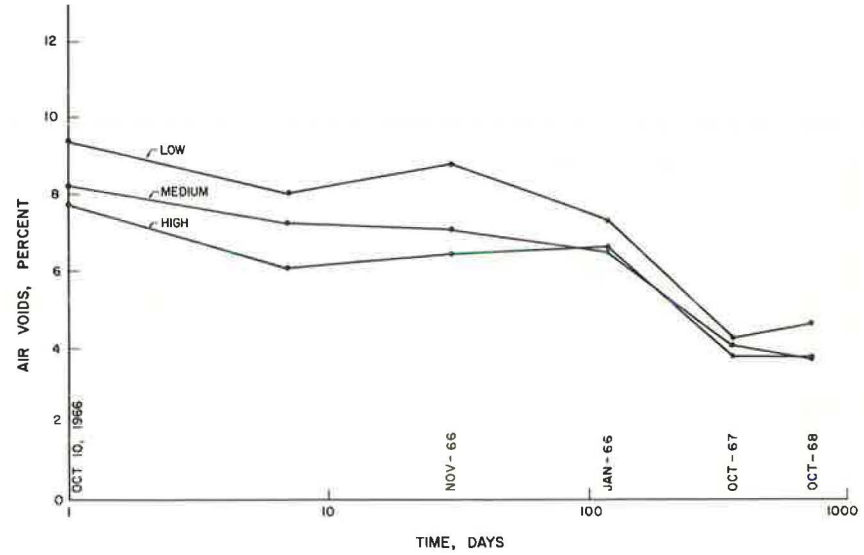

Figure 4. Pavement densification with time for various compactive efforts, inner wheel path, Sherman test section.

Because both the aggregate and asphalt characteristics varied widely, and the temperature at breakdown rolling was low (6 of 15 test sections, Table 1), little definitive information could be gained as to the factors controlling the initial density of pavements. However, these data indicate that it is important that compaction equipment follow the lay-down machine as closely as possible when thin lifts and cool weather are encountered during construction as the temperature drop of a mix increases its resistance to compaction.

As noted previously, individual test sites were subjected to different compactive efforts; however, little density variation was noted on most of the projects (Table 3). Furthermore, it is difficult to determine if the density of the pavements after 2 years

TABLE 3 PERCENT AIR VOIDS IN FIELD SAMPLES

Test Section	Sub-Section	Wheel Path	1 Day	1 Week	1 Month	4 Months	1 Year	2 Years
Childress US 287 25-42-9	A*	I**	10.20	9.34	7.16	4.20	4.15	3.70
		B**	9.62	9.66	8.73	5.92	6.23	5.23
		O**	10.53	9.84	7.60	4.55	4.17	3.90
	B*	I	8.69	8.45	5.60	3.39	3.90	3.32
		B	8.45	8.10	6.88	5.18	5.60	5.22
		O	9.20	8.15	6.26	3.97	3.93	4.08
	C*	I	8.58	8.33	6.81	3.81	3.84	3.98
		B	8.93	8.77	8.43	5.38	5.85	5.92
		O	9.03	9.72	7.80	5.11	5.11	4.70
Matador US 70 25-145-8	A	I	5.71	6.50	6.05	6.25	4.47	5.79
		B	6.25	6.42	6.02	5.94	4.62	4.57
		O	7.11	7.11	7.43	7.31	5.23	7.33
	B	I	7.68	7.79	8.77	7.47	5.36	6.77
		B	7.38	7.41	6.92	7.39	5.20	5.80
		O	9.06	8.58	9.19	9.88	7.90	8.92
	C	I	3.94	4.96	4.65	5.38	4.15	4.12
		B	5.56	6.40	6.16	6.19	3.50	4.11
		O	7.61	7.80	7.14	6.43	5.43	5.72
Sherman SH 5 1-47-3	A	I	9.32	8.05	8.80	7.39	4.29	4.66
		B	7.10	5.43	5.74	6.96	4.28	4.65
		O	7.19	7.21	5.62	5.64	2.70	3.33
	B	I	8.26	7.30	7.12	6.60	4.05	3.75
		B	6.99	5.96	5.63	6.45	4.36	4.75
		O	7.49	6.08	5.83	5.49	2.99	3.73
	C	I	7.77	6.14	6.49	6.72	3.80	3.79
		B	6.31	5.15	5.11	6.30	4.51	4.26
		O	6.82	5.78	4.66	5.09	3.13	4.31
Cooper SH 24 1-136-3	A	I	10.94	9.54	9.12	6.29	6.57	6.62
		B	10.43	9.30	9.23	6.70	6.33	6.30
		O	10.21	10.33	9.08	6.87	5.88	6.18
	B	I	10.85	9.54	9.29	6.92	6.32	6.17
		B	8.43	7.44	7.47	5.63	6.22	5.80
		O	10.82	9.34	8.63	7.04	6.72	6.50
	C	I	9.21	8.03	8.04	5.81	5.72	6.02
		B	7.93	8.00	6.91	5.54	5.33	5.72
		O	8.47	8.12	7.35	5.91	5.06	5.48
Cumby IH 30 1-9-13	A	I	8.02	6.92	6.94	3.06	1.95	1.79
		B	5.87	5.14	5.36	3.14	2.74	2.51
		O	7.11	6.27	6.22	3.40	1.88	1.59
	B	I	5.51	5.38	5.48	2.40	2.22	1.71
		B	4.08	4.64	4.77	2.87	2.31	2.05
		O	4.75	5.03	4.68	2.18	2.01	1.99
	C	I	4.77	6.01	4.84	2.85	1.56	1.60
		B	3.91	4.29	4.56	3.37	3.30	2.04
		O	4.50	4.28	4.59	2.20	1.64	1.52
Clifton SH 6 9-258-7	A	I	9.86	8.18	6.94	7.62	6.67	6.12
		B	9.65	8.97	8.90	8.45	7.39	8.45
		O	9.74	8.08	7.87	7.66	7.38	7.35
	B	I	9.89	7.02	6.47	6.07	5.46	6.23
		B	8.59	8.30	8.19	7.90	7.15	8.42
		O	9.13	7.98	6.96	7.19	6.82	6.59
	C	I	7.78	7.60	6.63	5.93	5.53	5.07
		B	7.68	7.62	7.21	6.93	6.60	6.61
		O	8.18	7.72	6.72	6.19	6.39	6.11
Waco US 84 9-55-8	A	I	7.23	5.52	2.48	1.80	2.59	1.95
		B	7.60	6.52	4.00	4.04	3.70	3.61
		O	7.58	5.89	2.53	2.57	3.01	2.36
	B	I	7.39	5.27	2.86	2.71	2.26	1.57
		B	6.77	5.18	3.75	3.07	2.76	2.30
		O	7.14	4.90	2.76	2.11	2.71	2.81
	C	I	6.35	4.55	3.05	2.57	2.22	1.89
		B	5.50	3.84	2.97	3.12	2.32	1.72
		O	5.55	3.85	2.34	1.97	2.34	2.25
Robinson US 77 9-209-1	A	I	9.41	7.79	8.56	6.34	5.08	5.03
		B	8.25	6.50	7.78	4.96	5.00	4.95
		O	8.71	7.34	6.75	6.07	4.06	5.05
	B	I	8.53	7.14	7.91	5.27	4.40	3.92
		B	7.62	6.90	9.31	5.72	4.91	4.77
		O	9.40	7.44	6.13	6.02	5.06	4.53
	C	I	7.01	6.86	7.43	4.50	5.42	4.73
		B	4.79	4.48	6.75	3.61	4.79	3.96
		O	6.39	5.89	4.99	4.62	5.66	3.73

TABLE 3 PERCENT AIR VOIDS IN FIELD SAMPLES
(Cont'd)

Test Section	Sub-Section	Wheel Path	1 Day	1 Week	1 Month	4 Months	1 Year	2 Years
Milano SH 36 17-185-4	A	I	19.23	17.96	18.00	16.77	16.31	16.85
		B	21.47	17.69	18.83	18.31	16.78	17.26
		O	19.71	18.55	18.10	17.55	17.14	17.35
	B	I	20.79	18.47	18.37	17.33	17.16	16.19
		B	21.39	18.36	17.97	17.89	17.41	16.80
		O	20.96	18.64	19.06	18.17	17.93	17.70
	C	I	17.85	17.46	17.60	17.21	16.59	17.12
		B	20.02	17.26	17.45	17.85	16.42	15.81
		O	18.54	16.75	16.93	17.83	15.42	15.17
Bryan Spur 308 17-599-1	A	I	21.46	17.38	16.90	15.91	14.22	14.48
		B	19.41	18.19	18.91	16.76	16.50	19.66
		O	17.31	16.21	17.37	15.61	13.85	17.98
	B	I	18.76	18.24	17.96	16.23	15.78	15.00
		B	17.40	16.94	18.45	16.16	15.98	15.60
		O	16.33	16.85	17.44	14.57	13.86	14.45
	C	I	18.73	17.68	17.45	14.95	14.97	18.11
		B	17.12	16.09	17.00	14.33	13.26	12.67
		O	16.69	15.59	15.79	14.06	13.94	13.67
Tamina IH 45 12-110-4	A	I	13.75	8.84	8.25	6.13	5.75	5.52
		B	13.07	9.32	7.48	6.39	6.39	5.90
		O	13.74	9.34	7.12	6.73	5.95	4.98
	B	I	12.72	8.80	7.80	6.18	5.55	5.00
		B	11.18	8.96	7.20	7.01	6.07	6.57
		O	13.56	9.12	6.94	5.92	5.44	5.68
	C	I	11.28	6.81	5.63	5.61	5.12	5.35
		B	10.01	7.91	6.89	7.36	5.84	6.14
		O	12.57	7.72	6.35	5.92	5.33	4.97
Conroe FM 1485 12-1062-35	A	I	11.53	11.59	11.65	9.38	9.44	9.96
		B	10.81	11.82	10.94	9.61	9.13	9.50
		O	9.81	10.28	8.93	8.88	7.89	7.51
	B	I	12.34	11.09	9.90	8.24	8.23	8.20
		B	10.54	10.42	10.02	8.13	7.94	8.50
		O	10.04	9.33	7.76	7.26	6.31	6.54
	C	I	11.87	11.09	10.10	9.08	8.58	8.56
		B	10.45	11.25	10.91	8.58	8.91	8.94
		O	9.68	9.03	8.38	7.52	7.08	6.33
Baytown Spur 330 12-508-7	A	I	19.71	11.45	7.18	5.97	4.91	5.52
		B	23.03	10.30	7.87	7.13	6.36	7.23
		O	23.55	11.94	7.64	6.34	4.73	5.42
	B	I	25.88	11.66	7.49	6.12	5.23	5.30
		B	25.12	10.35	8.53	7.60	6.78	8.05
		O	25.34	11.59	7.42	6.09	5.04	6.34
	C	I	11.70	11.31	7.77	6.00	4.97	4.75
		B	10.60	10.44	7.90	7.13	6.43	6.71
		O	11.38	10.80	7.71	5.90	5.15	3.48
Orange SH 12 20-499-3	A	I	11.69	7.97	7.58	6.28	5.49	5.27
		B	12.56	8.40	9.00	7.79	8.39	8.31
		O	12.33	7.67	6.08	6.06	6.49	5.70
	B	I	10.02	7.02	6.41	5.42	5.28	4.66
		B	11.50	8.20	9.11	7.53	7.16	6.95
		O	11.62	7.58	7.16	5.58	5.94	5.47
	C	I	8.51	6.43	6.09	4.68	5.27	4.63
		B	8.56	9.10	8.72	5.93	6.03	5.33
		O	7.92	7.24	6.78	4.92	4.71	4.48
Bridge City IH 87 20-306-3	A	I		8.22	8.97	8.11	8.76	8.45
		B	11.60	9.14	8.17	8.38	8.39	8.28
		O	12.10	9.49	7.83	7.95	8.27	7.58
	B	I	13.83	10.12	8.49	8.71	8.77	8.32
		B	13.63	11.36	9.83	9.96	9.36	9.32
		O	13.33	9.48	7.30	7.78	6.89	7.85
	C	I	13.51	10.30	9.47	8.80	8.54	7.28
		B	11.72	10.26	7.99		9.50	8.11
		O	14.12	9.27	7.36	8.26	7.43	9.10

*Subsection A - half as many roller passes as subsection B
*Subsection B - normal roller procedure for particular project
*Subsection C - twice as many roller passes as subsection B

** I - inner wheel path
** B - between wheel path
** O - outer wheel path

of service is dependent on initial density (Fig. 5). Thus, the majority of the pavements were compacted to an air void content within 2 to 3 percentage points of each other regardless of the initial compactive effort; and the resulting densities after 2 years of service are within a range of 1 or 2 percentage points of each other, having decreased from 4 to 6 percentage points during 2 years of service.

Material Properties

The properties of the asphalts and aggregates affect the long-term densification of a pavement as well as its initial densification. Those material properties that tend to increase the resistance of a pavement to initial compaction behave in the same manner for the long-term density increase because of mechanical and environmental loading.

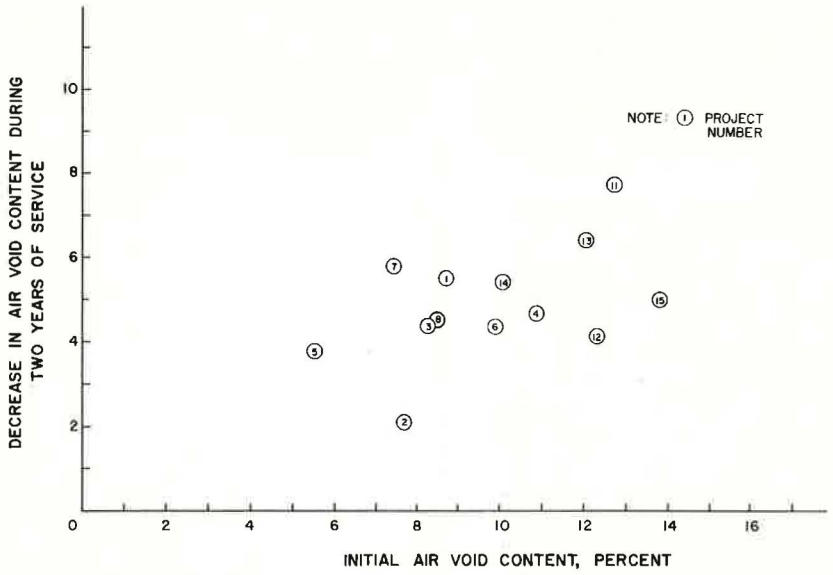

Figure 5. Density change as a function of initial compaction.

Insufficient data were available from these test sites to define accurately the effect of aggregate absorption, aggregate surface characteristics, aggregate gradation, asphalt temperature-viscosity relationship, and mix design on long-term densification of pavements.

Asphalt hardening has been correlated to a certain degree with air void content and degree of interconnectibility of air voids (9). In addition, data collected in this study suggest the same trend (Fig. 6).

Weather Conditions

Density increases between the wheelpaths have been noticed in several long-term density studies (5, 8) as well as this study (Figs. 1 and 2). These data indicate that the air void content between the wheelpaths is lower than either the inner or outer wheelpath in most cases; however, this difference is usually less than 2 percentage points.

Gallaway (10) has suggested that density gain between the wheelpaths may be due to thermal cycling. Therefore, both the seasonal variations and daily cycling in temperatures were obtained for the projects from information obtained from U.S. Weather Bureau stations near the test sites. These data suggest that the seasonal temperature extremes are greater in the northern part of the state (Childress, Matador, Sherman, Cooper, and Cumby) than in the more southerly and coastal projects (Tamina, Conroe, Baytown, Orange, and Bridge City). The summer average monthly temperatures are about the same for all locations.

Daily temperature variation for selected weeks in the winter, spring, summer, and fall was also obtained. These data indicate that daily temperature variation in the panhandle region of Texas (Childress and Matador) has a greater cyclic temperature change than the more southerly coastal areas throughout the year.

These temperature data do not satisfactorily explain the reason for densification between the wheelpaths. The amount of difference noted among the values of air void content in the various locations across the pavement cannot be simply related to the different seasonal and daily temperature environments (Table 3). These data together with data published by Palmer and Thomas (5) on pavements in New York indicate that the entire pavement cross section compacts to approximately the same degree of density

and at approximately the same rate independent of initial compaction, seasonal variations in temperature, and daily variation in temperature for the range of traffic and environments to which these pavements have been subjected.

The date of construction is important in that it determines the temperature of the pavement during its early life and thus its susceptibility to compaction by traffic. Three test sections were compacted in the late fall or early winter in the northern part of the state (Matador, Sherman, and Cumby, Table 3 and Fig. 2). All of these pavements remained at essentially the same density until the warmer spring and summer months elevated the pavement temperature to a level sufficiently high for compaction to continue.

As shown in the preceding, little pavement densification occurred during the colder months. Thus if thermal cycling is a cause of densification between the wheelpaths, it is not evident during the colder months on several of the projects.

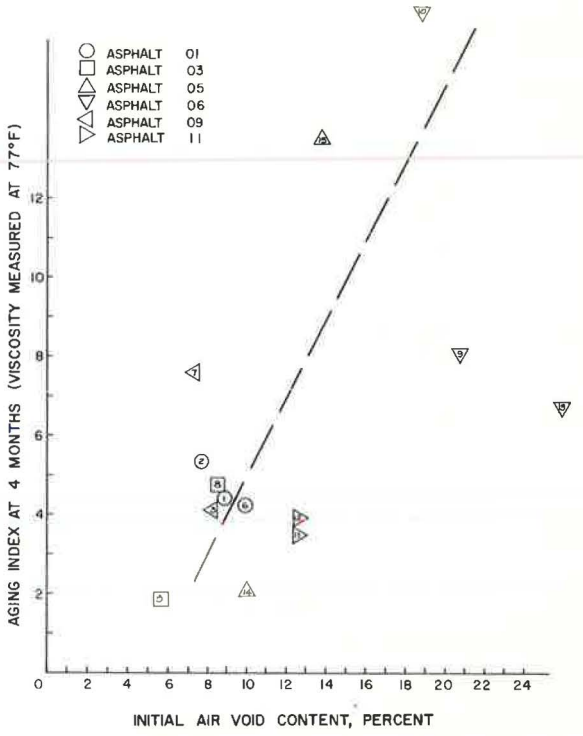

Figure 6. Relationship between asphalt hardening and initial air void content.

The calculated thermal strains in the pavement that are due to daily cycling in temperature are slightly greater in the winter as the daily temperature change is larger. However, the stiffness of the mix is much lower in the summer months, and therefore it is easier for the aggregate particles to arrange themselves in a more dense arrangement. Unfortunately the pavements that were constructed during the warmer months were subjected to traffic immediately after construction, and a check to determine if densification was due to a daily cycling in temperature during the warmer months could not be made.

Traffic

The effect of traffic on long-term pavement density has been established by a number of investigators, including Palmer and Thomas (5), Campen (6), Arena et al. (11), McLeod (12), and Zube (13). These data suggest that the pavement density is primarily related to traffic.

Volume of Traffic—Data reported in this study (Fig. 7) indicate that pavements densify a greater amount with increased traffic independent of the effects of other variables. This trend may explain the density increase in the wheelpaths; however, it does not explain the density increase between the wheelpaths. For example, 3 test sites were not subjected to traffic for various lengths of time after construction (Table 3). The Childress project was opened to traffic 1 week following construction, and consequently the pavement did not densify during the first week. The Cumby project was not open for traffic for 1 month. Little density change is noted during this period. Baytown was opened to traffic 1 month after construction; however, a large amount of densification occurred during this period because the contractor used this pavement as a haul road.

Type of Traffic—The distribution of wheel loads on a pavement will influence the density gain of a pavement with time. For pavements of adequate design, the greater

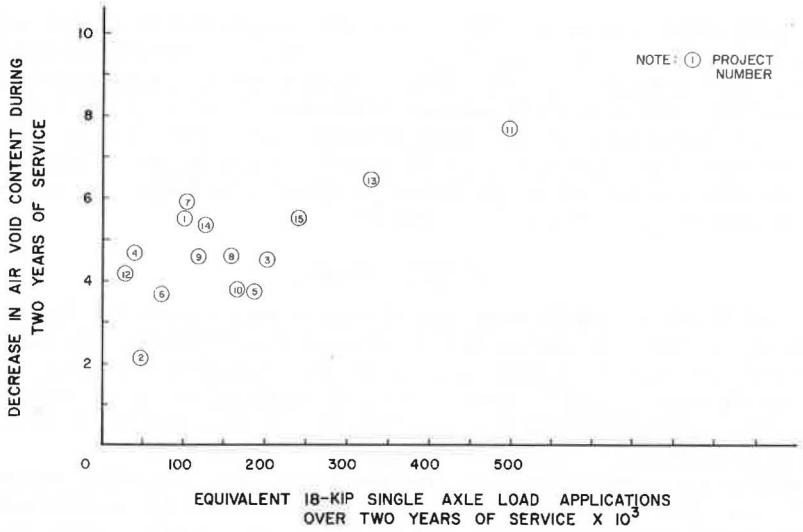

Figure 7. Relationship between increase in density and traffic during 2 years of service.

the number of heavy axle loads the greater the density increase due to traffic will be. This suggests that not only the percentage of trucks must be considered but also the wheel load distribution. The equivalent 18-kip wheel load concept considers both of these factors.

Yearly Distribution of Traffic—The distribution of traffic throughout the year will influence the compaction of a pavement. If the heavy traffic is predominant during the warm months, a greater amount of densification will occur than if the heavy traffic used the highway in the cold months. This is primarily due to differences in asphalt viscosity.

Traffic Distribution Across the Lane—The traffic distribution across the lane was investigated in hopes that it will explain the increase in density noted between the wheelpaths. Data have suggested (14) that 10 to 16 percent of the wheel loads a pavement experiences may be in the center of the pavement. The distribution used by the Portland Cement Association suggests that very little traffic uses the central part of the pavement. However, visual examination of several test sections with 13-ft-wide lanes suggests that these data may be incorrect as the vehicles seem to wander in the lane a significant amount, and therefore a larger portion of the wheel loads actually comes in contact with the center portion of the pavement than would otherwise be expected.

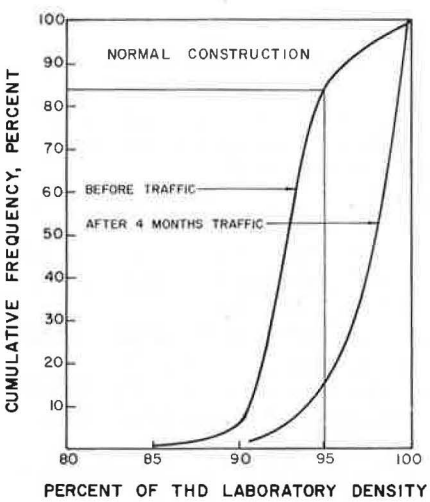

Figure 8. Cumulative frequency relative density.

Comparison of Field and Laboratory Results

If the data for all 15 test sections are considered collectively, a histogram can be prepared and a cumulative frequency distribution chart can be plotted. The chart for the relative densities before traffic and after 4 months of traffic is shown in Figure 8. From these curves it can be

seen that, after construction and before any traffic is allowed on the pavement, 85 percent of the pavement samples from the normal construction operations had not attained 95 percent of the laboratory density. After 1 week of traffic, approximately 50 percent of these pavements had reached 95 percent laboratory density. After 4 months, 80 percent had reached 95 percent of laboratory density. After 2 years of service, all except 2 of the pavements had reached at least 95 percent of this density. The data further show that one-third of the pavements did not densify to the desired 2 to 6 percent air void content after 2 years of service (Table 3).

CONCLUSIONS

1. Data collected in this study as well as others suggest that the long-term density gain of asphalt concrete pavements is a function of many factors. The most important factors as indicated earlier are the susceptibility of asphalt to hardening, the volume of traffic and its nature, and the time of year of construction. It is evident that most pavements will densify with time provided they do not have high initial density and provided they are subjected to heavy wheel loads in warm weather.
2. Densification noted between the wheelpaths closely paralleled the density gain in the wheelpaths. The reasons for this trend are not clear. A possible explanation exists if we consider thermal cycling as a cause of densification. This, however, implies that the predominant forces creating compaction in all sections of the pavement are due to thermal cycling and not traffic associated loads. It is believed that the compaction between the wheelpaths is predominantly related to wheel loads rather than thermal considerations as 2 of the pavements studied exhibited no density increase for periods of up to 1 month without traffic. If thermal cycling creates densification, the induced stresses should have been active during this period and a density increase should have taken place. None was noted.
3. The range of air void content decrease was 2 to 8 percentage points during 2 years of service. The voids in a majority of the pavements were reduced 3 to 6 percentage points.
4. Eighty percent of the total 2-year compaction, due to traffic and environmental effects, was complete within 1 year of service on all of the projects studied.
5. The majority of the pavements were compacted to an air void content within 2 to 3 percentage points of each other regardless of the compactive effort. The resulting densities after 2 years of service are within a range of 1 or 2 percentage points regardless of the location of the core with respect to the wheelpaths of the traffic.

REFERENCES

1. Manual of Testing Procedures. Texas Highway Department, Austin, Vol. 1, Feb. 1963.
2. Epps, J. A., Gallaway, B. M., Harper, W. J., Scott, W. W., and Seay, J. W. Compaction of Asphalt Concrete Pavements. Texas Transportation Institute, Texas A&M Univ., College Station, Res. Rept. 90-2F, 1970.
3. Kenis, W. J. Progress Report on Changes in Asphaltic Concrete in Service. HRB Bull. 333, 1962, pp. 39-65.
4. Bright, R., Steed, B., Steel, J., and Justice, A. The Effect of Viscosity of Asphalt on Properties of Bituminous Wearing Surface Mixtures. Proc., Assn. of Asphalt Paving Technologists, Vol. 35, 1966, pp. 164-188.
5. Palmer, R. K., and Thomas, J. J. Pavement Density—How It Changes. Proc., Assn. of Asphalt Paving Technologists, Vol. 37, 1968, pp. 542-574.
6. Campen, W. H., Smith, J. R., Erickson, L. G., and Mertz, L. R. The Effect of Traffic on the Density of Bituminous Paving Mixtures. Proc., Assn. of Asphalt Paving Technologists, Vol. 30, 1961, pp. 378-388.
7. Gallaway, B. M. Laboratory and Field Densities of Hot-Mix Asphaltic Concrete in Texas. HRB Bull. 251, 1960, pp. 12-17.
8. Pauls, J. T., and Halstead, W. J. Progressive Alterations in a Sheet Asphalt Pavement Over a Long Period of Time. Proc., Assn. of Asphalt Paving Technologists, Vol. 27, 1958.

9. Heithaus, J. F., and Johnson, R. W. A Microviscometer Study of Road Asphalt Hardening in the Field and Laboratory. Proc., Assn. of Asphalt Paving Technologists, Vol. 27, 1958, pp. 17-31.
10. Gallaway, B. M. Discussion of "Pavement Density—How It Changes." Proc., Assn. of Asphalt Paving Technologists, Vol. 37, 1968, p. 577.
11. Arena, P., Shah, S. C., and Adam, V. Compaction of Asphaltic Concrete Pavement with High Intensity Pneumatic Roller. Highway Research Record 178, 1967, pp. 75-92.
12. McLeod, N. W. Influence of Viscosity of Asphalt Cements on Compaction of Paving Mixtures in the Field. Highway Research Record 158, 1967, pp. 76-115.
13. Zube, E. Compaction Studies of Asphalt Concrete Pavement as Related to the Water Permeability Test. HRB Bull. 358, 1962, pp. 12-31.
14. Effect of Controlled Truck Axle Loadings on Concrete Pavements: Final Report on Road Test One—MD. HRB Spec. Rept. 4, 1949.